Flood dynamics, surface water retention and availability in the semiarid Cuvelai-Basin, southern Angola and northern Namibia

Robert Arendt

Cover picture:

Section of the Iishana system north of Oshakati, April 2021.

Freie Universität Berlin

Fachbereich Geowissenschaften

Institut für Geographische Wissenschaften

Flood dynamics, surface water retention and availability in the semiarid Cuvelai-Basin, southern Angola and northern Namibia

Inauguraldissertation

zur Erlangung des akademischen Grades

Doktor der Naturwissenschaften (Dr. rer. nat.)

Vorgelegt von

Ralf Robert Arendt

Berlin, 17.05.2022

Erstgutachter: **Prof. Dr. Achim Schulte**

Freie Universität Berlin
Fachrichtung Angewandte Geographie,
Umwelthydrologie und Ressourcenmanagement
Malteser Straße 74 – 100
12249 Berlin

Zweitgutachter: **Prof. Dr. Robert Jüpner**

Technische Universität Kaiserslautern
Fachbereich Bauingenieurwesen
Fachgebiet Wasserbau
Paul-Ehrlich-Straße 14-482
67663 Kaiserslautern

Tag der Disputation: **12.07.2022**

Eidesstattliche Erklärung

Hiermit versichere ich, dass die vorliegende Arbeit von mir selbstständig verfasst wurde und ich keine außer den angegebenen Hilfsmitteln und Quellen verwendet habe. Alle Gedanken in schriftlicher wie in bildlicher Form, welche aus fremden Quellen übernommen wurden, sind als solche gekennzeichnet. Die Arbeit wurde bisher keinem Prüfungsamt in gleicher oder ähnlicher Form vorgelegt.

Robert Arendt

Berlin, den 17.05.2022

Acknowledgements

Die Anfertigung der vorliegenden Arbeit wäre ohne die Unterstützung einiger Personen nicht möglich gewesen. Diesen Personen möchte ich daher danken.

Mein besonderer Dank gilt in erster Linie meinem Doktorvater Herrn Prof. Dr. Achim Schulte, welcher mir stets mit fachlicher und konstruktiver Kritik zur Seite stand und mich während der zahlreichen gemeinsamen Geländeaufenthalte in Namibia immer tatkräftig unterstützt hat.

Ebenso gilt mein besonderer Dank meinem zweiten Doktorvater Herrn Prof. Dr. Robert Jüpner, der mich ebenfalls in Namibia begleitete. Auch er stand mir stets hilfreich mit Rat und Tat zur Seite und hatte immer ein offenes Ohr für meine Probleme.

Ein großer Dank gilt auch meinen Kolleg*innen - allen voran Herrn Dr. Christian Reinhardt-Imjela. Seine wissenschaftliche Kreativität war stets Inspiration für mich. Für die zahlreichen Diskussionsrunden und für seinen hilfreichen Input danke ich ihm.
Auch meiner Kollegin Leona Faulstich möchte ich danken. Unsere gemeinsame Zeit in Namibia und die gemeinsame Arbeit an unseren Dissertationen werde ich nie vergessen.

Mein Dank gilt auch dem Forschungsnetzwerk Geo.X und der Deutschen Hydrologischen Gesellschaft, welche meine Forschungsaufenthalte finanziell unterstützt haben.

Ich möchte auch allen anderen Kolleg*innen für die tolle Arbeitsatmosphäre und ihre Unterstützung danken, namentlich: Maria v. Bodecker, Dr. Kai Hartmann, Marielle Geppert, Oliver Isau, Dr. André Assmann, Dr. Tobias Ullmann, Dr. Sandro Martinis und Lorenz Beck sowie allen namibischen Partnern, allen voran: Prof. Frank Kavishe, Dr. Petrina Johannes, Prof. Damas Alfred Mashauri, Dr. Joachim Lengricht und seiner Frau Barbara Lengricht.

Abschließend möchte ich meiner Mutter Heike Kreischer, meiner Freundin Rebekka Schmid und meinen Freunden für deren moralische Unterstützung danken.

Contents

List of Figures

List of Tables

List of Symbols and Abbreviations

1D	One-dimensional
2D	Two-dimensional
3D	Three-dimensional
ADEM	Adjusted Digital Elevation Model
ALOS	Advanced Land Observing Satellite
AORE	Atlantic Ocean Region East satellite (Inmarsat)
AORW	Atlantic Ocean Region West satellite (Inmarsat)
ArcGIS	Expert Software to process geo data, developed by the company ESRI
ArcMap	Main component of ArcGIS for visualizing data
ASAR	Advances Synthetic Aperture Radar
ASMC	Antecedent Soil Moisture Conditions
BeiDou	Chinese “Běidǒu” means “big bear” – Chinese version of GPS (People’s Republic of China)
BKG	Bundesamt für Kartographie und Geodäsie (Federal Agency for Cartography and Geodesy)
CB	Cuvelai Basin
CNES	Centre national d’etudes spatiales
CQ	Coordinate Quality
DEAL	Open Access agreement for Germany between Universities and publishing companies
DEM	Digital Elevation Model
DEM-BS	Digital Elevation Model – Blue Spot
DLR	Deutsches Zentrum für Luft- und Raumfahrt (German Aerospace Center)
DOP	Dilution of Precision
DTM	Digital Terrain Model

EGNOS	European Geostationary Navigation Overlay Service
ESA	European Space Agency
ESOC	European Space Operations Centre
ET	Evapotranspiration
ETp	potential Evapotranspiration
GAGAN	GPS Aided Geo Augmented Navigation
GDOP	DOP incl. 3 position coordinates and clock offset in solution
GFZ	Deutsches GeoForschungsZentrum (German Research Centre For Geoscience)
GLONASS	Globalnaja Nawigazionnaja Sputnikowaja Sistema (Russian Federation)
GNSS	Global Navigation Satellite System
GPS	Global Positioning System (United States of America)
HSG	hydrological soil groups
HYSOGs	Global Hydrologic Soil Groups for Curve Number-Based Runoff Modeling
IDW	Inverse distance weighting (deterministic method for multivariate interpolation)
Inmarsat	British Satellite Telecommunication Company
IOR	Indian Ocean Region satellite (Inmarsat)
ITCZ	Intertropical Convergence Zone
ITRF2014	International Terrestrial Reference System (Number ‘2014’ describes the version)
JAXA	Japan Aerospace Exploration Agency
LiDAR	Light Detection and Ranging
MODIS	Moderate Resolution Imaging Spectroradiometer
MSAS	Multi-functional Satellite Augmentation System
MWE	Maximum Water Extent Mask
NRA	Namibian Roads Authority
PALSAR	Phased Array L-Band Synthetic Aperture Radar

PDOP	DOP incl. 3 position coordinates
POR	Pacific Ocean Region satellite (Inmarsat)
PPP	Precise Point Positioning
PPP-Wizard	Software for correcting PPP data
QZSS	Quasi-Zenith Satellite System
RaMaFlood	Rapid Mapping of Flooding
Rh	Hydraulic radius
RMSE	Root Mean Square Error
RTK	Real Time Kinematic data correction via base station
RTKLIB	an Open Source Program Package for GNSS Positioning
RTKPPP	Real Time Kinematic Precise Point Positioning
RTX	Real Time data correction via satellite
SA/V-rate	Surface Area to Volume ratio
SASSCAL	Southern African Science Service Centre for Climate Change and Adaptive Land Management
SBAS	Satellite Based Augmentation System
SCS-CN	Soil Conservation Service - Curve Number
SRTM	Shuttle Radar Topography Mission
TanDEM-X	TerraSAR-X-Add-on for Digital Elevation Measurements in X-Band
TerraSAR-X	Terra Synthetic Aperture Radar in X-Band
TRMM	Tropical Rainfall Measurement Mission
UAV	Unmanned Aerial Vehicle
UHF/VHF	Ultra High Frequency / Very High Frequency
USDA	United States Department of Agriculture
UTM	Universal Transverse Mercator
WAAS	Wide Area Augmentation System

Abstract

Located in the western part of the Cuvelai Basin, the Iishana system is a transboundary region covering parts of southern Angola and northern Namibia. Hydrologically, this region is characterized by a network of episodically water-bearing channels in which numerous pans are embedded. These pans, which fill up during the rainy season, form an important water resource for the rural population, especially for agricultural and domestic use.

The Iishana system is one of the most densely populated areas in southwestern Africa, and this high population trend is increasing (NamStat 2013). To date, the majority of the population (80–90%) currently lives in rural areas. However, (small) cities are experiencing steady growth.

The semi-arid climate in this area has distinct rainy and dry seasons and is characterized by high interannual variability, resulting both in intense droughts and in strong flood events. As a result, water is sometimes a scarce resource in this region. The strong population growth and the temperature increase predicted as a result of global climate change will put further pressure on available water resources. However, as this region is also subject to volatile rainfall dynamics, in addition to droughts, the Iishana system also experiences repeated, severe flood events. Most recently, flood events occurred in 2008 to 2011, 2013, and 2017, resulting in the loss of life, the loss of crop yields and consequent loss of livelihood for many people, and the destruction of key infrastructure elements.

To date, there has been no complex 2D-hydrodynamic model for the Iishana system and no transferable modeling approach to identify potential locations for water storage and facilitate the planning and development of flood retention measures.

In this study, various methods have been developed and applied to address these issues. This has allowed for the validation of existing findings as well as the discovery of new insights, which are briefly summarized below.

First, an investigation was performed to test the influence of topography on hydrology, with a special emphasis on infrastructure elements. The focus here was on improving the raw DEM

for subsequent calculations. For this purpose, filter corrections were performed on the TanDEM-X raw data, and road dams, culverts, and bridges were recorded by means of kinematic surveys.

As a result, the definition of the flow paths was improved. It became clear that northern roads, especially those running from east to west, have a strong influence on the runoff behavior in the study area due to their height and their orientation orthogonal to the water flow of the Iishana.

Based on the corrected DEM and the application of a modified Blue Spot Analysis, further new findings emerged. Approximately 190,000 pans with a total storage volume of about 1.9 km³ and a total area of 4,021 km² were identified. The part of the study area located in Angola accounts for two thirds of the potential storage volume while only one third of the storage volume is in Namibia. Furthermore, about one third of all pans are located in the episodically water-bearing channels.

Based on previous results in other regions, a calculation of the surface-volume relationship (SA/V rate) was performed for the first time for the Iishana system. This enabled the identification of about 2,000 pans that are primarily suitable for an expansion of storage volume.

Using continuous and spatio-temporally varying TRMM precipitation data, a 2D-hydrodynamic modeling and reconstruction of the 2008/2009 flood event was performed using the FloodArea model.

Although the results represent a snapshot, they nevertheless contribute to an improved understanding of the interconnected runoff system and highlight potential flood hazards. Depending on the weighting of evapotranspiration in the calculation of the model, the potential storage volume can be quantified between 0.116 km³ and 0.547 km³. The total inundation area was calculated at 1.860 km². In addition, three main runoff paths were identified, of which the central and the eastern runoff paths pose a particular threat to the regional capital of Oshakati.

Furthermore, with the help of the model, for the first time it was possible to identify areas where, after the end of the rainy season, water availability is naturally shortest (Namibia) or longest (Angola).

Based on these numerous, new results, scenario calculations for neighboring catchments as well as calculations for other precipitation periods can be performed in the future. Thus, the duration of water availability after the end of a rainy season can be determined and possible locations for retention measures can be identified for various locations.

Zusammenfassung

Das Iishana System liegt im Grenzgebiet zwischen Süd-Angola und Nord-Namibia und bildet den westlichen Teil des Cuvelai-Etosha Beckens. Hydrologisch ist die Region durch ein Netzwerk episodisch wasserführender Gerinne geprägt, in das zahlreiche abflusslose geschlossene Hohlformen (Senken) eingebettet sind.

Die während der Regenzeit aufgefüllten Senken bilden eine wichtige Wasserressource für die Bevölkerung in den ländlichen Gebieten, insbesondere für die landwirtschaftliche Nutzung und als häusliches Brauchwasser. Die Region gehört zu den am dichtesten besiedelten Räumen im südwestlichen Afrika – Tendenz steigend (NamStat 2013). Hiervon lebt derzeit der Großteil der Bevölkerung (80-90 %) im ländlichen Raum. Die (Klein)-Städte verzeichnen jedoch einen stetigen Zuwachs.

Das semiaride Klima mit ausgeprägten Regen- und Trockenzeiten ist durch eine hohe interannuelle Variabilität mit intensiven Dürreperioden aber auch starken Hochwasserereignissen gekennzeichnet. Dies führt dazu, dass Wasser zuweilen eine knappe Ressource in diesem Raum darstellt. Das starke Bevölkerungswachstum und die im Zuge des globalen Klimawandels vorhergesagte Temperaturerhöhung steigern den Druck auf die Ressource Wasser zusätzlich. Im Zusammenhang der volatilen Niederschlagsdynamik kommt es jedoch neben den Dürreperioden auch immer wieder zu starken Hochwasserereignissen, wie zuletzt in den Jahren 2008 bis 2011, 2013 und 2017. Damit verbunden ist der Verlust von Menschenleben, der Ausfall von Ernteerträgen und der damit einhergehende Wegfall der Lebensgrundlage für viele Menschen sowie die Zerstörung wichtiger Infrastruktureinrichtungen.

Bislang mangelte es an einer komplexen 2D-hydrodynamischen Modellierung des Iishana Systems sowie an einem übertragbaren Modellansatz zur Ableitung von potenziellen Standorten für Wasserspeicher und Hochwasserrückhaltemaßnahmen.

Zur Lösung der beschriebenen Problematiken wurden verschiedene Methoden entwickelt und angewandt. Dadurch konnten sowohl bestehende Erkenntnisse validiert als auch neue Erkenntnisse gewonnen werden, welche nachfolgend kurz zusammengefasst sind:

In einem ersten Schritt wurde der Einfluss der Topographie auf die Hydrologie unter besonderer Berücksichtigung von Infrastrukturelementen untersucht. Der Schwerpunkt lag hierbei auf der Verbesserung des Basis-DGM für nachfolgende Berechnungen. Dazu wurden Filterkorrekturen an den TanDEM-X Basisdaten durchgeführt und mittels kinematischer Vermessungen Straßendämme, -durchlässe und Brücken erfasst.
Im Ergebnis konnte die Definition der Fließwege verbessert werden. Es wurde deutlich, dass besonders die nördlichen, von Ost nach West verlaufenden Straßen, auf Grund ihrer Höhe und ihrer Ausrichtung orthogonal zur Fließrichtung der Iishana einen starken Einfluss auf das Abflussgeschehen im Untersuchungsgebiet haben.

Auf Grundlage des korrigierten DGM und der darauf aufbauenden Anwendung einer modifizierten Blue Spot Analyse ergaben sich weitere neue Erkenntnisse.
Es konnten ca. 190.000 abflusslose Senken mit einem Gesamtspeichervolumen von ca. 1,9 km³ und einer Gesamtfläche von 4.021 km² identifiziert werden. Dabei entfällt 2/3 des potenziellen Speichervolumens auf den angolanischen Teil des Untersuchungsgebietes und nur 1/3 auf den namibischen Teil. Weiterhin wurde sichtbar, dass ca. ein Drittel aller abflussloser Senken in den episodisch wasserführenden Gerinnen liegen.

Auf vorangegangenen Analyseergebnissen aufbauend erfolgte für das Untersuchungsgebiet eine erstmalige Berechnung der Oberflächen-Volumenbeziehung (SA/V-Rate). Damit war es möglich, ca. 2.000 Senken zu bestimmen, welche sich primär für eine Erweiterung des Speicherpotenzials eignen.

Mittels kontinuierlicher sowie räumlich und zeitlich variierender TRMM Niederschlagsdaten, wurde abschließend mit dem Modell FloodArea eine 2D-hydrodynamische Modellierung und Rekonstruktion des Hochwasserereignisses 2008/2009 durchgeführt.

Wenngleich die Ergebnisse eine Momentaufnahme darstellen, leisten sie dennoch einen Beitrag zum verbesserten Verständnis über das interkonnektive Abflusssystem und ermöglichen es, die Hochwassergefahren aufzuzeigen. Je nach Gewichtung der Evapotranspiration im Modell konnte das potenzielle Speichervolumen im Modellausschnitt auf 0,116 km³ bis 0,547 km³ quantifiziert werden. Die Bestimmung der Überschwemmungsfläche ergab ein Areal von 1.860 km². Zudem ließen sich insgesamt drei Hauptabflussbahnen identifizieren, wovon die zentrale und die östliche Abflussbahn eine besondere Gefahr für die Regionalhauptstadt Oshakati darstellen. Des Weiteren ist es mit Hilfe der Modellergebnisse erstmals möglich, Gebiete zu identifizieren, in denen die Wasserverfügbarkeit nach Ende der Regenzeit auf natürliche Weise am kürzesten (Namibia) bzw. am längsten (Angola) gewährleistet ist.

Auf Basis der zahlreichen neuen Ergebnisse lassen sich zukünftig sowohl Szenarienberechnungen für benachbarte Einzugsgebiete als auch Berechnungen für andere Niederschlagsperioden durchführen. Die Dauer der Wasserverfügbarkeit nach dem Ende einer beliebig gewählten Regenzeit kann hiermit bestimmt und dafür mögliche Standorte im Gelände geschaffen werden.

1 Introduction

Climate change and a constantly rising global population and economy are leading to more and more pressure on the world's water resources. At the same time, the frequency of droughts and flood events is increasing. All of this is simultaneously impacting highly condensed habitats and leading to crop failures and associated starvation as well as damage to critical infrastructure. These consequences are particularly difficult for economically vulnerable countries.

At the present, the transboundary region of northern Namibia and southern Angola is one of the fastest growing regions in southwestern Africa. Both the rural population and the growing urban centers are heavily impacted by seasonal droughts and floods. This necessitates the adaption and optimization of current water resource management in this region.

1.1. Definition of terms

The investigations for this thesis focused on the Namibian section of the study area. The reason for this was, and still is, the easier access to study sites, resulting in the greater feasibility of conducting research and collecting data. The security of the researchers also played a role in limiting the research focus to this section of the study area. However, throughout the study, attempts were always made to consider the entire study area of the Iishana system in a holistic manner.

In the literature, there are currently two parallel interpretations of the term ‘Iishana system’. Faulstich et al. (2018) describe it as numerous and partially isolated pans (singular Oshana) scattered across northern Namibia and southern Angola.

However, other authors, such as Cunningham et al. (1992), refer to the Iishana system as a network of episodically discharging channels, thus defining individual parts or strands of the network as Oshana, to which pans are related.

This paper will rely on the latter definition, in which the Iishana system is inevitably associated with the numerous pans.

At the beginning of this study, the term 'Iishana system' was often used synonymously with the term 'Iishana region'. However, an Iishana region does not conceptually exist. Rather, the Iishana system is located within distinct regions in south-central Angola and north-central Namibia. The system covers the region of Cunene, a federal state in Angola, and the regions of Omusati, Oshana, Ohangwena and Oshikoto, all federal states in Namibia.

The regional capital of the four Namibian states is the city of Oshakati. In Angola, the regional capital of Cunene is the city of Ondjiva.

Thus, when the Iishana region is mentioned, it refers to the Iishana system in the Angolan and Namibian regions as specified above.

1.2. Motivation

The transboundary Iishana system in the western Cuvelai Basin is characterized by severe and recurrent drought and flood events (Figs. 1-1 & 1-2). From a scientific standpoint, both natural events have long been studied, however, past research has always addressed them separately.

To better explore the Iishana system's potential as a water resource, and the risks it poses as a flooding hazard, this thesis considers drought and flood events together and studies their effect on the sources of water in the area. The current local water supply in the region can be categorized into three main sources:

1. Water supply via the Kunene River in southwestern Angola and northwestern Namibia. Water is impounded on the Angolan side of the Iishana system and conveyed to the regional capital of Oshakati via the Calueque-Oshakati Canal, which runs past the Namibian town of Ruacana and is an open canal about 155 km long. Between Ruacana and Oshakati there are four water treatment plants associated with the canal. The

amount of water that can be delivered through the canal depends heavily on the surface runoff generated in the northern part of the Iishana system (Klintenberg et al. 2007). Therefore, during more intense droughts, water shortages can still occur, which in turn can lead to conflicts in water distribution. Beyond this, many residents are not able to pay for treated water due to their low income. As a result, they can only resort to untreated water (groundwater or surface water).

2. Groundwater from perched aquifers. Unlike classic aquifers, perched aquifers are predominantly groundwater lenses (with low-depth water tables), which are superimposed on the actual deep aquifers.

   Water is extracted from these perched aquifers via hand-dug and open wells. Therefore, these wells are often more heavily contaminated by pollutants such as animal feces. Another disadvantage of this water resource is its high degree of mineralization and turbidity. Despite these conditions, perched aquifers still represent an important water resource due to the widespread scarcity of water in the region (Himmelsbach et al. 2018, Hamutoko et al. 2017, Wanke et al. 2014, Kluge et al. 2008).

3. Surface water stored in the Iishana and natural pans. During a pronounced rainy season, surface runoff accumulates in the net-like, episodically flowing Iishana. During this time, water availability in the region is exceptionally good. But towards the end of the rainy season, and as evapotranspiration increases, water quality deteriorates (Faulstich et al. 2018). Over time, as evapotranspiration persists and water continues to run off toward Lake Oponono (located south of Oshakati), water availability in the Iishana system declines rapidly. Finally, the only remaining water can be found in the pans. Throughout this process, the water quality also continues to deteriorate.

   Despite its low quality, this water is still very important, especially for the rural community, because it often represents the last easily accessible water resource. Thus, the local people are regularly forced to use this water to supply their households, to

irrigate their fields, and to water their livestock (Kluge et al. 2008, Klintenberg et al. 2007).

These three water resources are the primary methods for people to access water in the Iishana system. The Calueque-Oshakati Canal running from Angola to Namibia largely ensures the water supply for residents of Oshakati as well as for people settling along the canal.

In addition, there are some subsistence residents who have access to water via hand-dug wells. This option is viable only for those living close to a usable perched aquifer. The remainder of the population relies entirely on the water of the Iishana or the water that remains in the pans after the rainy season.

Despite the essential nature of the water in these Iishana and pans, this particular resource has not yet been adequately investigated through scientific models. As a result, the Iishana system has great unrecognized potential in terms of flood retention and increasing resilience against future drought events.

Figure 1-1: Flooded agricultural landscape with water-filled pans in north-central Namibia, April 2021.

Figure 1-2: Flooded suburban area north-east of Oshakati, located near an Oshana, April 2021.

1.3. Research questions and aims

This dissertation utilizes data from a study begun in 2017 on water resource management in the western Cuvelai Basin located in northern Namibia and southern Angola. The study focused on the overarching topics of water quantity and quality in the Iishana system. This region, and its unique water system, is the focus of much scientific work as it represents an intersection between volatile water availability and quality, and its use for subsistence by humans, livestock, and agriculture.

The aim of this work is to better understand the complex flow processes and interconnectivity of ephemeral and endorheic river channels in the Iishana system in order to determine the system's water retention potential and the availability of water in natural and artificial pans. Furthermore, this work also aims to contribute to a future flood risk management plan, e.g. by identifying locations for potential retention measures and areas of risk.

This study will answer the following research questions:

1. What impact does the technical infrastructure have on the runoff system in the study area?

2. What quantitative and qualitative characteristics can be attributed to artificial and natural pans, and what contribution can the pans provide in the context of optimized water resource management?

    a) What information can be obtained about the number, location, distribution patterns, and connectivity of pans?

    b) What metrics (area, volume, and depth) can be attributed to these pans?

    c) Based on the information obtained previously, can individual pans be identified for development as temporary storage within an integrated water resource management framework?

3. How can the runoff processes of the Iishana system be described and how much water remains in the system immediately after the end of a rainy season?

To answer these questions, different methods were applied and combined. To start, the underlying elevation model (DEM), the TanDEM-X model, was rectified with the help of different filter algorithms to enable a topographic calculation of the flow paths. The next step was the implementation of the technical infrastructure elements (road dams, culverts and bridges) and the investigation of their influence on the flow paths and directions.

With the help of the adapted DEM and a modified Blue Spot Analysis, it was possible to identify natural pans for the entire Iishana system. The metrics of these pans could then be determined, leading to initial findings on their retention potential. By calculating the surface area volume rate (SA/V), potential sites for retention measures could be localized.

Finally, 2D-hydrodynamic modeling (FloodArea) was used to visualize runoff processes in a spatially and temporally differentiated manner. For this purpose, the flood event of 2008/2009 was selected for modeling because of the high volume of available data relating to this event. The model focused heavily on the flow processes made evident by the flood event. Thus, spatially and temporally variable knowledge could be gained on parameters such as flow velocities, flood depths and the total amount of water left in the system after the rainy season.

By the end of this work, the existing knowledge gaps about this particular Iishana drainage system will be filled and contribution to water resource management will have been given.

1.4. Structure of this dissertation

Chapters 2 to 4 represent several publications that describe in detail the research objectives and results of this thesis (Tab. 1-1). All of the publications listed were conceptualized, edited, and written by the thesis author, as evidenced by the first authorship listing. The co-authors, however, were also involved in general research for the project and contributed by creating appropriate frameworks, carefully revising the manuscripts, and, at times, helpfully initiating changes in perspective. All of these scientific articles have been peer-reviewed and are ranked internationally. In addition, all articles were originally submitted and published in English.

Table 1-1: Chapters in this dissertation, their related publications or manuscripts, and their publication status.

Chapter	Publication	Status
2	Arendt R, Faulstich L, Jüpner R, Assmann A, Lengricht J, Kavishe F, Schulte A (2020): GNSS mobile road dam surveying for TanDEM-X correction to improve the data base for floodwater modeling in northern Namibia. *Environmental Earth Science 79:333.* https://doi.org/10.1007/s12665-020-09057-5	Published in: June, 2020 Environmental Earth Science
3	Arendt R, Reinhardt-Imjela C, Schulte A, Faulstich L, Ullmann T, Beck L, Martinis S, Johannes P, Lengricht J (2021): Natural Pans as an important Surface Water Resource in the Cuvelai Basin – Metrics for Storage Volume Calculations and Identification of Potential Augmentation Sites. *Water 13:177.* https://doi.org/10.3390/w13020177	Published in: January, 2021 Water
4	Arendt R, Reinhardt-Imjela C, Faulstich L, Schulte A, Assmann A, Jüpner R, Johannes P T, Mashauri D A (in review): Hydrodynamic modeling of ephemeral flow in the Iishana channel system of the Cuvelai Basin – North Namibia. *River Research and Application*	Submitted in: April, 2022 River Research and Application

2 GNSS mobile road dam surveying for TanDEM-X correction to improve the database for floodwater modeling in northern Namibia

Link to online publication: https://doi.org/10.1007/s12665-020-09057-5

Abstract

The aim of this study is the improvement of the TanDEM-X elevation model for future floodwater modeling by implementing surveyed road dams and the use of filter algorithms. Modern satellite systems like TanDEM-X deliver high-resolution images with a high vertical and horizontal accuracy. Nevertheless, regarding special usage they sometimes reach their limits in documenting important features that are smaller than the grid size. Especially in the context of 2D-hydrodynamic flood modelling, the features that influence the runoff processes, e.g. road dams and culverts, have to be included for precise calculations. To fulfil the objective, the main road dams were surveyed, especially those that are blocking the flood water flowing from south Angola to the Etosha Pan in northern Namibia. First, a Leica GS 16 Sensor was installed on the roof of a car recording position data in real time while driving on the road dams in the Cuvelai Basin. In total, 532 km of road dams have been investigated during 4 days while driving at a top speed of 80 km/h. Due to the long driving distances, the daily regular adjustment of the base station would have been necessary but logistically not possible. Moreover, the lack of reference stations made a RTK and Network-RTK solution likewise impossible. For that reasons, the Leica *SmartLink* function was used. This method is not dependent on classic reference stations next to the GNSS sensor but instead works with geostationary satellites sending correction data in real time. The surveyed road dam elevation data have a vertical accuracy of 4.3 cm up to 10 cm. These precise measurements contribute to rectifying the TanDEM-X elevation data and thus improve the surface runoff network for the future floodwater model and should enhance the floodwater prediction for the Cuvelai Basin.

2.1. Introduction

This study is part of a broader research project in northern Namibia concerning the topics of floods and droughts and their effects on water quality in the Iishana region (Fig. 2-1). Regarding floods, ongoing investigations are made to understand the hydrological system characterized by ephemeral Iishana. These net-like distributed pans may fill with water during the rainy season and inundate leading to large floods that negatively affect the Iishana region and its inhabitants. Consequences include the loss of lives and high economic losses. Up to now, a synoptic flood forecast system is only available for the entire African continent, produced by the National Oceanic and Atmospheric Administration and its Climate Prediction Center. Detailed flood routing and prediction systems are neither available at a regional level, nor for the study area. Nevertheless, efforts have been made to prevent susceptible areas

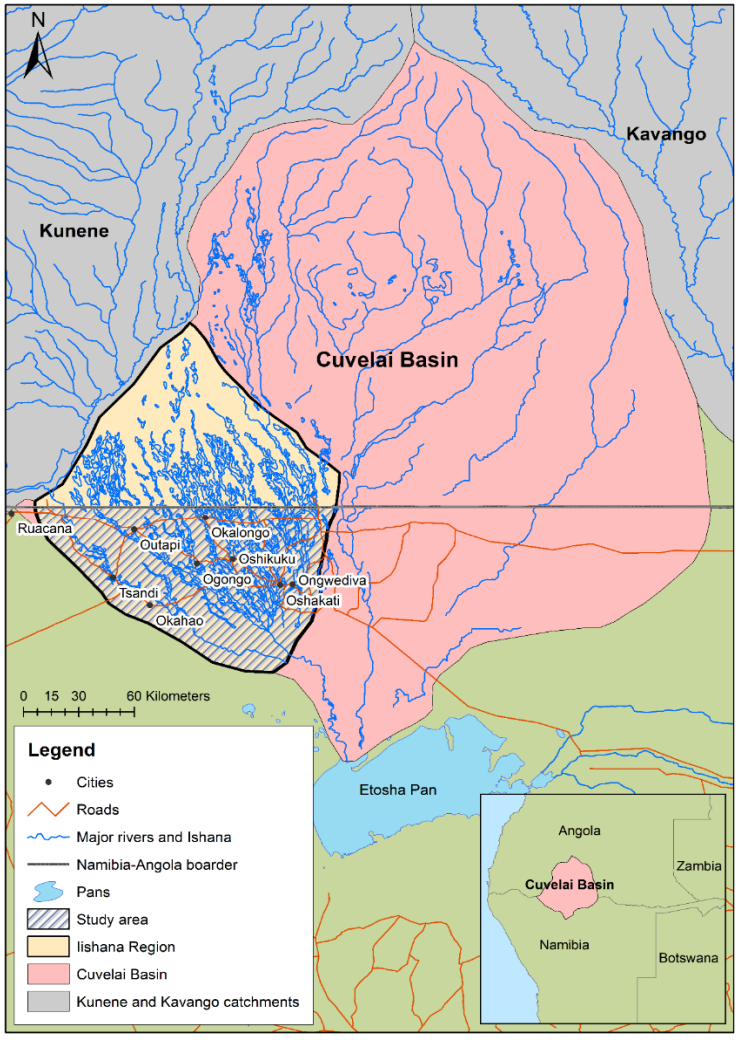

Figure 2-1: Overview of the Cuvelai Basin and the study area of the Iishana region (source: Faulstich et al. (2018), database: UN-OCHAROSA (2018) and Digital Atlas of Namibia (2016), edited by Robert Arendt).

from floods: for example, the Namibian Early Flood Warning System, which was a sensor web-based pilot project starting in 2008.

However, due to the large costs the project was not founded until the end (Mandl et al. 2012) and no longer exists. Further work has been done by Skakun et al. (2012), who extracted the maximum flood extents from satellite images for flood risk assessment. In addition, Awadallah & Tabet (2015) estimated flood extents via remote sensing data. Goormans et al. (2015) set up the first hydrological and hydrodynamic model for the Iishana region. They focused on the city region of Oshakati and modeled the effect of a dyke, which was planned by the Ministry of Regional and Local Government, Housing and Rural Development - Oshakati Town Council in 2012 (Bethune et al. 2012) and was in some parts realized. Nevertheless, it still does not cover the whole Iishana region. For this reason, the aim is to develop a 2D-hydrodynamic flood model covering the whole Iishana area (Fig. 2-1). The objective is to provide flood risk maps as well as routable flood paths. Finally, retaining-measures will be suggested and the flood model will contribute to an early warning system in the context of a broader flood risk management plan. Therefore, the model requires many input parameters like data on land use, hydrology, topography and others.

This paper focuses on the topography in the study area and discusses the digital elevation model and its improvement in accuracy for flood model calculations in a further step by correcting TanDEM-X elevation data via GNSS data. Therefore, this study is less about the detailed approach of GNSS physics itself and more about the application and combination of GNSS techniques for enhancing database for further flood modeling.

Today's modern satellites provide high-resolution images and have a high vertical and horizontal accuracy. For example, the TanDEM-X mission which delivers a digital elevation model for the whole planet with a horizontal accuracy of around 12 m and in vertical up to 2 m at least (Rizzoli et al. 2017). From the hydrological point of view, this is a great improvement to former resolutions like 20 m horizontal and 16 m to 10 m vertical accuracies of the Shuttle Radar Topography Mission (Mukul et al. 2017; Smith 2003). These advancements are important for experts modelling in the field of floods, creating more exact

flood risk maps and improving the results of flood models. It becomes clear that accuracy is a factor of certainty, even more so if model results are later used for flood forecasts. To enhance the vertical accuracy of the entire DEM, different filter algorithms have been used. Moreover, water surface interferences have been corrected by masking out (Wendleder et al. 2013) and using interpolation procedures. With these methods, natural and anthropogenic hydrological obstacles, like parts of vegetation and water-induced interferences or buildings, could be equalized.

Anthropogenic obstacles, in this specific case road dams (Fig. 2-2), have been surveyed in real time by a GNSS sensor. These road dams play a significant role in the Iishana region, which is characterized by a very low relief where almost every small sink or elevation influences the flow dynamic. Using the GNSS sensor to localize specific points precisely on the ground has been a common method used in industry and science for years (Knoop et al. 2017; Arroyo-Suarez et al. 2005; Gao et al. 2005; Bisnath et al. 2003). If using a differential system an accuracy in a millimeter range is readily achieved. However, differential GNS-systems always need a base station in a certain range, otherwise the accuracy decreases dramatically up to a loss of connection. For example, the Leica GS16 System works properly up to 1 km in differential mode.

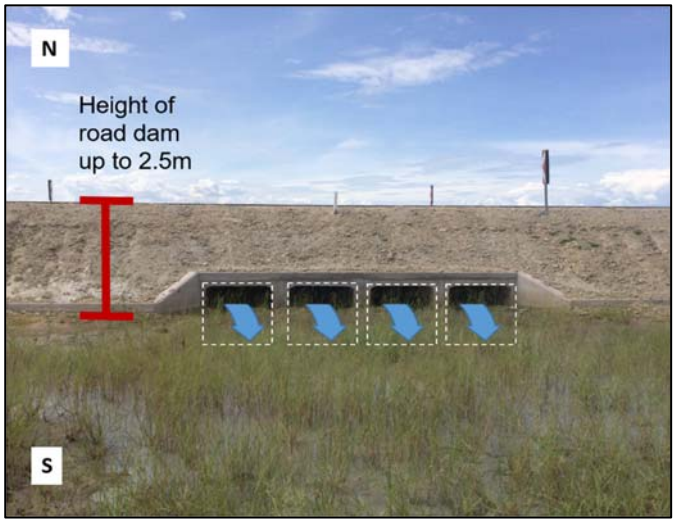

Figure 2-2: High road dam crossing an Oshana in transverse direction. Water flows from north to south through the culverts. The culverts (white dotted boxes) are heavily sedimented. (Photo & editing: Robert Arendt 2018).

If this is not wide enough for a certain use, it is possible to use the common Real-Time Kinematic (RTK) or Network-RTK mode, like other GNS-Systems. Both RTK solutions receive their correction data either from a single or even from a network of reference stations a few kilometers nearby. These systems use UHF/VHF radio signals or mobile phone networks to send their correction data to the GNSS sensor. This technique is very well known in vehicle navigation and in cases of precision farming (Knoop et al. 2017; Shrivathsa & Panjwani 2017; Gebbers and Adamchuk 2010; Skog and Handel 2009; Dixon 2006). The accuracy of (Network-) RTK generated GNSS data differs in a sub-centimeter range. In terms of precision farming, the vehicles are driving slowly with a maximum speed of 11 km/h. Even here, their work range is limited by the availability of reference stations and their application is expensive (Perez-Ruiz & Upadhyaya 2012). Moreover, potential connection losses lead to reduced accuracy up to a meter range.

To become more independent, the Satellite Based Augmentation System (SBAS) was formerly invented for the offshore industry in the early 1990s (Barboux 2000). Offshore platforms need to be constructed precisely, although they are usually located far away from the coast. In these remote areas, no reference stations are available. This method nowadays is called Real-Time Precise Point Positioning. In this case, the GNSS system receives the correction data directly from a geostationary satellite, which makes it applicable all around the world (Perez-Ruiz & Upadhyaya 2012; Skog and Handel 2009).

In this study, a Leica GS16 Sensor was installed on the roof of a car. While driving along the road dams with a maximum speed of 80 km/h, elevation surveys were automatically corrected in real time via the commercial Leica SmartLink function within a centimeter of accuracy. After the days of recording, the data were corrected by eliminating outliers and redundant measurements. In a next step, the elevation data were implemented into the post processed TanDEM-dataset for further hydrodynamic calculations.

2.2. Materials and methods

2.2.1. Study area

Namibia's climate is strongly influenced by the cold Benguela current along the west coast of South Africa leading to arid and semi-arid conditions. Determined by the Intertropical Convergence Zone (ITCZ), rainy season runs from October to April and dry season from May to September.

A hydrologically diverse region therein is the transboundary Cuvelai Basin, which itself is bounded to the north by the Kunene River and Okavango River in Angola and by the Etosha Pan on the south in Namibia. The western edge is defined by the city of Ruacana and the eastern edge lies between the cities of Okongo and Mpungu Vlei.

The Cuvelai Basin is divided into eight major drainage zones (Mendelsohn et al. 2013).

In this case, the study area is part of the Iishana region, consisting of the Western Oshana Zone and the Central Oshana Zone (Cunningham et al. 1992). Reduced to the Namibian state territory, it is marked to the north by the Namibian-Angolan boarder. The western edge is marked by the city of Ruacana and in the east by the city of Oshakati (Faulstich et al. 2018) (Fig. 2-1). The annual amount of precipitation is between 350 up to 550 mm increasing from west to east and is characterized by high rainfall variability. The potential evaporation rises in the same direction from 2,600 to 3,200 mm (Persendt et al. 2015; Mendelsohn et al. 2013). The terrain is about 1,100–1,200 m a.s.l. and has a very flat slope ranging from 0.5 to 1.0 m/km (Mendelsohn et al. 2013). The surface hydrology is featured by a large ephemeral river system and is affected by irregular floods during rainy seasons (Kundzewicz et al. 2014; Shifidi 2014; Skakun et al. 2012; Kuliwoye 2010). These low slope, net-like troughs and sinks run in a northwesterly to southeasterly direction. The water depth during floods is about 1–7 m. Namibia gains most of its rainfall in the study area. The soils are profitable for agricultural use. These circumstances lead to the fact that around 40% of Namibia's population lives in the northern region (Mendelsohn et al. 2013). Nevertheless,

next to near-surface Aeolian and fluvial sediments of clay deposits, lime and silicate crusts, produce low infiltration capacities and high surface runoff (Goudie & Viles 2015; Nguno & Angombe 2011; Hüser et al. 2001).

These facts result in widespread flooding during rainy season. While most of the surface water comes from the Angolan side of the Iishana region, floods are intensified by local convective rain events. Fatal floods in the recent past have occurred in 2008, 2009, 2010, 2011 and 2013. The large inundations affected human lives, caused huge damage to health, extensive damage to property and technical infrastructures like roads, bridges and dams (Awadallah & Tabet 2015; Bischofberger et al. 2015; Persendt et al. 2015; Filali-Meknassi et al. 2014; Mufeti et al. 2013; Mandl et al. 2012; Skakun et al. 2012).

2.2.2. The hydrodynamic model

In this particular study, the specific flood prediction problem is a combination of multiple factors. The large catchment of about 10,000 km² and the TanDEM-X raster resolution of 12.5 m needs a model that is able to handle the amount of data in an adequate time. Moreover, the model needs the ability to incorporate culverts and bridges. Furthermore, the relief is very flat (slope ranging from 0.5 to 1.0 m/km), the flow speeds of floods is low (Cunningham et al. 1992) and even low obstacles can substantially change the flow behavior instantly. Nonetheless, at the same time, these areas affected by floods should be recorded as precisely as possible. Therefore, the hydrodynamic model ‘FloodArea’ will be used in a future step to calculate the runoff, flow concentration, flow velocity, backwater situations and inundation depth for variable time steps. ‘FloodArea’ is based on a simplified hydraulic approach including hydrodynamic calculations for the simulation of large areas with high spatial resolution (< 1 m) (Fritsch et al. 2016). Successful applications have been made in large-scale simulations of catchments sized up to 3,000 km² in Germany (Assmann et al. 2013). As mentioned above, the hydrodynamic calculation itself will not be discussed in this

work. Further literature regarding ‘FloodArea’ is reported in Anders et al. (2016), Fritsch et al. (2016) and Assmann et al. (2013).

2.2.3. Road dams and culverts

According to the cited TanDEM-X accuracy, small objects like road dams are not displayed. These road dams are elongated artificial fillings of earth material or rock on which a road runs. A road dam is designed to elevate and thus overcome geomorphological and topographical obstacles and thus has a landscape-shaping effect. It must not be compared to flood protection dams, because its construction is altogether simpler and not suitable as a flood protection measure. The road embankment has no overflows or other auxiliary structures, with the exception of culverts. Its structure is not designed for the lateral pressure of large water masses and additionally hinders natural flow processes and drainage channels.

Most of the roads in the study area are almost orthogonally affected by the Iishana system (Fig. 2-3), and the major cities are connected by the shortest route and lowest construction costs. During most of the year (normal rainy season and dry season), this infrastructure is not negatively affected by water. In the case of an “Efundja”, a local name for a major flood, they become vulnerable to overspilling and erosion (Mendelsohn et al. 2013).

On one hand, these road dams change the flow directions and hinder flow processes, which have to be taken into account by the hydrodynamic model. There is a water buildup and settlement structures in this area are more affected by the floods. Of course, during this time, these important infrastructure facilities cannot be used. As an example for the benefit of measuring and implementing these road dams into the DEM, the divergence in elevation between the Tan-DEM-X raw data and the GNSS measured values shows differences ranging from 0.125 up to 1.955 m (section 2.3.2.).

On the other hand, culverts and bridges have to be included and incorporated into the model. The consideration of small structures like low walls or road dams is crucial to analyze flow

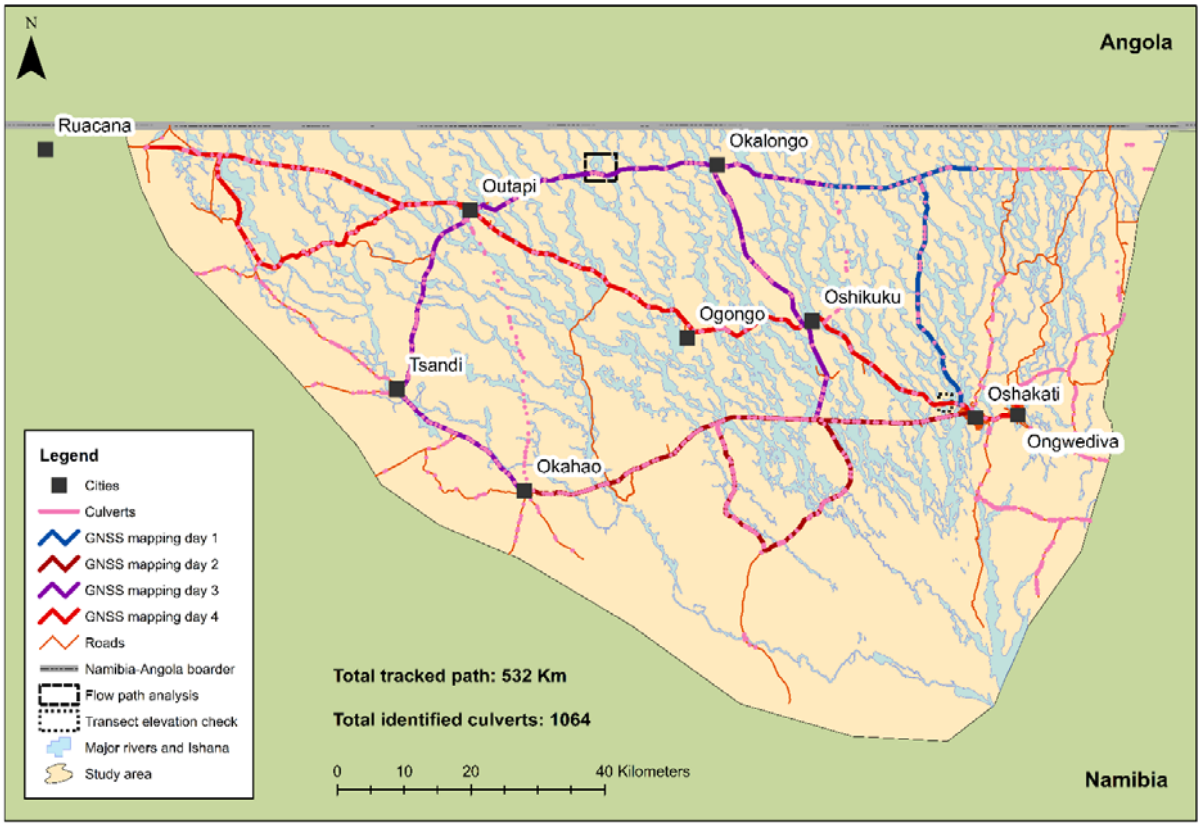

Figure 2-3: Map including the surveyed road dams and culverts, source: Faulstich et al. (2018), database: UN-OCHAROSA (2018) and Digital Atlas of Namibia (2016), edited & mapping by Robert Arendt.

paths and assess the influence of flow velocity (Fritsch et al. 2016). Therefore, over 1,000 culverts and bridges were mapped via Google Earth satellite images and have been cross-validated during the field trip via a hand hold Garmin e-Trex GPS (Fig. 2-3).

A high-resolution DEM including significant obstacles is essential for the accuracy in modeling surface runoff. An accurate DEM increases the predictive capacity of the flood model in terms of a better identification of main flow paths and local sinks, the locations of high flow depths and accelerated flow velocities (Fritsch et al. 2016). The exact magnitude of the advantage cannot yet be described until the model has been run, but can be assumed as enhanced as the flow path analysis shows in the results (section 2.3.3.). This analysis was done three times with different pre-settings. The fist flow path calculation considered the TanDEM-X raw data set by using just the 'Fill' function in advance. Otherwise, there would be no flow path calculation possible. The second calculation also used the filter algorithms (section 2.2.7.). The third calculation included more than 1,000 culverts and

bridges (Fig. 2-3). The flow path calculations were done according to the work of Persendt & Gomez (2016) and used the D8-algorithm as a simple approach for a validation process.

2.2.4. GNSS and real-time kinematic precise point positioning

The surveying of positions with the Global Navigation Satellite System (GNSS) is a common method for personal navigation and is ubiquitous. It is omnipresent, whether while driving with cars or for navigation during outdoor activities, in science and industrial sectors, or for surveying and lane detection (Knoop et al. 2017). Currently, few GNS Systems are available. The most prominent and first developed GNS System is the American Global Positioning System (GPS) that emerged in the 1990s (Zumberge et al. 1997). At the same time, many different positioning systems are available. The European Space Agency (ESA) developed the Galileo Program. There is the Chinese system BeiDou and the Russian system GLONASS, which have been working parallel to GPS for many years (Liu et al. 2017; Li et al. 2015; Skog & Handel 2009). GNSS positioning is the most basic technique and founded on the measurement of pseudo-range (Shrivathsa & Paniwani 2017).

Main disturbances in positioning appear in the ionosphere and the troposphere. Therefore, different methods exist to decrease these errors. One strategies is the use of an a-priori model to estimate the residual effects from measurements (Shrivathsa & Paniwani 2017). In case of ionospheric delays, only around half of it can be deleted and errors of several meters can still occur. Another strategy to improve the accuracy is to measure the delay by collecting data with a dual-frequency receiver. These devices are more expensive (Shrivathsa & Paniwani 2017; Skog & Handel 2009).

Higher accuracies can be reached by Relative Positioning with the integration of proximate static reference stations, e.g. with Network-RTK stations. With these techniques, common mode errors for GNSS receivers in a terminated area are estimated by a nearby stationary reference station that transmits the corrected information to the rover typically via UHF radio signals (Xu 2012). The common mode error increases with distance between the rover and

the base station (Skog & Handel 2009). In differential mode, a pseudo-range measurement can reach accuracies within a centimeter up to millimeter dimension (Shrivathsa & Paniwani 2017). Combining the pseudo-range measurements and carrier-phase measurements improves the accuracy even more by providing unknown carrier phase cycle ambiguities and fix them to their integer value (Knoop et al. 2017; Teunissen & Khodabandeh 2014; Ge et al. 2008). Negative aspects of differential or relative GNSS positioning are the large and costly data transfer and the need of a dense local network of reference stations in a (Network-) RTK mode (Knoop et al. 2017; Shrivathsa & Paniwani 2017).

During the last 20 years, precise point positioning (PPP) achieved powerful advancements, which significantly led to increasing accuracy. It developed from former single-frequency constellation (just GPS) to multiple GNSS constellations like GPS, GLONASS, BeiDou and Galileo (He 2015; Li et al. 2015; Cai & Gao 2007). It further enhanced from single over dual up to triple frequencies and from ambiguity-float to ambiguity-fixed solutions (Liu et al. 2018). Moreover, as a key for base station-independent work, it evolved from post-processing to real-time processing (Dixon 2006), usable in a static or even in a kinematic mode, via a globally distributed network of reference stations and geostationary satellites (Liu et al. 2018; Bisnath & Gao 2009; Kaplan & Hegarty 2005). Thus, PPP developed into a method able to measure precise point positions in a kinematic mode and correcting in real-time - real-time kinematic precise point positioning (RTKPPP) (Bisnath & Gao 2009). The main applications for RTKPPP are in the field of precision farming (Perez-Ruiz & Upadhyaya 2012; Dixon 2006) and marine constructions (Arroyo-Suarez et al. 2005). PPP almost works like a Differential GNSS but instead of calculating the position relatively to a nearby ground or base station, it uses correction data send via a geostationary satellite. This technique provides accurate position data almost all over the globe in a decimeter, up to centimeter quality (Liu et al. 2018; Knoop et al. 2017; Shrivathsa & Panjwani 2017; Bisnath & Gao 2009; Kaplan & Hegarty 2005; Hatch et al. 2003). In a PPP system, the receiver uses the clock and orbit information of the satellite itself, and also the correction data from a relatively sparse global tracking network on the ground (Li et al. 2015). This stationary network calculates the

correction for all visible satellites and the ensemble of this correction data is formatted into a binary message. This message is then sent to the Hub where it is uplinked to the geostationary satellite (Liu et al. 2018; Knoop et al. 2017; Shrivathsa & Panjwani 2017; Bisnath & Gao 2009; Kaplan and Hegarty 2005; Hatch et al. 2003). The geostationary satellite broadcasts the information to the receiving antenna on the ground (Fig. 2-4). The communication runs in the L-band format for GPS constellation (Li et al. 2015; Skog & Handel 2009; Kaplan & Hegarty 2005; Hatch et al. 2003). A dual-frequency receiver reduces the amount of reference stations needed to attain high accuracy (Shrivathsa & Panjwani 2017; Hatch et al. 2003). The satellite-based correction data is usually offered by commercial service providers (Liu et al. 2018; Bisnath & Gao 2009) like VERIPOS Apex/Apex²/Apex⁵, OmniSTAR G2, TERRASTAR-D, NavCom, Trimble CenterPoint RTX and SartFire. For open

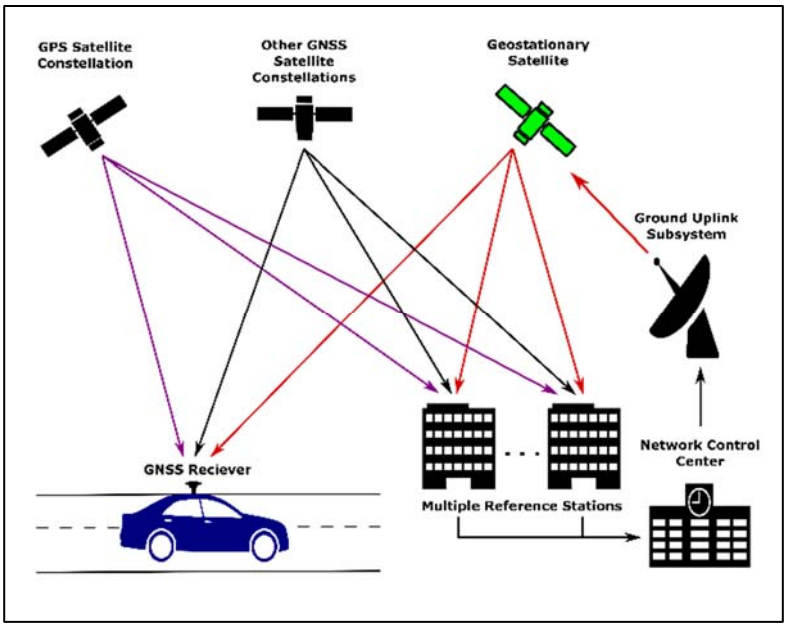

Figure 2-4: Operation of Real-Time-Kinematic Precise Point Positioning (source: edited after NovTel Inc. (2015), modified by Robert Arendt).

source use, the PPP-Wizard and RTKLIB are available (Jokinen 2014).

Nowadays, different providers like the BKG (Bundesamt für Kartographie und Geodaesy), CNES (Centre National d'Etudes Spatiales), DLR (Deutsches Zentrum für Luft- und Raumfahrt), ESA/ESOC (European Space Agency/ European Space Operations Centre), GFZ (Deutsches GeoForschungsZentrum) deliver freely accessible correction data. More

and detailed information regarding the topic of post-processing is discussed in Wang et al. (2018). A cutout of the globally distributed reference stations can be seen in Li et al. (2015) and are further explained in Skog & Handel (2009).

To achieve an accuracy of up to 5 cm a convergence time of 20–60 min is normally needed, depending on the actual number and geometry of visible satellites. To prevent a loss of tracking or a lock on a minimum of satellites, an open sky is needed as well as a continuously unobstructed environment (Knoop et al. 2017; Bisnath & Gao 2009). On the other hand, the use of PPP has its advantages in isolated and remote locations, expansive areas and regions where a reference station infrastructure is not generally available or is too costly (Bisnath & Gao 2009).

2.2.5. Sensor specifications

The Leica Viva GS16 smart antenna is a multi-frequency GNSS Sensor running together with the Leica CS20 Field Controller. Signal tracking is working with GPS (L1, L2, L2C, L5), GLONASS (L1, L2), BeiDou (B1, B2, B3 limited), Galileo (E1, E5a, E5b, Alt-BOC, E6 limited), QZSS (in future), SBAS (WAAS, EGNOS, MSAS, GAGAN) and L-band. The intern Satel M³-TR4 radio modem has 555 channels which leads to a high sensitivity and fast acquisition. The sensor can be used as a normal GNSS (absolute point positioning), in differential modus as a base station or rover as well as in a real-time-kinematic modus (RTK) with adaptive on-the-fly satellite selection (relative positioning). The RTK single baseline performance is about 8 mm + 1 ppm horizontal and 15 mm + 1 ppm in vertical. In the Network RTK mode an accuracy of 8 mm + 0.5 ppm horizontal and 15 mm + 0.5 ppm in vertical can be reached. Post-processed data measured in a static phase with long observation time can have an accuracy of about 3 mm + 0.1 ppm horizontal and 3.5 mm + 0.4 ppm vertically. The specialty of the sensor is its commercial SmartLink worldwide correction service based on the VERIPOS Apex correction service (In this study Apex² service). The SmartLink and SmartLink fill function is a remote Precise Point Positioning system with an accuracy up to

3 cm in 2D. The measurement precision, accuracy and reliability is dependent on various factors like the number of available satellites, observation time, atmospheric conditions, multipath and others. The convergence time needed to gain full accuracy can take 20 up to 40 min. More general sensor information can be read in Leica GS 16 manual (Leica Geosystems AG 2018).

Using the SmartLink function means that permanent corrected data can be received from a geostationary satellite (RTKPPP, derived via 7 different geostationary satellites - 25E, 98 W, 143.5E, AORE, AORW, IOR, POR) (Fig. 2-4). The accuracy in the commercial SmartLink mode is lower than in the RTK mode but it is independent of proximate reference stations and applicable all over the world. A statistical post-processing is not required because the SmartLink software automatically corrects the ionospheric and tropospheric delay as well as orbit and clock lags with help of the geostationary satellite information.

The geometric arrangement of the satellites, called Dilution of Precision (DOP), is given as GDOP (3 position coordinates plus clock offset in solution) and PDOP (Position of 3 coordinates) (Hurn 1989). A negative aspect of this commercial service is the stochastic black box, where the user has no option to look at the correct functional model and the proper intra- and inter-system weighting of observations behind (Kazmierski et al. 2018; Kazmierski 2018).

Further negative aspects of using commercial correction data instead of the free available data, for example of the CNES are its high costs and less accurate results against post-processed data.

However, depending on the task and its required accuracy it can make investigations less complex for the end-user.

2.2.6. Measurement setup and processing strategy

For mapping the road dams, the GS 16 Sensor was installed on the roof of a 4 × 4 car (Figs. 2-5, 2-6). The offset between the sensor and the street surface was measured with a Leica LaserDisto 8 and results in 1.93 m (Fig. 2-6). The sensor was connected via Bluetooth with the Leica CS20 Field-Controller in the car. This was programmed to take points automatically every 25 m or more frequently if there is an elevation change of more than 0.3 m in between that distance. The range was chosen according to the TanDEM-X digital elevation model,

Figure 2-5: Leica GS 16 Sensor installed on the roof of a car (photo: Robert Arendt 2018).

Figure 2-6: Measurement setup – Toyota Hilux with GS 16 sensor on the car roof (photo & editing: Robert Arendt 2018).

which has a raster resolution of 12.5 m. A higher waypoint resolution would have been possible but was not necessary because most of the time no significant elevation change was recognized in between a higher raster resolution, as previous fieldwork has shown.

The coordinate reference frame used by Apex² is ITRF2014. Due to the settings of the Field Controller CS20 it was automatically transferred into ITRF2008 and later measurements were reassigned in a geodetic format with ellipsoid and datum WGS 84, further given in Cartesian projected coordinate system UTM 33 S. Selectable satellite systems were GPS, GLONASS, Galileo and BeiDou. The Leica SmartLink option was selected by activating the Augmentation System so signals from geostationary satellites and their real-time correction data could be received. As mentioned above, the used commercial function is based on the VERIPOS Apex² system that only allows the receiving of real-time correction data for GPS

and GLONASS. That is why real-time correction data for BeiDou and Galileo could not have been received. The quality of the received correction data is guaranteed by the ISO 17123-8. More information about the processing strategy can be read in Tab. 2-1. The satellite cut-off angle was set on 10°. A DOP limit was not determined in advance but verified in the post-evaluation.

Each of the four surveying days (Fig. 2-3) started and ended at the campus site of the University of Namibia in Ongwediva. Before driving commenced, the GS16 was installed on the car and a convergence time of 20 to 40 min was given until the sensor achieved a 1D accuracy of lower than 10 cm.

Due to the limitation in time and parallel projects, the focus was on the main roads and required:

1. Transverse course to the flow direction of the Iishana and
2. Security for the drivers, passengers and the car.

Therefore, some remote gravel roads lacking security had to be excluded, like the part between Okahao and Outapi, which was too dangerous to drive on. The road dams east of Oshakati and Ongwediva have been excluded, because the hydrological network is different from the western system and will not be investigated further (Fig. 2-3). In addition, a part of short track between Tsandi and Ruacana is ignored as the system is flowing almost parallel to the road, so that the road dam will not have any important influence on the flow dynamic in this part of the study area (Fig. 2-3). A longer track starting west of the city of Okahao leading east of Ogongo has been omitted in consequence of its flatness.

The driving speed spanned between 0 and 80 km/h. During breaks, for example at traffic lights, the speed was 0 meanwhile the speed on long straight route sections was constantly about 80 km/h. In general, the speed was adapted to the road conditions and traffic situation. Outliers like waypoints leading to parking lots have been excluded manually. Furthermore, it has to be considered that the transverse gradient of the roads, especially in wide curves, could not always be driven along the highest positions due to road traffic regulations. To

improve the process of validation, data from the Namibian Roads Authority (NRA) were utilized for cross validation. Three datasets M0092, M0133, M0123 were provided.

Table 2-1: Processing strategy.

Processing mode	real-time
Observables	Ionospheric-free linear combination code and carrier-phase measurements
Ambiguities	float
Signal frequencies	GPS: L1/L2, GLONASS: L1/L2
Inter-System weighting	VERIPOS Apex²
Elevation cut-off angle	10°
Sampling rate	25m and/or change in elevation >30cm
Troposphere delay modeling	VERIPOS Apex²
Receiver clock	VERIPOS Apex²
Satellite orbits and clocks	VERIPOS Apex²
Code and phase biases	VERIPOS Apex²
Solution type	kinematic, VERIPOS Apex²
Correction models	VERIPOS Apex²

(compliant to the ISO 17123-8 standard)

The NRA partly measured the same roads and their heights within a distance of 500 m with the TRIMBLE R10 GNSS receiver in 2015. Likewise using a proprietary provider for real time correction in motion, they took the Trimble Continental CenterPoint RTX data. Similar to the measuring campaign of this study, they drove along the roads with a maximum speed of 80 km/h recorded in ITRF2014 coordinate reference frame, which was later converted into a WGS 84 format. They also measured while connected to the GPS and GLONASS systems. Another part in the set up was the PDOP value. If the value rose more than 0.5 m surveying ceased. Even in this investigation, post-processing was not necessarily done because of the real-time correction. The NRA could not give information that is more detailed. Nevertheless, both datasets measured nearly the same coordinates, just with another commercial device and software but still in the same mode.

Other cross validation methods, such as double and triple measurements or single point long time static measurements, have not been executed due to the lack of time in the field campaign. The results of the two kinematic measurement campaigns of 2015 and 2018 were

later compared for cross checking and to validate their deviations and similarities giving a hint of the overall reliability of the results.

The major challenge was to find coordinates that are at an equal location for further comparison. Most of the surveyed points could not been taken for validation because both campaigns measured in opposite directions and at different distances (25–500 m). Therefore, a buffer of 3 m was set around the coordinates of the 2018 campaign and intersected with the NRA data. The setting of 3 m was chosen under the condition that every pair of points had to be as close as possible for a significant comparison. Otherwise, if the buffer was set smaller almost no pairs of points were left for comparison. Finally, 18 points were close enough to each other for further comparison imitating a double measurement at these locations.

2.2.7. DEM pre-processing and correction

The correction of the TanDEM-X data set took place in several steps. In step one, outliers in elevation and indifferences caused by water were sought for exclusion. Therefore, the data package of the TanDEM-X data set includes different additional information layers (Wessel 2016). In this case, the TanDEM-X Water Indication Mask was used for excluding the strong inconsistencies (Wendleder et al. 2013).

The generated holes have to be interpolated to adapt the surface to the surrounding area. This was done with the Image Analyzer in ArcGIS. Here, the mask function was used with a minimum value of 0 and a maximum value of 3,034 for band 1. As a result, missing values were set to NoData. Afterwards gaps were filled with the Elevation void fill function (Short Range IDW Radius “off” and Max. Void Width “fill all”). Then, smaller sinks were filled with the standard Fill function of ArcGIS to eliminate further voids. Subsequently extreme values were reduced by a low-pass filter 3 × 3 (Pipaud et al. 2015). The last step is about the implementation of the GNSS records. Therein a 25 m buffer was set around the GNSS point data. Afterwards, a Kernel interpolation between the GNSS points was set in between the

buffer area. Then, the new dataset was implemented by the ArcGIS function Mosaic to new raster.

2.3. Results

2.3.1. GNSS performance

The measurement setup could be applied on all road dams as planned. At the end, 16,590 points were taken and around 532 km of main road dams were tracked (Fig. 2-3). Nevertheless, in the post-evaluation of the recorded data, it became clear that points were not taken exactly every 25 m as was defined in the automatic mode. Most points were taken in a range between 25 and 27 m. Moreover, a large amount of points was taken in distances up to 49 m. Statistically, points have been collected within a mean of every 32.08 m.

Nevertheless, the overall GNSS performance shows PDOP and GDOP values within an excellent to ideal rating between 3.5 and 1.2 (Tabs. 2-2, 2-3) (Dutt et al. 2009; Langley 1999). It should be mentioned that the performance rating originally was invented for GPS only (Langley 1999).

In addition, the 1D, 2D and 3D coordinate quality (CQ) is also determined in a decimeter to a sub-decimeter range, where 1D describes the vertical accuracy, 2D the horizontal accuracy and 3D the spherical (vertical and horizontal) accuracy. As reported in Tab. 2, the range of total accuracy in the sector of 3D coordinate quality spans from 5.0 to 10.0 cm, where 10 cm was the cut off limit. Points with a lower accuracy were excluded in the post-evaluation process. The calculated 3DCQ mean is about 7.1 cm with a standard deviation of 1.1 cm and a skewness of 0.544. The 1D and 2D coordinate quality is even better (Tab. 2-2).

Table 2-2: Overview of used satellites and accuracies of the recorded GNSS data.

Satellites used	Day 1	Day 2	Day 3	Day 4
GPS	7 - 8	7 - 10	7	10
GLONASS	6 - 7	4 - 8	7	6
Total detected	17 - 21	11 - 20	16 - 17	18 - 19
Accuracy				
PDOP	1.4 - 1.7	1.2 - 2.1	1.2 - 2.9	1.3 - 2.8
GDOP	1.6 - 2.0	1.2 - 2.2	1.3 - 3.5	1.2 - 2.3
1DCQ [cm]	7.1 - 9.9	4.3 - 9.0	4.7 - 10.0	4.4 - 10.0
2DCQ [cm]	3.2 - 5.4	2.4 - 6.3	2.5 - 6.2	2.4 - 7.8
3DCQ [cm]	7.8 - 9.9	5.0 - 10.0	5.3 - 10.0	5.0 - 10.0

Table 2-3: Explanation of DOP quality, after Langley (1999) in Dutt et al. (2009).

DOP Value	Rating
1	ideal
2-4	excellent
4-6	good
6-8	moderate
8-20	fair
20-50	poor

2.3.2. GNSS and TanDEM-X cross validation

The cross-validation of the two surveying campaigns (Tab. 2-4) between Leica and Trimble shows differences in height between 0.006 and 0.585 m with a mean difference of 0.154 m and a median difference of 0.091 m. The standard deviation is about 0.160 m with a skewness of 1.386 and a variance of 0.026. The calculated RMSE is about 0.219.

Moreover, the measurements of the 2018 campaign with the Leica instrument were compared to the TanDEM-X raw data at the same positions. Obviously, the range is larger. The minimum deviation is 0.125 m and the maximum deviation is up to 1.955 m, with a mean difference of 0.418 m and a median of 0.471 m. The standard deviation is 0.973 m with a skewness of − 1.138 and a variance of 0.947. The calculated RMSE is about 1.059.

Table 2-4: Cross validation of measurements with Leica, Trimble and the TanDEM-X.

Leica Point ID	Height Leica [m]	Trimble Point ID	Height Trimble [m]	Horizontal distance between Points [m]	Absolute vertical deviation Leica & Trimble [m]	Height TanDEM-X [m]	Absolute vertical deviation Leica & TdX [m]	Statistics for vertical deviation of Leica & Trimble data	Statistics for vertical deviation of total measured points of Leica at TdX raw data position
3410	1129.933	256	1129.927	2.449	0.006	1129.423	0.510	Mean value [m]	Mean value [m]
9948	1127.953	35	1127.961	2.732	0.008	1129.241	1.288	0.154	0.418
10968	1124.560	97	1124.576	2.955	0.016	1124.000	0.560		
7422	1125.875	47	1125.852	2.908	0.023	1126.000	0.125	Median [m]	Median [m]
3476	1128.586	260	1128.642	2.593	0.057	1129.250	0.664	0.091	0.471
9807	1128.516	26	1128.574	2.880	0.058	1127.661	0.856		
9987	1128.039	37	1127.981	2.912	0.058	1126.044	1.995	Stand. deviation [m]	Stand. deviation [m]
10712	1125.969	82	1125.906	2.425	0.063	1126.309	0.339	0.160	0.973
10098	1127.549	43	1127.631	2.837	0.083	1127.276	0.273		
4541	1132.345	345	1132.246	1.045	0.099	1131,327	1.018	Skewness	Skewness
10762	1125.696	85	1125.570	2.688	0.126	1125.227	0.470	1.386	-1.138
3080	1127.226	234	1127.087	1.594	0.139	1126.000	1.226		
10748	1125.774	84	1125.574	2.949	0.200	1126.006	0.233	Variance	Variance
11039	1124.491	101	1124.257	2.455	0.234	1123.000	1.491	0.026	0.947
9744	1128.929	21	1129.170	2.989	0.241	1128.019	0.910		
4628	1133.556	340	1133.891	2.300	0.335	1133.921	0.365	RMSE	RMSE
4683	1132.567	337	1133.000	1.172	0.433	1133.292	0.724	0.219	1.059
4835	1131.988	328	1132.573	3.000	0.585	1131.723	0.265		
								Min / Max [m]	Min / Max [m]
								0.006 / 0.585	0.125 / 1.955

2.3.3. Corrected TanDEM-X

The TanDEM-X Transect Elevation Check of Fig. 2-7 shows two different lines and a blue plain of height along a transect, which can be found in Fig. 2-8. The black line indicates the height of the TanDEM-X raw data set before any calculation. The red dotted line designates the same path after the correction of water interferences and the application of filtering algorithms as described before (DEM pre-processing and correction). Up to here, the topography is smoothed and represents a more realistic and natural image. Sharpe edges could be equalized and some overestimated parts (water interferences and vegetation patches) have been lowered while other underestimated parts have been raised. Until that point, the road dam is still not clearly visible.

The plain blue specifies the final corrected DEM (Fig. 2-7) including the surveyed road dam, which is visible also in Fig. 2-8. Except for the road dam where more than a meter deviation is evident, differences in a sub-meter range could be detected. As shown in Fig. 2-8, the

application of the different filter algorithms and the correction of the water-induced interferences have been successful, so the road dam is clearly visible and the high outrage peaks are eliminated.

The value of the results becomes clearer in Fig. 2-9. The effect of the road dams and the modifications including culverts and bridges leads to a change in flow behavior, here emphasized in a change of flow direction. The calculated flow paths change significantly between the raw TanDEM-X model and the two edited models where additional filter algorithms were applied and culverts and bridges have been included.

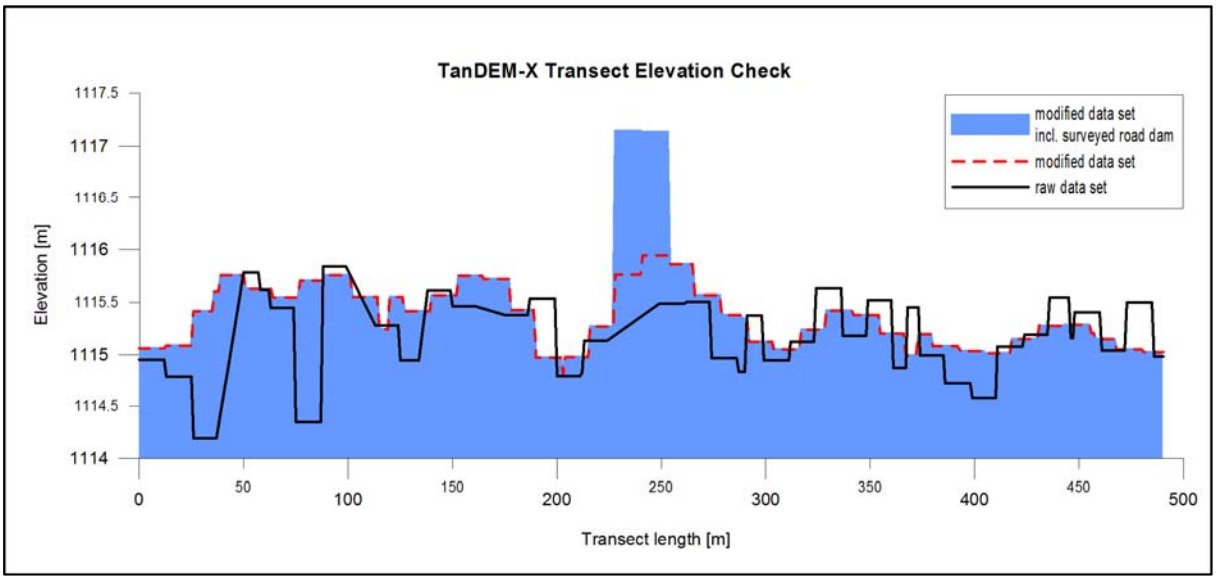

Figure 2-7: TanDEM-X Transect Elevation Check (located in Figure 2-3, 2-8 & 2-9).

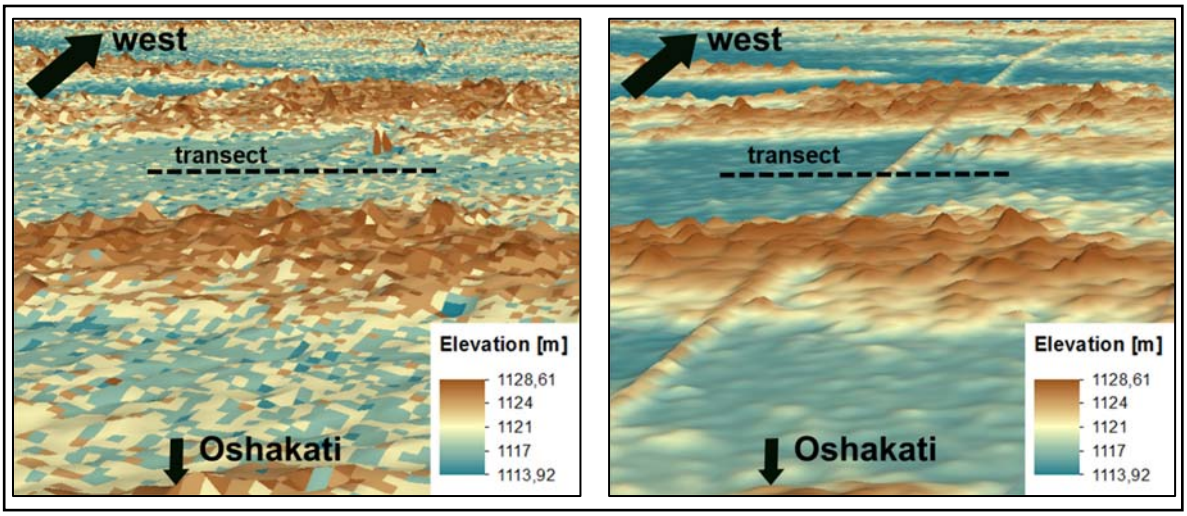

Figure 2-8: TanDEM-X scene before correction (left) and after correction (right). Both scenes face in a western direction with exaggeration x 12 and the indication of the transect of Figure 2-7 (also located in Figure 2-3).

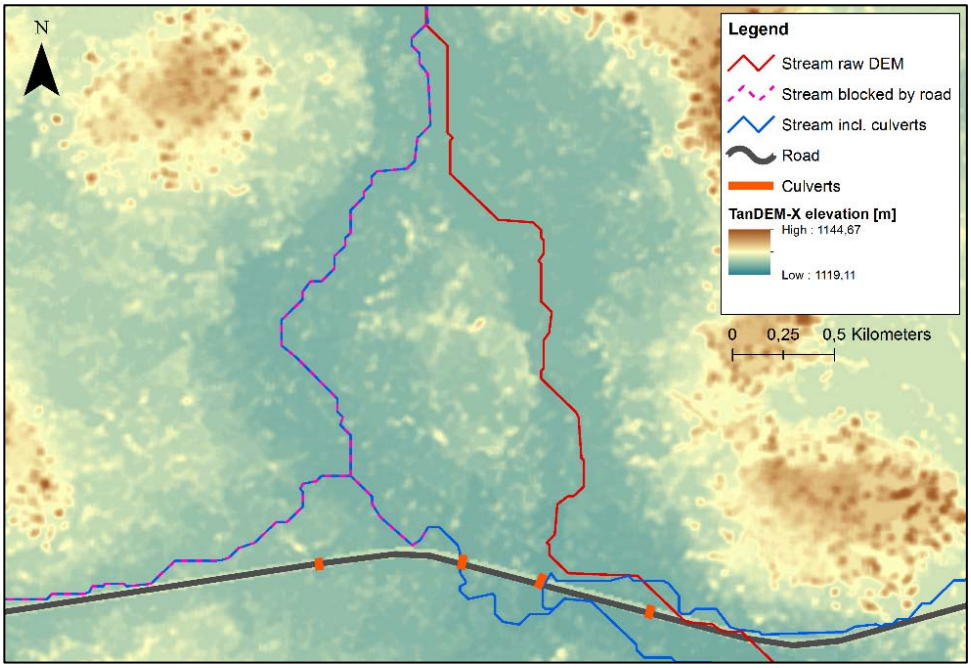

Figure 2-9: Three different flow path calculations with ArcGIS illustrated in one image. Red stream definition based on the raw TanDEM-X model only used the 'Fill' function. Purple dotted Stream is calculated after the application of additional filter algorithms and the inclusion of the road dams. The blue Stream also includes the culverts and bridges. The road dams and culverts are influencing the flow dynamics.

2.4. Discussion

Due to left hand-traffic, data points were usually collected while driving on the left side of the roads. It has to be acknowledged, that road dams are normally transversely inclined in curves. Therefore, some of the collected point data in curves are not always representing the highest part of the road dam cross section. Nevertheless, in a few parts, the attempt was made to drive the highest profile through the curves to gain the maximum height of the road dam. These circumstances led to small differences between the left and right roadsides, which theoretically has to be added to the general vertical accuracy (1DCQ).

Airfreight costs could be saved, as just one sensor was necessary instead of two and no additional equipment. Moreover, time and work force was saved, because no differential station had to be set up every 1 km nor always had to be guarded by staff. Even the long

convergence time of 30–40 min at the beginning of the measurement session was no problem at all, since this time was used to prepare the daily fieldwork.

According to Langley (1999), the GDOP and PDOP values had excellent to ideal rates. This explanation of quality was formerly developed for GPS only. Even the 1D, 2D and 3D coordinate accuracy shows a decimeter to sub-decimeter deviation. Nonetheless, coordinates could not have been detected 100% accurately every 25 m as was planned and set in the settings. It is assumed that the top speed of 80 km/h might be too high if points information were recorded every 25 m. Regarding future measurements, either the top speed has to be limited or the record span has to be widened. First estimations indicate that it is more about velocity. Some extreme outliers can be explained by an exceeding of top speed for example, due to overtaking, and others may be caused by a longer software calculation time.

It can be assumed that multipath effects were not important, due to the sparsely vegetated and very flat landscape being only rarely interrupted by trees or buildings. Multipath effects caused by the white metal roof of the car cannot be determined nor excluded. Literature did not give any hints about necessary protection measures for roof top installed GNSS sensors, nor any numbers for multipath measurement errors.

The filter algorithm used leads to a substantial improvement. The evaluation of the transect as well as Figs. 2-7 and 2-8 shows that most of the interferences could be eliminated successfully and the geomorphology is obviously more perceptible. Nonetheless, the delivered water mask did not cover all water surfaces, especially very small ones sometimes were not covered. As a consequence, the low-pass filter smoothed these objects but some of them still exist as small dunes. However, regarding the work of Wendleder et al. (2013), it can be assumed that around 70% of the water bodies were detected. Further statistics regarding the used water mask are pending and have to be evaluated in a next step.

The validation of the measured data was limited due to the use of commercial real-time correction data. This caused a black-box effect in which not all data quality parameters were visible. Long-term single point measurements and double and triple measurements could

not have been done due to limitation of time and parallel investigations in the field. Therefore, the only chance to get an idea of the vertical accuracy was the comparison of the data with former measured data from the Namibian Roads Authority. In this case, different systems were used but with almost the same settings, measuring in motion with the same speed and the use of a commercial real-time correction service. Statistical analyses showed a sub-decimeter median value. Nonetheless, even for the data of the NRA individual quality values were missing due to the commercial real-time correction service used.

To achieve real-time correction data that is free of charge different providers like the CNES can be addressed for future measurements. In addition, post-processing would contribute to increased accuracy (Kazmierski et al. 2018; Kazmierski 2018; Wang et al. 2018). For example, with the new VERIPOS Apex^5 system, receiving of correction data including BeiDou and Galileo would have been possible to increase data quality. Even with the CLK91 stream via CNES free available correction data including all 4 satellite systems could have been received (Wang et al. 2018).

To some extent, the final total estimated error in height consists of different single errors and cannot be assessed in a concluding number due to various factors: the position of the car on the street (top or down of the turn), the uncertainty of the commercial real-time correction data (partially black-box), the TanDEM-X itself (vertical/horizontal accuracy), and filter algorithms and interpolation procedures used. It becomes clear that a millimeter accuracy cannot be reached at all. Nonetheless, the aim of the work - to improve the TanDEM-X data set for further flood modelling - has been achieved.

2.5. Conclusions

The application of the different filter algorithms and the correction of the water-induced interferences have been successful, so road dams have been made clearly visible and high outrage peaks were eliminated. These modifications including culverts and bridges also lead to a change of flow directions. The automatically recorded points present excellent up to

ideal GDOP and PDOP values with vertical accuracies about 4.3 cm up to 10.0 cm. The validation procedure shows huge vertical differences between GNSS measurements and the TanDEM-X raw model ranging from about 0.125 m up to 1.955 m with a median of 0.471 m. Elevation differences between two GNSS systems have shown significantly less differences in accuracy ranging between 0.006 and 0.585 m with a median of 0.091 m. These circumstances clearly illustrate the necessity of measuring smaller infrastructures for an accurate representation in the digital elevation model.

With this investigation, a scientific contribution has been made towards understanding the topographic basis of the Iishana system. Previously developed hydrological models in the Iishana region were focused on small sub-basins rather than on the entire system. The survey results reported here provide a scientific base for developing a trans-boundary flood model in the Iishana region of Angola and Namibia, which would contribute towards an innovative adaptation of water management to climate change. The potential and originality of this research project is to bridge the knowledge gaps and to contribute to the scientific base for sustainable water resource management in the region.

The results underline the significance of a preprocessing of TanDEM-X data and the importance of incorporating road dams, culverts and bridges when a high quality floodwater prediction model is sought.

2.6. Acknowledgements

Open Access funding provided by ‘Projekt DEAL’. We thank the German Aerospace Centre (© DLR 2017) for their delivery and support with the TanDEM-X data (Proposal ID: DEM_HYDR1285). Further, we thank the Leica Geosystems AG for their quick and helpful technical support during our field campaign in March 2018. Moreover, we thank the "German Association for International Cooperation (GIZ) GmbH" (Windhoek, Namibia office, Prof. Dr. Heinrich Semar) for the logistical support of the field campaign in September 2017 and March 2018. We are grateful for the collaboration with the University of Namibia (Campus

Ongwediva) and the Namibian Roads Authority (Windhoek, Mr. Horst Schommarz) for providing us with data. We also thank Mr. Benjamin Rommel (Freie Universitaet Berlin) for constructing the special tools for the sensor installation.

2.7. Funding

This research was supported by the Freie Universitaet Berlin and the “Research Network for Geoscience in Berlin and Potsdam – Geo.X”.

3 Natural Pans as an Important Surface Water Resource in the Cuvelai Basin – Metrics for Storage Volume Calculations and Identification of Potential Augmentation Sites

Link to online publication: https://doi.org/10.3390/w13020177

Abstract

Numerous ephemeral rivers and thousands of natural pans characterize the transboundary Iishana system of the Cuvelai Basin between Namibia and Angola. After the rainy season, surface water stored in pans is often the only affordable water source for many people in rural areas. High inter- and intra-annual rainfall variations in this semiarid environment provoke years of extreme flood events and long periods of droughts. Thus, the issue of water availability is playing an increasingly important role in one of the most densely populated and fastest growing regions in southwestern Africa. Currently, there is no transnational approach to quantifying the potential storage and supply functions of the Iishana system. To bridge these knowledge gaps and to increase the resilience of the local people's livelihood, suitable pans for expansion as intermediate storage were identified and their metrics determined. Therefore, a modified Blue Spot Analysis was performed, based on the high-resolution TanDEM-X digital elevation model. Further, surface area–volume ratio calculations were accomplished for finding suitable augmentation sites in a first step. The potential water storage volume of more than 190,000 pans was calculated at 1.9 km³. Over 2,200 pans were identified for potential expansion to facilitate increased water supply and flood protection in the future.

3.1. Introduction

The Iishana system is part of the western CB (Cuvelai Basin), which crosses the border between southern Angola and northern Namibia. The basin is one of the most densely

populated areas in southern Africa; around 40% of all Namibian inhabitants live in this region. The high population density is expected to increase drastically at a growth rate of 1.4% in the next several years (NamStat 2013). Projections for the year 2041 anticipate a population count 27% higher than what exists today (NamStat 2014). One factor driving this growth is the presence of slightly more fertile soil than in the rest of the country (Persendt & Gomez 2016). The cultivation of rain-fed sorghum and millet and the practice of stock farming are the most important sources of rural income (Luetkemeier & Liehr 2019; Luetkemeier et al. 2017).

The semiarid climate of the region is characterized by a single rainy season between November and April (annual precipitation of 350–550 mm) and a potential evaporation rate of up to 3,200 mm/a. Additionally, high seasonal, inter- and intra-annual climate variability frequently leads to extreme events, such as floods and droughts. These are the major factors controlling and limiting the development and safety of the local people's livelihood, food security, and water availability (Gaughan et al. 2016; Shifidi 2016; Persendt et al. 2015; Reason & Smart 2015; Kundzewicz et al. 2014; Mendelsohn et al. 2013).

Severe droughts struck in the late 1980s and mid-1990s. More recently, a longstanding drought has lasted from 2014 to 2019, with normal rainfall in 2017. This has caused a tremendous food insecurity for people in Namibia and Angola. Although the occurrence of droughts in semiarid environments is to be expected, awareness of and preparedness for drought events in the Iishana system is rather low (Luetkemeier et al. 2017; Seely et al. 2003).

In addition to these drought events, flood disasters occurred recently in 2008, 2009, 2010, 2011, and 2013. These events caused fatalities and significant damage to property, crop yield, and livestock, as well as damage to the technical infrastructure of the region (Bischofberger et al. 2016; Shifidi 2016; Awadallah & Tabet 2015; Persendt et al. 2015; Filali-Meknassi et al. 2014; Skakun et al. 2014; Mufeti et al. 2013; Mandl et al. 2012). However, floods are also very important because they replenish the water system, which supports the local people's livelihood through dry seasons (Cunningham et al. 1992). The episodic surface water supports crop growth, provides fish and water grazing areas for livestock (Seely et al. 2003).

The Kunene River is an important headwater for the Iishana system. It flows along a portion of the border for southwestern Angola and northwestern Namibia, respectively. The river water is diverted from Angola to the Namibian part of the Iishana system by the 155 km Calueque-Oshakati Canal and is purified in a chain of four water works. Water availability strongly depends on the discharge of the northern part of the basin (located in southern Angola) (Klintenberg et al. 2007), where the annual rainfall is much higher (550–950 mm) than the rainfall in northern Namibia (350–550 mm) (Mendelsohn & Weber 2011). Considering the low income in rural areas, many people are not able to pay for treated water. As such, water distribution conflicts are more than likely in periods of intense droughts and increasing water shortage (Luetkemeier et al. 2017; Seely et al. 2003). Some residents interviewed by Shifidi (2016) have even reported that they have no access to piped water and thus depend on ground or surface water. In this context, the term “groundwater” includes not only deep aquifers but also shallow perched aquifers accessed by boreholes and hand-dug wells (Kluge & Polak 2018). In rural areas, people construct small, hand-dug wells, which can be up to 20 m deep (Zimmermann 2013; Cunningham et al. 1992). However, groundwater in the transboundary Iishana system is highly mineralized and often not suitable for human consumption (Faulstich et al. 2018; Kluge et al. 2008).

Shallow, interconnected ephemeral and endorheic river channels associated with thousands of small pans and natural depressions characterize the landscape in this region (Ngula Niipele & Chen 2019; Luetkemeier et al. 2017; Persendt & Gomez 2016; Shifidi 2016; Awadallah & Tabet 2015; Goormans et al. 2015; Mendelsohn et al. 2013; Zimmermann 2013; Kluge et al. 2008; Cunningham et al. 1992) (Figs. 3-1, 3-2). These pans serve as an important source of water supply for agricultural and domestic use. Since the surface water of the ephemeral Iishana (singular Oshana) does not persist over the dry season, several adaptation strategies have been developed over the decades. For example, shallow artificial depressions are dug in the Iishana by local people to increase water retention. Such depressions are usually 3-5 m deep and collect the local rainfall and the Iishana runoff (Zimmermann 2013; Cunningham et al. 1992) (Fig. 3-1a). Another technique to store water (Beyer et al. 2018) is the use of a

Stengel-Dam (Stengel 1963) (Fig. 3-1d). Among all these measures, the common aim is to reduce the population's drought vulnerability. From an integrative perspective, such adaptation measures are necessary to increase water storage. Simultaneously, they help to prevent widespread devastation caused by floods.

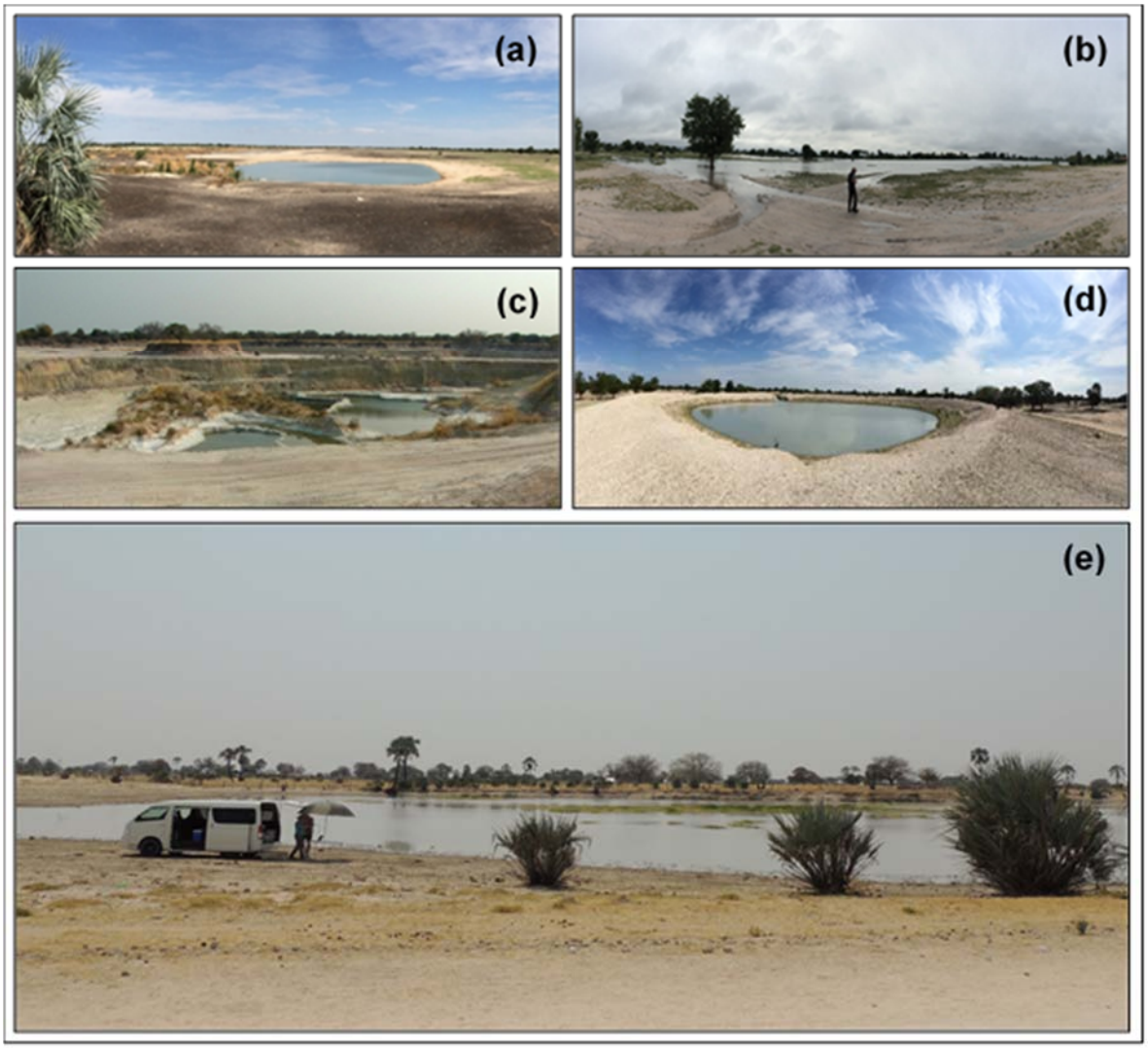

Figure 3-1: Typical hydrological landforms in the Iishana system: (a) man-made deepened pan in an Oshana, (b) large pan in an Oshana, (c) borrow pit filled with groundwater, (d) artificial Stengel dam for water harvesting, and (e) typical Oshana with water filled pan; photos by R. Arendt 2017.

It must be assumed that climate change will lead to more hydro-meteorological extreme events in the near future, which will cause further floods and droughts in the Iishana system. Therefore, increased pressure on the rural population living in a subsistence economy is to be expected (Luetkemeier & Liehr 2019; Luetkemeier et al. 2017), highlighting the need for a comprehensive assessment of the water balance for the entire transboundary basin.

Most preceding research on floods and droughts in the Iishana system focused on the estimation of the flood extents (Müller et al. 2018; Awadallah & Tabet 2015; Goormans et al. 2015; Skakun et al. 2014; Mandl et al. 2012), flood modeling (Mufeti et al. 2013), the description of flood impacts on livelihoods (Shifidi 2016), and drought hazard assessment (Luetkemeier 2017). Thus, most studies concentrated on selected parts of the Iishana system, but never on the entire region. Additionally, research has been carried out by McBenedict et al. (2019); Wanke et al. (2018); Wanke et al. (2014); Zimmermann (2010); Miller et al. (2010) to analyze the water supply function and quality of hand-dug wells. However, there is no quantitative information on the water storage and supply function of the natural pans in the Iishana system. Nor does information exist about the types, distribution, connectivity, and storage volume of natural and artificial pans. Thus, this study aims to comprehend the hydrological complexity of the entire Iishana system by identifying and classifying the pattern, volume, depth, and distribution of its small, natural water pans. These patterns were identified and characterized by using a Blue Spot Analysis, which was based on the high-resolution TanDEM-X DEM (digital elevation model). Further, surface area–volume ratio calculations were undertaken for determining suitable augmentation sites.

3.2. Materials and methods

3.2.1. Study area

The Iishana system is located in the western part of the CB (Miller et al. 2010) (Fig. 3-2). The size of the total CB is about 97,620 km². The Iishana system covers about 18,370 km². Approximately 1.2 million people live in this region (34% in Angola and 66% in Namibia) (Digital Atlas of Namibia 2016; Persendt & Gomez 2016; Mendelsohn & Weber 2011). The study area is bounded by the Kunene River and Okavango River (Angola) in the north and by the Etosha Pan (Namibia) in the south.

The topography is characterized by very flat slope angles with average gradients of 1‰ in Angola to 0.5‰ in Namibia. With an elevation of about 1,200 to 1,100 m, the flat terrain

plunges into the Etosha Pan (Mendelsohn et al. 2013). The Iishana system is defined as a diffuse network of shallow and ephemeral channels (Ngula Niipele & Chen 2019; Luetkemeier et al. 2017; Persendt & Gomez 2016; Shifidi 2016; Awadallah & Tabet 2015; Goormans et al. 2015; Mendelsohn et al. 2013; Zimmermann 2013; Kluge et al. 2008). Their sizes are highly dynamic with widths reaching from 1,750 m to 100 m and depths ranging from 1 to 7 m (Mendelsohn et al. 2013).

Several shallow depressions (natural pans) have formed due to a lack of morphologically well-defined discharge channels. These isolated pans connect to broad, undefined channels once they are filled with local rainwater (Persendt & Gomez 2016).

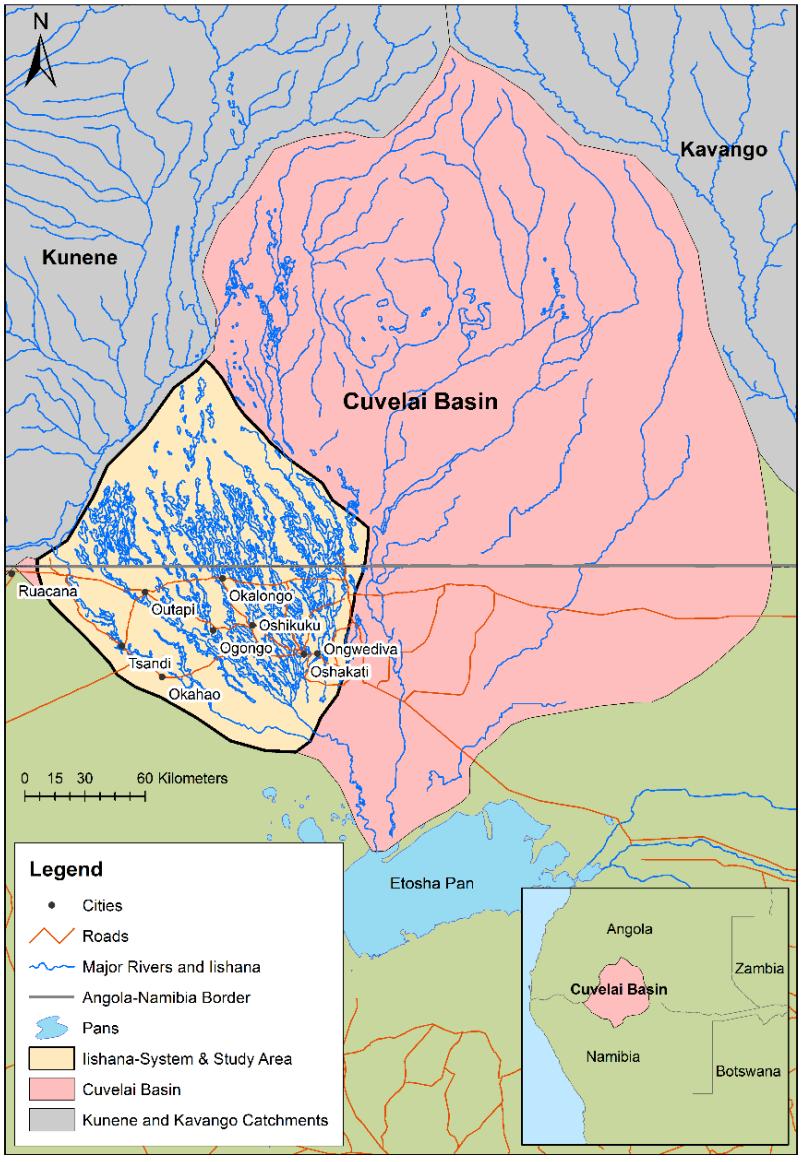

Figure 3-2: Overview of the Cuvelai Basin and the study area of the Iishana system, database: Digital Atlas of Namibia (2016); UN-OCHAROSA (2018).

Some of these channels have been covered by windblown sand, especially towards the southeast where drier conditions are present. As a result, the southern Iishana system is characterized by tens of thousands of small pans, which are usually never connected to each other (Mendelsohn et al. 2013) except during heavy flood events.

The elevated areas between the Iishana consist of Kalahari sand. These locations are feasible for crop production and subsistence rain-fed agriculture (Persendt & Gomez 2016). In the lower Iishana areas, aeolian and fluvial sediments are present. These are frequently characterized by fine-grained material (clay fraction), calcite and, according to own investigations, also by silicate crusts. This composition supports low infiltration capacities and high surface runoff (Faulstich et al. 2018; Goudi & Viles 2015; Hipondoka 2005; Hüser et al. 2001).

In terms of climate, the CB spans between a subtropical north and a semiarid south. The potential evaporation in the Iishana system increases from west to east from 2,600 to 3,200 mm/a (Persendt et al. 2015; Mendelsohn et al. 2013). The annual precipitation increases from about 350 up to 950 mm along the same gradient. The rainy season runs from October to April and the dry season from May to September. A high interannual rainfall variability, causing floods and droughts with all their consequences, as mentioned in the preceding section (Gaughan et al. 2016; Shifidi 2016; Reason & Smart 2015; Kundzewicz et al. 2014), characterize the climate.

3.2.2. DEM preprocessing

This study was based on the TanDEM-X DEM, which provides a horizontal spatial resolution of around 12 m and a vertical resolution of less than 1 m (i.e., information on the surface elevation is stored in floating point precision). The relative vertical accuracy is less than 2 m for regions with subtle topography (slope < 10°) (Rizzoli et al. 2017). From a hydrological point of view, the DEM is a great improvement compared to former DEMs (e.g. the SRTM

DEM), which provided spatial resolutions of up to 20 m and accuracies of 16 m horizontally and 10 m vertically (Mukul et al. 2017; Smith & Sandwell 2003).

In using the DEM, two challenges had to be addressed prior to the Blue Spot Analysis. First, the DEM comes with some local inconsistencies and errors, which are due to phase-unwrapping problems caused by water surfaces. This effect typically manifests in locally restricted, highly increased elevation values (up to tens of meters compared to the surrounding terrain). Second, the DEM is a surface model, and the provided information displays the height of the terrain plus the height of man-made objects, vegetation, etc. A removal of these objects (along with the above-mentioned errors) is preferred for the hydrographic modeling. The processing steps, outlined in Fig. 3-3a, were applied to account for these issues and the Water Indication Mask (Water Mask), which comes along with the DEM (Wessel 2016), was used to remove inconsistencies over water surfaces (Wendleder et al. 2013). The resulting gaps were interpolated with the help of the Image Analyzer Function of ArcGIS, called 'Eliminate void and fill' (Arendt et al. 2020).

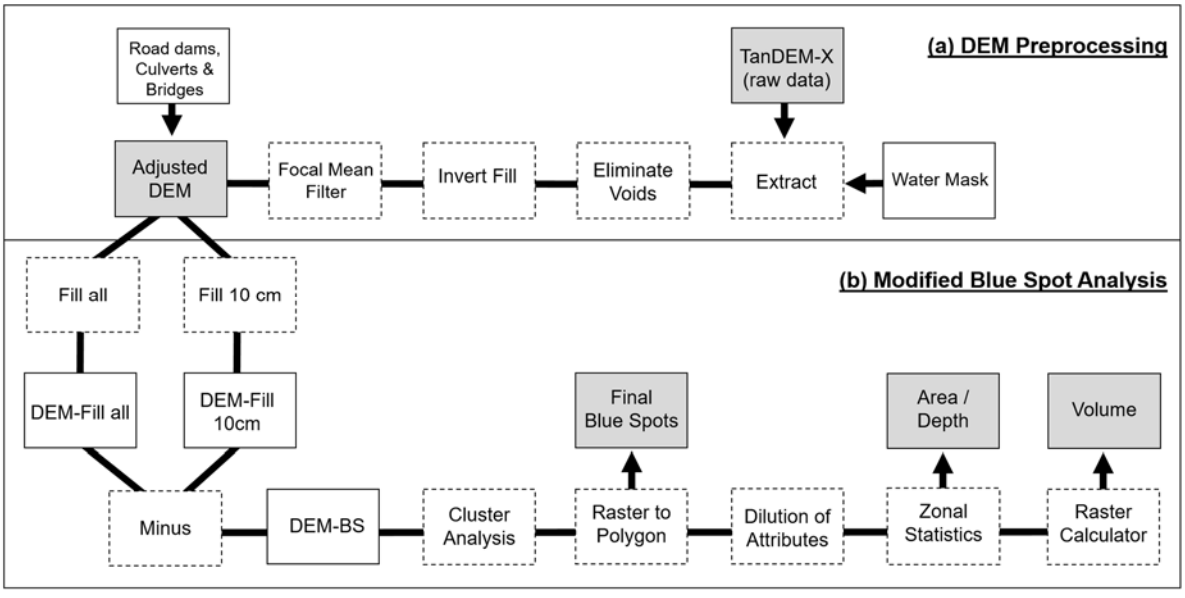

Figure 3-3: The TanDEM-X DEM preprocessing chain connected with the Modified Blue Spot Analysis. (a): A DEM preprocessing is necessary before any further analysis; (b): The affiliated modified Blue Spot Analysis after the preprocessing.

In the following, the Invert Fill algorithm (Fig. 3-3a) was applied. This method is based on the approach of Rutzinger et al. (2006) and the Fill-function algorithm implemented in ArcGIS. First, the previously edited DEM was inverted with the help of the raster calculator by multiplying the DEM raster values by minus one. Second, the ArcMap Fill-function algorithm was used to fill the inverted peaks. Next, the inverted and the filled DEM were retransformed with the raster calculator by multiplying them by minus one again. As a result, the former inconsistencies, which appear as peaks in the DEM, were removed, but natural pans remained.

In the next step, vegetation obstacles were reduced with a 3 × 3 Focal Mean Filter to produce the ADEM (adjusted digital elevation model). Finally, major road dams, culverts and bridges were implemented. Details on the origin of the data used and the specific procedure of implementation can be read in (Arendt et al. 2020).

3.2.3. Modified Blue Spot Analysis

The following approach is based on the ADEM and aims to identify natural pans (Nielsen et al. 2011). The Blue Spot identification took place in several steps (Fig. 3-3b):

First, the ADEM was filled by the ArcGIS Fill function with a threshold of 10 cm to account for possible artifacts and noises (Jenson & Domingue 1988). This means all pans were filled to 10 cm for equalization. Second, the ADEM was entirely filled to the pour point of all pans (not using a limiting threshold). These two results were subtracted to create the Blue Spots in the new raster layer called DEM-BS (Digital Elevation Model–Blue-Spots) (Balstrøm 2015). In further post-processing, the results of the Blue Spot Analysis were cleaned and separated into unique groups through the use of the Boundary Clean, Majority Filter, and Region Group tools (Grim 2012).

Finally, the data was transformed into a Feature Layer (i.e., vector geometry). From the resulting polygons, the attributes of area, depth, and sum were calculated amongst other

relevant attributes. To calculate the volume values of each Blue Spot (Fig. 3-4), the area was multiplied by the sum of the pixel depth then divided by the count of pixels (Eq.1).

$$\text{Volume } (m^3) = \text{Area } (m^2) \times \text{Sum(pixel depth)(m)/Count} \quad (1)$$

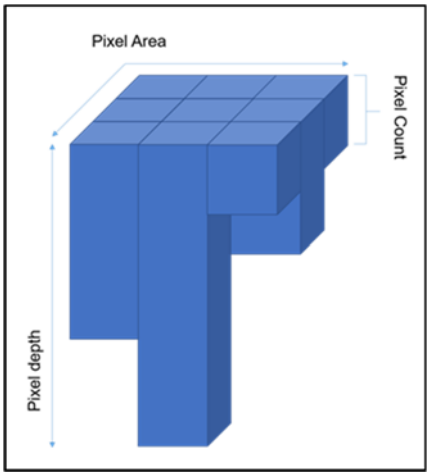

Figure 3-4: Schematic representation of a Blue Spot.

3.2.4. Validation

For validation, a mask was developed in cooperation with the Julius-Maximilians-University of Würzburg and the German Aerospace Center. This mask represents the maximum water coverage in the entire Iishana system for a specified period. This MWE (Maximum Water Extent Mask) was developed using a multisensor approach (Rättich et al. 2020). It includes data from 12 different spaceborne remote sensors, which, in turn, are located on seven different satellites. The multispectral satellites used are Landsat-5 and Landsat-8, and the radar satellites are ALOS/PALSAR, ALOS-2/PALSAR-2, Envisat ASAR, Sentinel-1, and TerraSAR-X (Tab. A-1).

All available images for three rainy seasons with floods were examined, covering the months of October to September during the years 2007/2008, 2008/2009, and 2016/2017. Single water masks were extracted for each available image within the three study periods. Detailed methods can be found for Landsat-5 and -8 data in Wieland & Martinis (2019), for Sentinel-1 radar data in Twele et al. (2016), and for TerraSAR-X in Martinis et al. (2015a). The remaining

data can be found in the RaMaFlood (Rapid Mapping of Flooding) process description of Martinis et al. (2015b). In addition, these water masks were used to calculate the total duration of annual floods (Rättich et al. 2020) during the three study periods. If one pixel had two consecutive water detections, it was considered to be flooded and was assigned to the annual water mask for its respective study period. This subdivision fueled further investigation, which will be described in another study. Finally, the three individual annual water masks were merged into one mask, the MWE mask. Permanent water surfaces were excluded from the outset. Since one year with 365 days is not completely covered by any of the three study periods, water bodies are defined as permanent if the number of days with water presence within the total duration layer is higher than the maximum possible number of days minus 30 (Pekel et al. 2016).

The validation process took place in two major steps and is outlined by an example in Fig. 3-5.

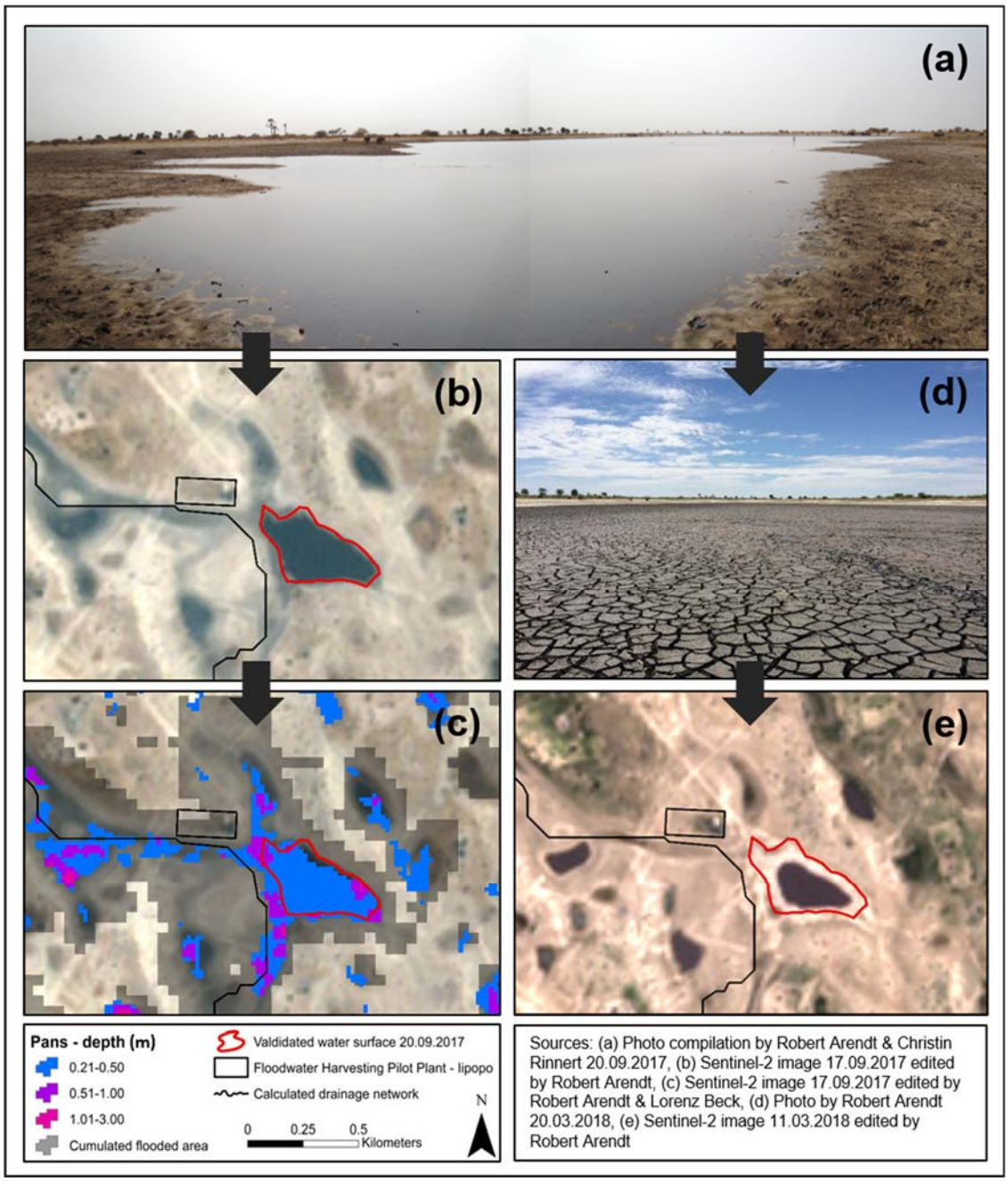

Figure 3-5: Validation process of pan detection. Example also represents focus area 4, annotated in Fig. 3-6. Subfigure (a) shows the situation and water extend on site in 2017. The red shape in subfigure (b) determines the surface water area of (a) and corresponds to the water surface area detected via the satellite data in 2017 (b). Subfigure (c) shows the result of the calculated depths and extent of the pans. Additionally, the gray areas show the maximum flood water extent detected in the past. In subfigure (d) the appearance of the depression in a dried out state is illustrated. This condition was documented by photo in 2018 after a drought event. Subfigure (e) shows the same dry pan by a satellite image including the former red shape of the water extend of 2017. Here, the dark area does not represent water, but dry sediments.

In total, 11 photos of water-filled pans were taken in the countryside and in the city of Oshakati (Figs. 3-6, 3-7 FA 2) for ground truth control. Ten of these pictures were taken between the 5th and 7th of March 2018, ranging from one to three days after a heavy rain event. This work was done at the same time as the road dam survey and culvert detection study, which were conducted during the field trip in March and April of 2018. Details of the survey can be read in Arendt et al. (2020). One photo was taken during the study's first field trip on the 20th of September 2017 in Iipopo. This exception was included because it is the best-documented site in the study area.

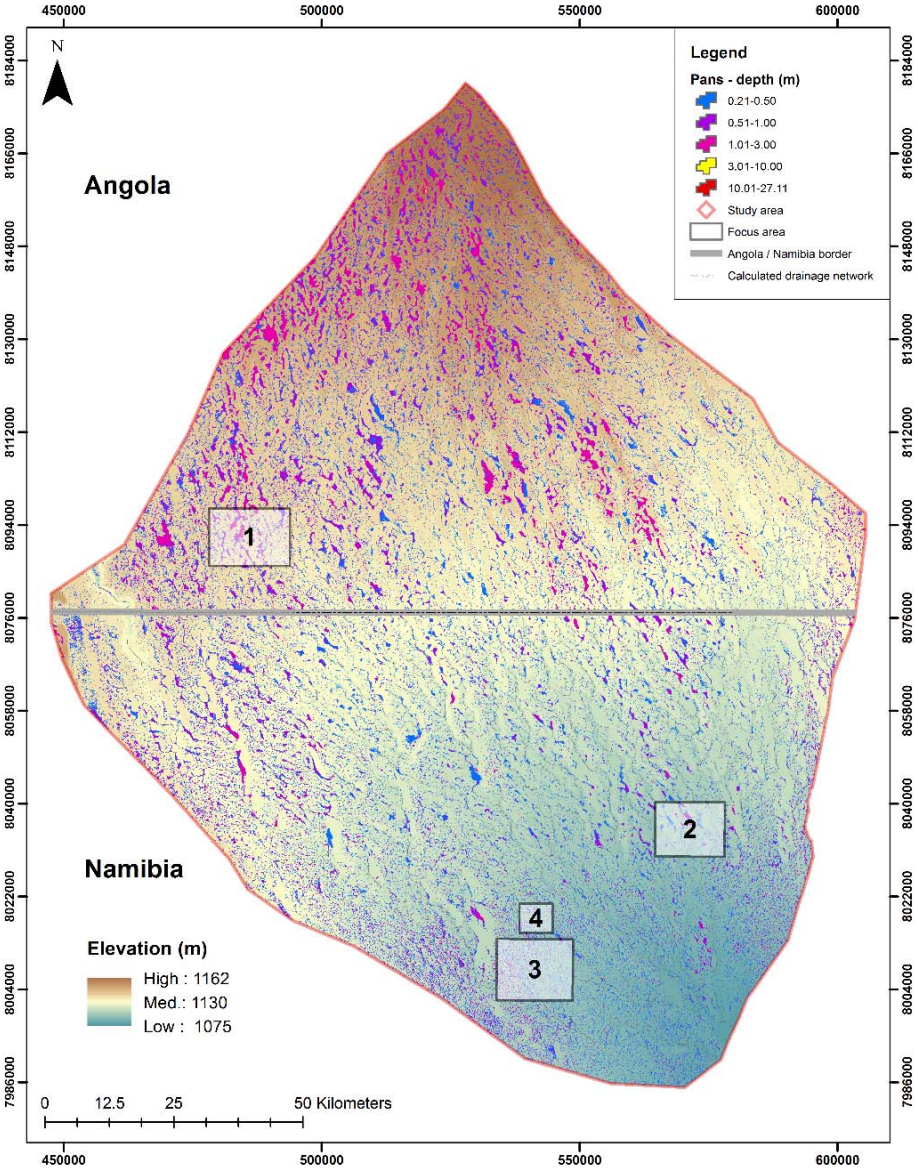

Figure 3-6: Pans and their depths in meters for the entire transboundary Iishana system. Detailed information for focus areas 1–3 can be found in Fig. 3-7. Focus area 4 represents the example for validation and is shown in Fig. 3-5.

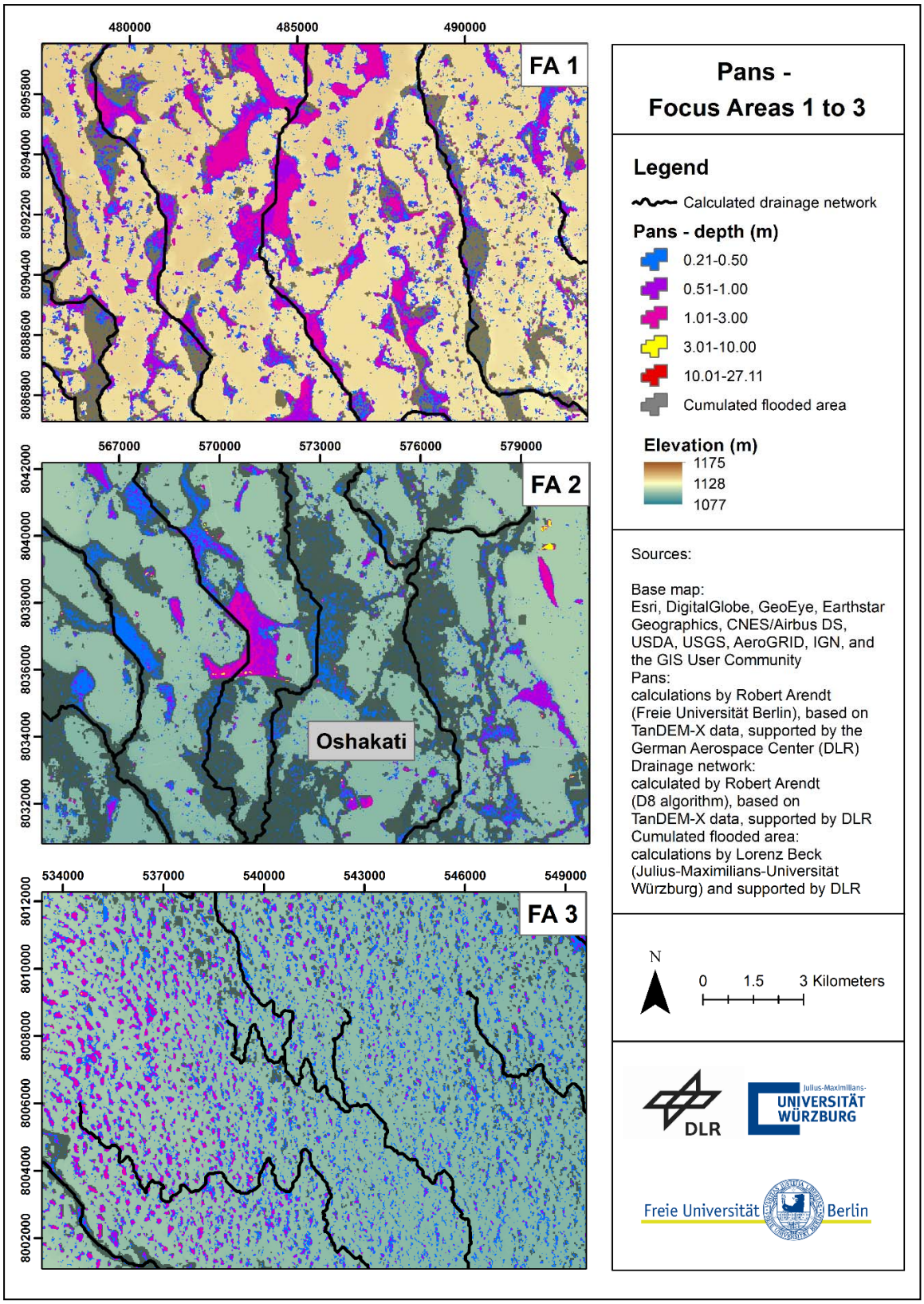

Figure 3-7: Pans in focus areas 1–3 in Angola and Namibia as shown in Fig. 3-6. FA 1: Large and deep pans in the southwestern part of the Angolan Iishana system; FA 2: Fewer but still large pans around the town of Oshakati in the southeastern part of the Namibian part of the Iishana system, pans highlighted in yellow represent borrow pits; FA 3: Thousands of small and isolated pans in the southern part of the Iishana system in Namibia.

Subsequently, the results of the Blue Spot Analysis (calculated pans) were compared to the onsite pictures.

Next, the same calculated pans (Blue Spots) were compared to the MWE validation Mask. In both comparisons, overlapping analysis was performed by visual examination. For each approach, this process determined whether or not a Blue Spot matched both the photo and the MWE.

3.3. Results

The Iishana system is typically considered and described as a unified and coherent hydrological system (Fig. 3-6). For better examination, references to individual focus areas are made (Fig. 3-7). At the same time, the landscape is artificially divided based on geopolitical boundaries in order to highlight possible hydrological potentials in a country-specific manner.

3.3.1. Surface area

The study location covers an area of 18,370 km², of which 8,726 km² belong to Angola and 9,644 km² to Namibia. The total area of all pans is about 4,021 km². Thus, the proportion of the total surface area is approximately 22% for Angola and 27% for Namibia.

The total number of all pans is 190,623, making an average of 10.4 pans per square kilometer. There are fewer pans in Angola (84,755) than there are in Namibia (106,089 pans). Likewise, the ratio of pans per square kilometer differs between the two states from 9.7 to 11.0, respectively (Tab. 3-1).

Table 3-1: Pan statistics listed by region: total Iishana system, Namibian territory, and Angolan territory.

		Surface Area (m^2)	Volume (m^3)	SA/V (m^{-1})	Depth (m)
Iishana system	Sum	4,021,400,469	1,877,297,618		
	Min	156	1	0.14	0.10
	Max	16,846,563	20,776,981	538.95	27.12
	Median	2500	612	4.16	0.24
	Mean	21,096	9848	5.20	0.29
	25%/Quartil	1094	254	2.75	0.16
	75%/Quartil	7656	2073	6.43	0.36
	sd	172,681	135,574	4.84	0.14
	Skew	38	63	29.49	62.65
	pans count: 190,623	pans/km^2 = 10.4			
Angola	Sum	2,355,694,219	1,259,943,689		
	Min	156	5	0.60	0.10
	Max	462,969	120,579	102.40	19.26
	Median	1875	568	3.48	0.28
	Mean	6207	1879	4.84	0.33
	25%/Quartil	781	188	2.02	0.17
	75%/Quartil	6094	2153	5.47	0.43
	sd	154,864	129,934	46.84	0.15
	Skew	27	44	143.53	47.92
	pans count: 84,755	pans/km^2 = 9.7			
Namibia	Sum	1,989,113,125	706,824,881		
	Min	156	<1	0.14	0.10
	Max	13,075,313	6,055,795	538.95	27.12
	Median	2656	567	4.55	0.22
	Mean	18,749	6663	5.60	0.25
	25%/Quartil	1250	236	3.12	0.15
	75%/Quartil	8438	2048	6.84	0.32
	sd	126,195	58,909	5.13	0.13
	Skew	40	43	32.58	43.47
	pans count: 106,089	pans/km^2 = 11.0			

The size of the smallest pan in both states is 156.25 m² and is valid as the smallest value for the entire study due to the methodological approach (raster resolution 12.5 × 12.5 m). The largest pan, with an area of around 16.8 km², lies in the Angolan territory. For Namibia, the largest pan is about 13 km². This size imbalance can be further observed in how the mean values and median values differ considerably, pointing to a skewed distribution. When looking at the entire study area, the mean area of pans is 21,096 m², while the median is 2,500 m². Similarly, the values of Angola show a mean of 23,978 m² and a median of 2,343 m² while the Namibian territory shows mean and median values of 18,749 and 2,656 m² (Tab. 3-1). These strong divergences between the mean and the median values result from a large number of small pans and a much smaller number of large pans, defined as outliers (Fig. 3-8).

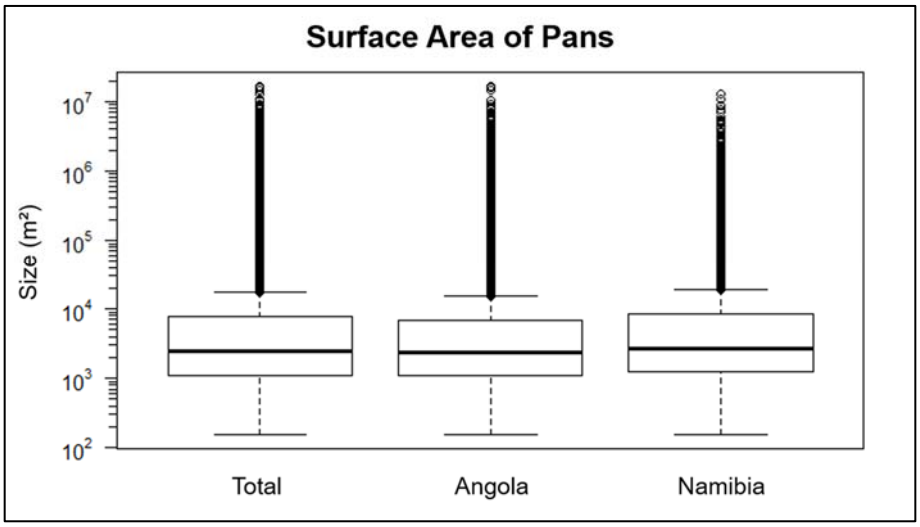

Figure 3-8: Surface area of pans in total, for Angola, and for Namibia, indicating the enormous number of outliers.

A comparison of the spatial distribution of the pans (Figs. 3-6 and 3-7) shows that on the Angolan side of the Iishana system there are fewer pans than there are on the Namibian side. For all three regions (the entire Iishana system, the Angolan portion, and the Namibian portion), the statistics show unimodal right-skewed distributions (Tab. 3-1). These are characterized by strong outliers (e.g., particularly large areas and all areas to be assigned to the right-skewed area are smaller) (Fig. 3-8). Furthermore, there is a lower density of pans in Angola (Tab 3-1). However, pans on the Angolan side are, on average, larger than those on the Namibian side. This is particularly evident along the more elevated areas in the north and

west, as well as in the southwest (Fig. 3-6 and 3-7 FA 1) and in the northeast portion of the study area, which extends to the city of Oshakati (Fig. 3-7 FA 2). The southern part of the study area is characterized by numerous, small pans that are not connected to the drainage network (Fig. 3-7 FA 3).

3.3.2. Depth

The depths of the pans range from 0.1 to 27.12 m throughout the Iishana system (Tab. 3-1). The lowest depth is limited to 0.1 m according to the methodological approach. It is also the most common value in both subareas, Angola and Namibia. Therefore, in Figs. 3-6 and 3-7 a fixation to a limit of 0.21 m was made for visual reasons. All values up to a depth 0.20 m were disbanded in order to better identify relevant information. The deepest value of 27.12 m was identified on Namibian territory; the deepest value on the Angolan side is 19.26 m (Tab. 3-1).

The median and average depths for the entire area are 0.24 and 0.29 m. In the country-specific calculations, these values differ just slightly, although pans on the Namibian side are often shallower (Tab. 3-1). A similar picture emerges when looking at the quartiles: the vast majority of pans are very shallow, with depths of less than half a meter. When looking at the maximum depth values, it must be taken into account that borrow pits (Fig. 3-1c) result in higher depth values (yellow areas in Fig. 3-7 FA 2).

3.3.3. Volume

The total volume of all pans was approximately 1.9 km³ and thus, as an example, corresponds to less than 0.1% of the volume of Lake Victoria, which measures 2,424 km³. It is striking that about 67% of the total calculated volume is allocated to the Angolan side and only 33% of the total volume is attributable to the Namibian territory. The volumes of individual pans range from 0.1 to 12,642,002 m³, with the largest pan volume being located in Angola. By comparison, the largest Namibian pan has a volume of about 6,055,794 m³ (Tab. 3-1).

The median and mean values of the pan volumes also differ from one another. For the entire study area, the median value for volume is 612 m³, whereas the mean value is 9,848 m³. A comparison between the pan volumes in Angola and Namibia shows that the median and mean values for Angola (668 and 13,810 m³) are considerably larger than those for Namibia (566 and 6,662 m³). From the 75% quartiles, it is obvious that the majority of pan volumes is lower than approximately 2,100 m³. Pans with a larger volume span from around 2,100 to 12,642,002 m³. The bottom line is that the volume of pans in Angola is about twice as large as the volume in Namibia.

3.3.4. Surface Area–Volume ratio

The SA/V value (ratio between the area and the volume of the pans) is an important metric to assess the water storage function of pans (Figs. 3-9 and 3-10). In deep pans with a small surface area, water loss by evaporation is much slower than in large, shallow depressions. For example, a reduction of 20% of the surface area results in a 20% reduction of evaporation (McJannet et al. 2008).

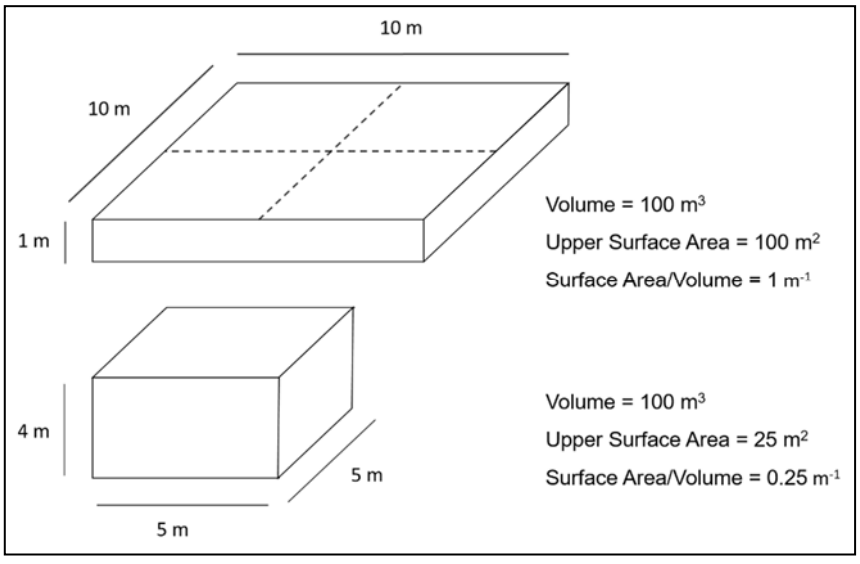

Figure 3-9: Surface area–volume ratio, after McJannet et al. (2008).

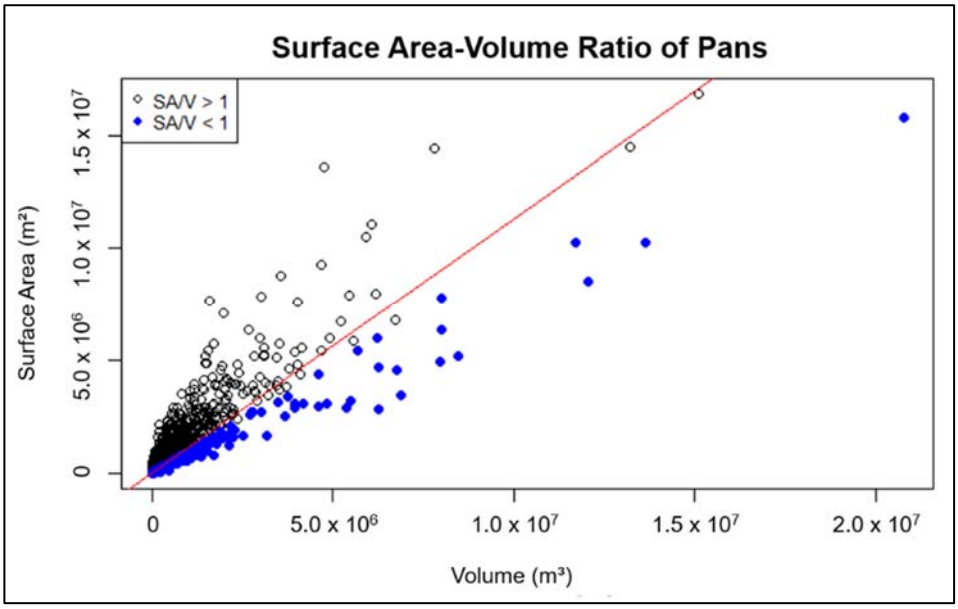

Figure 3-10: Surface area–volume ratio (SA/V) of all pans. Blue dots indicate the most suitable pans for enlargement.

The lowest SA/V ratio in the Iishana system is 0.14 m^{-1} and the highest ratio is 538.95 m^{-1}, both extremes are found on the Namibian side (Tab. 3-1). In the Angolan region of the study area, the lowest SA/V ratio is 0.60 m^{-1} while the highest value is 102.40 m^{-1}.

The overall assessment of the SA/V ratios indicates that the rates for the Angolan side are lower than those for the Namibian side, and so the problem of water loss due to evaporation has a bigger impact in the Namibian region.

Presuming that an optimum SA/V ratio is ≤1 m^{-1}, (McJannet et al. 2008) all values labeled blue in Fig. 3-10 show the most qualified pans for potential artificial enlargement to increase the storage function. Under this condition, 2,176 pans were identified as suitable for augmentation.

3.3.5. Example and synopsis

As a specific example, the water filled pan of an Oshana next to the small village Iipopo is used as a natural flood water harvesting measure (Fig. 3-5 a, b). Water is stored during the

rainy season and provides a resource throughout the dry season for irrigating cash crops like tomatoes (Bischofberger et al. 2016). The plantation is marked with a black rectangle and the remaining body of water is framed with a red polygon, both visible in Fig. 3-5 b, c, e. Picture (a) in Fig. 3-5 was taken at the end of the dry season in September 2017 and shows the remaining water stored in the pan (Fig. 3-5 a, b). A few months later in March 2018, after the rainy season, the pan dried out completely (Fig. 3-5 d, e). This was the result of little rainfall during the wet season of 2017/2018, which was a continuation of a 3- to 4-year-long drought period. This drought did not end until the rainy season of 2019/20.

The processed drainage network (D8-algorithm) and the cumulative flooded area in Fig. 3-5 c shows that the floodwater typically fills all pans and the Iishana up to a certain point, depending on the amount of precipitation that has fallen in Angola and Namibia during the rainy season. This case clearly demonstrates that the priory calculated pans (Fig. 3-5 c) match when compared to the water surface area validated in September 2009 (Fig. 3-5 a, b). Additionally, the MWE (Maximum Water Extent Mask) verifies that the results are correct.

Regarding the metrics of the pans, about one-third of the total and both the largest and deepest pans are located within potential flood plains and in the ephemeral runoff trajectories of the Iishana system. There are fewer pans, both by total number and per km², in Angola than there are in Namibia. In contrast, the Angolan part of the region represents slightly more than two-thirds of the potential total volume of 1.9 km³. This difference is also reflected in lower SA/V rates and, on average, slightly greater depths of the pans on the Angolan side. However, both sub regions and the entire study area are similar in having strong outliers in terms of area, size, volume, and depth, and thus they are all characterized by unimodal right-skewed distributions (Tab. 3-1).

3.4. Discussion

3.4.1. Error analysis

As noted by Ngula Niipele & Chen (2019), currently, no standardized validation procedures exist for the accuracy assessment of extracted discharge networks. Therefore, all methods applied must always consider the specific landscape characteristics of the individual study area, as well as those of the basic data used. This also applies to the current validation methods of pans.

Looking at the DEM data, possible errors can be found in the backscatter behavior of the radar signal. Rizzoli et al. (2017) describes a weak backscatter behavior on sandy surfaces, which could be improved by increasing the angle of the emitting sensor. Thus, the predicted error rate of all pixels for the global model could be reduced from 3% to 0.1%. Furthermore, a vertical accuracy of 2 m with a confidence interval of 90% is given. In the range of 50%, an accuracy of 1 m is given. This accuracy is remarkable, but it still casts a critical light on the results of the volume calculation here; minimal deviations can cause a significant volume change. Currently, a quantification of this potential error is not possible.

Moreover, it must be determined whether very small elements (e.g. pan 156 m²) are true pans or just errors resulting from water-induced interferences. In this study, the DEM preprocessing was based on an approach published in a preliminary work (Arendt et al. 2020) in which algorithms for hydrographic modeling were well established and considered accurate. As such, we believe that an accurate result for the spatial characteristics of pans was derived, especially considering that the topographic setting in the Iishana system allows for such small pans. Additionally, the ground truth control points, although few in number, confirmed these results.

Mendelsohn et al. (2013) emphasize that the northern Cuvelai Basin (in Angola) consists of broader channels while the southern part of the Iishana system consists of many smaller pans

measuring less than 100 m², traditional hand-dug wells, surface dams, and smaller ponds. Furthermore, Hipondoka (2005) describes the amount of pans as innumerable, and their size in the southern parts as minor due to the low topography. Additionally, Zimmermann (2013) describes these small ponds as having diameters of 4–5 m and depths of 8–9 m and small SA/V ratios. These smaller ponds would not be detected as natural pans due to the raster resolution. Therefore, the results only show the natural pans described by Mendelsohn et al. (2013) and Hipondoka (2005) and not the small artificial pans. Here the advantages of DEM resolution can be seen.

Other inaccuracies may occur in the generalization of pixel groups. The grouping of pixels (clustering) helped to reduce the enormous number of individual small pans measuring 156 m² (i.e. area covered by one pixel in the DEM). According to Mitchell (1999), this approach has advantages and disadvantages, which have to be considered during the evaluation of the results. The advantage is the reduction of outliers as well as the connection of pixels that actually belong together, which were separated due to the mixed-pixel effect. On the other hand, pixels that do not belong together may also be erroneously connected. However, since the advantages of this approach outweigh the reduction of outliers, this method was used in preprocessing.

The calculated flow paths and the MWE mask fit well together and have a high level of agreement. Therefore, reliability is high for the flow path analysis (Figs. 3-6 and 3-7).

The validation of the calculated pans, with the help of the identified flood areas, should also be viewed critically. This method increases the probability of the occurrence of a pan, but it does not show it in detail. Only validation by ground truth control, e.g., with photos, provides security. Nevertheless, the validation procedure shows a high degree of accuracy, as the result in section 3.3.5 shows (Fig. 3-5). Additionally, this method provides the best performance in rural areas.

3.4.2. Function as a water resource

The transboundary region suffers simultaneously from a poor socioeconomic performance and a high frequency of natural hazards, namely floods and droughts. Moreover, resilience in regards to climate change is insufficient (Luetkemeier et al. 2017; Kapuka 2020). Studies have shown that Namibia has more pans, in total, than Angola does, but those Namibian pans have less volume. Just one third of the total volume of pans belongs to Namibia. Additionally, individual pans with the largest volumes all appear in Angola. Considering the heightened ecosystem stress due to climate change with less precipitation, higher evapotranspiration and a growing population on the Namibian Iishana system, efforts should be undertaken to artificially deepen these natural reservoirs to sustain the people's resilience. However, how to start this approach?

In the past, efforts have been made to push the concept and implementation of rainwater-harvesting techniques, especially rooftop harvesting in rainwater tanks (Woltersdorf et al. 2015; Sturm et al. 2009). However, these are expensive for a rural population living under subsistence economy conditions. A rainwater-harvesting tank costs anywhere from USD 460 to 870 for a 10 m³ tank, depending on the material (Sturm et al. 2009). Meanwhile, many older, man-made depressions are no longer in use (Zimmermann 2013). Therefore, the answer to the water resource question should be to reactivate the man-made depressions. This approach will be cheaper because no costly material is required for construction. To implement this plan, selected pans would have to be identified and deepened (excavated) as retention measures. The SA/V ratio could be an essential factor in the analysis for identifying suitable pans for enlargement. It is clear that these natural pans play a major role now and in the future in supplying the local population and livestock with water.

Additionally, the differences in the pan depths indicate that the process of linear surface runoff dominates on the Angolan side of the study area. As the distance to the Etosha Pan

decreases, the ground slope also decreases, leading to a prevalence of extensive surface runoff.

It can be concluded that the deeper, linear forms in Angola are maintained by flood runoff while the shallow forms in Namibia are, perhaps, mainly filled during flood events. This is a question to be analyzed in future research. Consequently, the fluvial-morphology determines and affects the available water resource in the different parts of the study area.

Furthermore, one third of all pans are located in the inundation zone, making these spots major priority locations for enlargement. The use of the above-mentioned retaining measures on these pans would provide both flood protection and water storage capabilities. These priority locations would be filled by precipitation and floodwater, thus increasing the ability for water storage and enhancing the resilience of the rural population.

Accordingly, enlargement should be performed on pans that meet the following criteria:

(1) Pan must be close to a location with a high demand for water/flood protection;
(2) Pan must be primarily connected to the channel network within an inundation zone;
(3) Pan needs a low SA/V-ratio to counter the problem of high evaporation rates.

For the pans in the southern part of the study area, the situation is different. Here the pans are filled mostly by precipitation. Surface runoff usually finds no entry into the depressions, since these are often geomorphologically encapsulated (section 3.2.1). Therefore, it is proposed that these isolated pans be opened and connected via the calculated flow paths to enhance the probability that they will be filled during rainfall and surface runoff events. This can boost the water volume to better meet the increased water demand. Up until this point, this concept has only been applied for smaller, hand-dug pans in the northern regions (Zimmermann 2013).

3.5. Conclusions and outlook

Ephemeral rivers and numerous natural and artificial depressions hydro-morphologically characterize the semiarid and transboundary Iishana system between southern Angola and northern Namibia. A high inter- and intra-annual variation of precipitation regularly leads to floods and also to severe droughts.

Therefore, the aim of this work is to increase the resilience of the local people's livelihood by identifying suitable pans for expansion as intermediate storage. These pans will reduce the flood peak and provide water for drier periods.

The identification of the pans in this very topographically flat region was a great challenge. Therefore, a new strategy for processing the TanDEM-X elevation model was developed and applied in combination with a modified Blue Spot Analysis.

The validation of the results was done with the help of calculated flood masks. Additionally, photos were taken during a field trip to verify the ground truth. Thanks to the double validation approach, reliable statements could be made despite less available data.

More than 190,000 pans were identified. The total potential volume of these pans was determined to be 1.9 km³, with the Angolan territory accounting for about 2/3 of the volume and the Namibian territory only accounting for about 1/3. The total surface area of all pans is 4,021 km². This means that about one fifth of the entire region is covered by pans. A distinction between artificial and natural pans could be made by calculating the mean depths. It was shown that the pans are very shallow, measuring barely 30 cm deep on average. At the same time, however, there are also numerous outliers with significantly greater depths (Fig. 3-10), which will be the focus of investigation in the following work. Additionally, about one third of all pans are located inside the ephemeral flow paths.

Furthermore, the hydro-morphological differences of the pans between the northern area (Angola) and the southern area (Namibia) described in the literature can be confirmed

(Mendelsohn et al. 2013; Zimmermann et al. 2013; Hipondoka 2005). In depth, width and volume, the pans in the northern region are larger than those in the southern part of the Iishana system. In addition, the hydro-morphological characteristics of numerous small, isolated depressions in the very south can be confirmed.

In order to identify pans as potential water reservoirs, a further parameter was determined. The surface area–volume ratio takes into account the volume coupled with the surface of a pan and thus provides an important indication of the natural storage time of the water in the system with regard to the high evaporation rates in this region. With the help of these calculations, more than 2,000 pans were identified and could be considered for potential further enlargement.

A prioritization procedure should be applied for the selection of potential sites. According to the criteria described in section 3.4.2, potential sites should first be selected according to their distance from a settlement structure with increased water demand. In addition, the selection of the site should be based on its connection to the channel network in order to increase the probability of filling by flood or precipitation water. Non connected pans should at least be as close as possible to a drainage system in order to be artificially connected to it. To make the implementation worthwhile, the surface area of the pan should be large enough and, at the same time, should have a SA/V ratio smaller or equal to one.

Currently, a validation of the calculated volumes is missing. UAV flights were planned for April and September 2020. Using the Structure-from-Motion method, accurate 3D models of selected pans should be created, and the volumes calculated and compared with those derived from the DEM. Due to the COVID-19 pandemic and the resulting travel restrictions, this project has to be realized in the future.

For the first time in the literature to date, this investigation drew a detailed morphometric picture of the pans within the Iishana system. The relevance of this work is further demonstrated by the key characteristics of distribution and shapes as well as sizes and volumes. Especially with regard to climate change, this work provides initial answers for future

work on flood protection and water storage for years of drought, which should be a priority task to protect the local people's livelihood and enhance their resilience.

3.6. Acknowledgments

We thank the German Aerospace Centre (© DLR 2017) for their delivery and support with the TanDEM-X data (Proposal ID: DEM_HYDR1285). ALOS/PALSAR and ALOS-2/PALSAR-2 data are kindly provided by JAXA (Proposal number MTH 1153, PI number 3043). We are grateful for the collaboration with the University of Namibia (Campus Ongwediva).

3.7. Funding

The publication of this article was funded by Freie Universität Berlin.
This project was cofounded by the Geo.X-plattform and the Deutsche Hydrologische Gesellschaft.

4 Hydrodynamic modeling of ephemeral flow in the Iishana channel systems of the Cuvelai Basin - Northern Namibia

Abstract

The transboundary region of the Iishana system in the western Cuvelai Basin, between southern Angola and northern Namibia, is frequently affected by floods at irregular intervals. As a result, the predominantly rural, subsistence farming population experienced crop failures, human and economic losses. To date, very little is known about the generation of floods, flood concentration, and stormwater drainage dynamics in this region.

Therefore, in order to intensively study the runoff behavior and interconnectivity of the Iishana system, 2D-hydrodynamic modeling was used to reconstruct one of the latest major flood events during the rainy season from November 2008 to March 2009. The model focused on the eastern part of the Iishana system, which was most affected by floods and flood damage due to the high population density in and around Oshakati, the regional capital.

Two main streams were identified noteworthy because they merge and subsequently affect Oshakati. Water depths vary from 0.1 m to 14 m, with an average of 0.2 m, while water depths above 5 m were attributed to borrow pits. The inundation area ranged up to 1,860 km² and the amount of water left after the rainy season was determined between 0.116 km³ and 0.547 km³, depending on the amount of evapotranspiration (ET) considered in the model. Thus, in the Angolan part of the Iishana system, significantly larger quantities of water are available for longer periods of time during the subsequent dry season, whereas the system in Namibia stores less water, resulting in a shorter water retention period.

4.1. Introduction

This study focuses on the transboundary Cuvelai Basin between southern Angola and northern Namibia, specifically the Iishana system in its western region (Fig. 4-1 & 4-2). This area has

been the major focus of a broader research project dealing with the issues of floods, droughts, and water quantity and quality (Arendt et al. 2020 & 2021; Faulstich et al. 2018). Ephemeral and endorheic river channels, also known as Oshana (plur. Iishana), characterize this distinct region. They are shallow, net-like waterways with thousands of natural depressions and smaller pans embedded in the channel system (Ngula Niipele & Chen 2019; Luetkemeier et al. 2017; Persendt & Gomez 2016; Shifidi 2016; Awadallah & Tabet 2015; Goormans et al. 2015; Mendelsohn et al. 2013; Zimmermann 2013; Kluge et al. 2008; Cunningham et al. 1992). The area around the Iishana system has more fertile soil than other regions nearby (Persent & Gomez 2016). This leads to a high population density, which is still increasing (NamStat 2013).

During the rainy season between October and April, small flood events typically replenish the channel system (Fig. 4-1), which is greatly needed after a regular dry period. These floods are exacerbated by the flatness of the landscape in Northern Namibia unlike Southern Angola which has hills and mountains. This causes the water to flow from north to south and floods in Namibia are intensified by local convective precipitation. They bring fish, deliver water for agricultural, livestock, and domestic use and fill natural and artificial reservoirs (Arendt et al. 2021; Seely et al. 2003; Cunningham et al. 1992).

Figure 4-1: Northern Namibia, border region, left: large shallow inundated areas, right: flooded sorghum fields of a kraal.

Nevertheless, drought events can occur when the rainy season is too weak. Such events occurred in the late 1980s and mid-1990s. In more recent years, very frequent droughts

transpired between 2013 and 2019, with the exception of 2017 (Luetkemeier et al. 2017; Kerdiles et al. 2015; Seely et al. 2003).

On the other hand, major flood events occurred in 2008, 2009, 2010, 2011 and 2013, causing fatalities, the loss of livestock and crop yield, and damage to property and technical infrastructure (Arendt et al. 2021; Bischofberger et al. 2016; Shifidi 2016; Awadallah & Tabet 2015; Persendt et al. 2015; Filali-Meknassi et al. 2014; Mandl et al. 2013; Mufeti et al. 2013; Skakun et al. 2013).

Different studies on the Cuvelai Basin have tried to reconstruct past flood events by mapping their extents via time series satellite images or the application of different sensors (radar and optical) (Awadallah & Tabet 2015; Skakun et al. 2013; De Groeve 2010; Müller et al. 2018). Most studies attempted to forecast the probable extent of a flood event and show areas of high risk, but they accomplished this using a very coarse spatial resolution. Moreover, some studies did not include the transboundary aspect of the basin or the Iishana system (Awadallah & Tabet 2015; Skakun et al. 2013; De Groeve 2010). De Groeve (2010) established a real-time flood monitoring approach aiming to detect the beginning of flood events, but it offers no ability to predict further flood routing. Moreover, Mufeti et al. (2013) assembled a rainfall-runoff model for the 2009 flood event. The model delivered no information about flood inundation, but it did estimate the streamflow output based on a 90 m resolution SRTM digital elevation model.

The research by Goormans et al. (2015) reported the first approach using hydrodynamic flood modeling coupled with a hydrological model in the Iishana system. Focusing just on the boundary (approx. 20 km x 30 km) of the City of Oshakati (regional capital), they merged a 90 m resolution SRTM, a 50 m resolution DTM generated from aerial photographs, and a 5 m x 5 m LIDAR DTM as a base for further calculations with InfoWorks RS v10.5 (Innovyze Ltd, UK). Their aim was to calibrate the model with the help of the 2011 flood event. On that basis, they created a design flood to benchmark the local government's plans to construct a dike and diversion channel to protect the city of Oshakati against future floods.

So far, analysis of the area has ranged from rapid satellite and topographical-based screening to a first, small-scaled hydraulic and hydrodynamic assessment (Müller et al. 2018; Tyrna et al. 2018; Awadallah & Tabet 2015; Goormans et al. 2015; Skakun et al. 2013; De Groeve 2010). However, there is no 2D-hydrodynamic assessment of the total Iishana system, nor is there a transferable model approach available yet.

Therefore, the aim of this study is to generate information about flood routing in order to understand the interconnectivity of the Iishana system as well as the related filling of the Iishana depressions, which serve as an important water source for the rural population. Describing the runoff processes in the Iishana system, the model outputs provide metrics about inundation depths at different times during the rainy season and the amount of water remaining at the season's end. The model can be used for scenario calculations of future floods.

4.2. Materials and methods

4.2.1. Study area

The study area is part of the Iishana system located in the western part of the transboundary Cuvelai Basin (Fig. 4-2). The Iishana system covers an area of 18,370 km² and is characterized by a high population density (Mendelsohn et al. 2013). About 1.2 million people live in this area (34% in Angola and 66% in Namibia) (Persendt & Gomez 2016; Mendelsohn & Weber 2011). The study area itself is located in the eastern part of the Iishana system and has an area of 4,600 km². Here, in the far south, the town of Oshakati represents the main developing center of the region. The study area is semi-arid, being influenced by the cold Benguela Current and the Inner Tropical Convergence Zone (ITCZ). Precipitation increases from west to northeast from 350 to 950 mm a year. Evaporation rates increase along the same west-east gradient from 2,600 to 3,200 mm/a. The rainy season lasts from October to April, but it is most prominent from December/January to March. A high intra- and interannual variability in precipitation is

characteristic, which in consequence regularly brings floods and droughts (Gaughan et al. 2016; Shifidi 2016; Reason & Smart 2015; Kundzewicz et al. 2013).

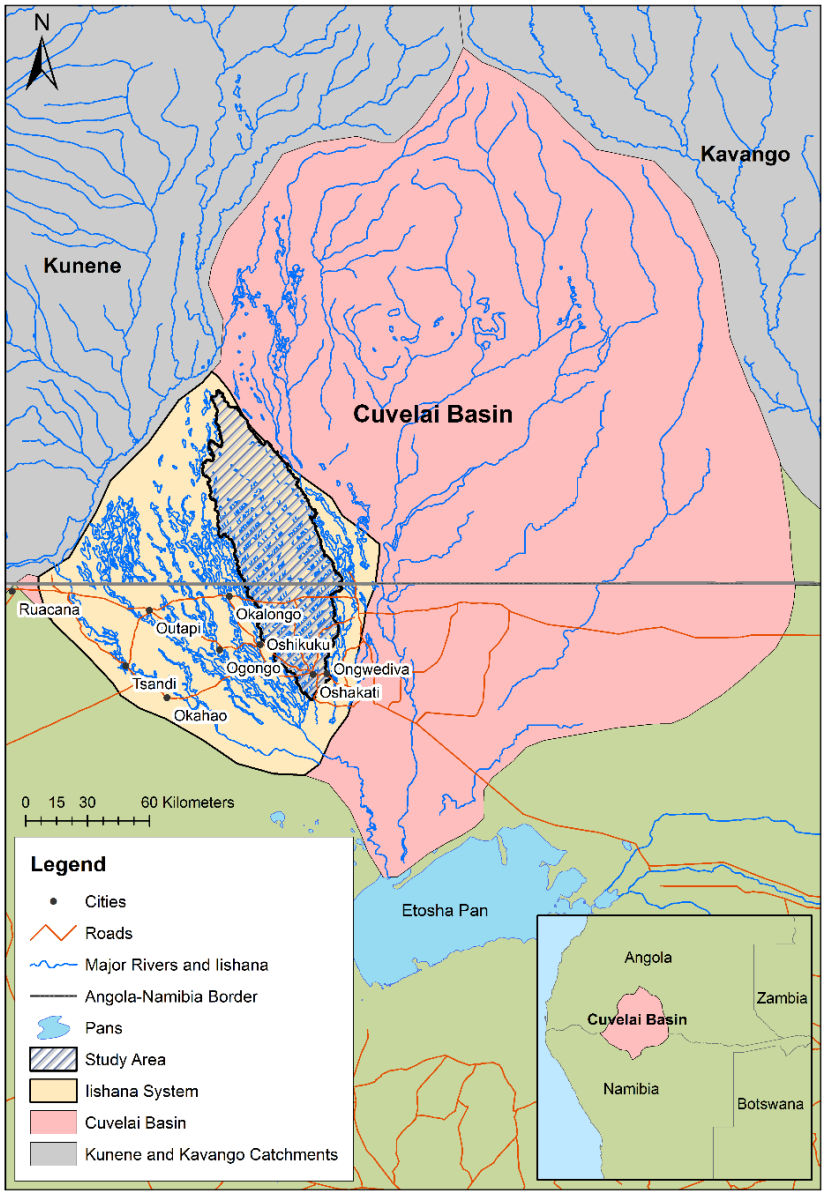

Figure 4-2: Map of the study area – model catchment, database: Digital Atlas of Namibia (2016); UN-OCHAROSA (2018).

The topography is flat with an elevation of approximately 1,200 m to 1,100 m and a northwest southeast gradient of only 0.5 ‰ to 1 ‰ (Mendelsohn et al. 2013). The surface hydrology is dominated by a diffuse network of shallow endorheic and ephemeral channels (Iishana), which run from northwest to southeast and ultimately drain in the Etosha-Pan. The width of the Iishana channels varies greatly from hundred meter to over 1,750 m with depths ranging between 1 and 7 m (Ibid.). The elevated areas between the Iishana consist of Kalahari sands.

These areas are used for communal farming, crop production and rain-fed agriculture (subsistence farming). The lower and intermediate Iishana areas are dominated by aeolian and fluvial sediments (clay fraction), calcite and silicate crusts (Faulstich et al. 2018; Goudie & Viles 2015; Hipondoka 2005; Hüser et al. 2001). Shallow natural pans have formed in these areas, which fill with water during sufficient local precipitation or flood events. At these times of inundation, the pans connect with each other to form a unique and characteristic inland delta (Arendt et al. 2021; Persendt & Gomez 2016; Hipondoka 2005; Van Der Waal 1991). The majority of surface water comes from the Angolan side of the transboundary region, with flood events often being amplified or intensified by local convective rainfall events.

4.2.2. Hydrodynamic modeling

There are many different models available for a 2D-hydrodynamic simulation of flooding processes (Achleitner et al. 2020), such as HYDRO_AS-2D (Nujić 2016), TELEMAC-2D (Ata 2017), HEC-RAS 2D (Desalegn & Mulu 2021), P-DWave (Leandro et al. 2014), JFolw (Bradbrook 2006) and FloodArea (Tyrna et al. 2018). They all have their advantages and disadvantages and slightly differ from one another in what hydraulic equations are used, whether they are raster-grid or mesh-based, and if they are open-source, commercial, or freeware. Moreover, some of the models have a variety of additional functions, such as the ability to couple with an urban drainage system, or deeper modeling capabilities for runoff generation and vertical hydrological processes. In this study, the software package FloodArea11 was used. Developed by the geomer GmbH in Heidelberg (Germany), FloodArea11 is designed as an ArcGIS extension (geomer GmbH 2017) and able to calculate water depth and flow velocity. The calculation of flow velocity is based on the Gauckler-Manning-Strickler equation for uniform flow (Manning 1891; Strickler 1923). The advantage of FloodArea for our study is its ability to implement temporally and spatially varying precipitation. A second major advantage is the computationally less demanding Manning-Strickler approach, which allows a simulation of large areas with a long continuous time series. The Manning-

Strickler approach presumes that, under uniform conditions, the bottom slope (S) equals the slope of the energy grade line (Tyrna et al. 2018).

The average velocity (V) within the cells is calculated from the Strickler coefficient (Kst), which represents the surface roughness, the hydraulic radius (Rh), and the slope (S) according to Eq. 2:

$$V = K_{st} * R_h^{2/3} * S^{1/2} \quad (2)$$

To derivate roughness coefficients, a supervised land use classification was produced with a Sentinel-2B image acquired in October 2017. On this basis, Strickler roughness coefficients could be estimated using the standard table from Chow (1959).

The discharge rate for each cell is calculated by multiplying the velocity (V) by the cross-sectional area of each pixel.

Flat topographies can lead to low flow velocities and high dispersion rates, which cause unrealistic inundation patterns. Therefore, FloodArea uses the D∞ algorithm developed by Tarboton (1997) for flood routing. For this purpose, the flow direction is determined as the direction of the steepest slope on plain and triangular aspect and is expressed as a steady flow direction degree. Moreover, it distributes the flow to two neighboring cells and calculates the flow direction limited to 16 fixed angles. In this study, the hardware allowed for the calculation of 10 cores simultaneously and needed 24 days in total to complete the model run.

For digital elevation data, a TanDEM-X model was used. It provides a spatial resolution of 12.5 m and a vertical accuracy of less than 2 m in very flat regions (Rizzoli et al. 2017). Before it could be used for hydrodynamic calculations, it was corrected by eliminating outliers and interferences due to backscatter effects from water surfaces or other inconsistencies. In addition, significant artificial objects below DEM spatial resolution were included, such as roads, dams, culverts, and bridges. The exact procedure for the DEM preprocessing is described by Arendt et al. (2020 & 2021), Wessel (2016) and Wendleder et al. (2013).

4.2.3. Precipitation

For modeling the 2008/2009 rainy season, data from the Tropical Rainfall Measurement Mission (TRMM, 'TMPA-RT Near-Real-Time Precipitation L3 day 0.25° x 0.25° V7') was used. The study area is covered by 15 precipitation tiles. For each tile, a daily rainfall time series was generated from the raster data for the period between November 26, 2008 and March 25, 2009. The daily data were disaggregated, complying with the hourly modeling time steps required by FloodArea. Therefore, a uniform hydrograph assuming constant rainfall between 3 and 5 p.m. was used according to typical convective rain events close to the ITCZ (Fig. 4-3).

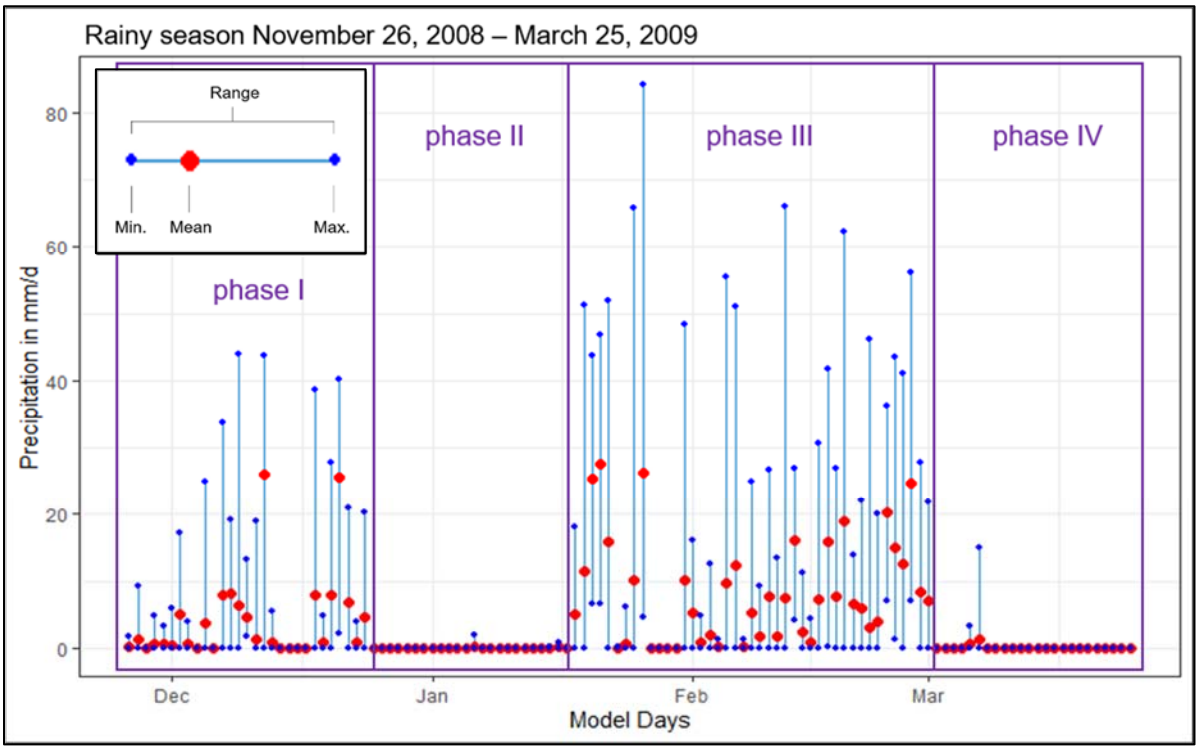

Figure 4-3: Summary statistics of the 15 TRMM precipitation raster cells covering the study area, including the four rainy and dry phases described in section 4.3.1.

4.2.4. Runoff generation

FloodArea simulates the flood wave propagation in the channel system. For the transformation of rainfall into runoff the SCS-CN method (USDA 2009) was used (Fig. 4-3 & Eq. 3).

$$S = \frac{1000}{CN} - 10 \quad (3)$$

$$Ia = S*\lambda \quad , \lambda = 0.1$$

$$, P > Ia = S*0.1$$

$$, P = 0; P < Ia = S*0.1 \quad (4)$$

$$P_{eff} = \frac{(P - Ia)^2}{(P - Ia) + S_{0.1}} \quad (5)$$

(Woodward et al. 2003, modified)

According to Woodward et al. (2003), a lower λ value of 0.1 was chosen to prevent an overestimation in runoff (Eq. 4 & 5).

As a first step, the hydrological soil groups (HSG) were extracted from the HYSOGs 250 m data set. This data set provides worldwide gridded hydrological soil groups for curve-number-based runoff modeling (Ross et al. 2018). To match the TRMM precipitation tiles, the data set was aggregated by a majority filter in ArcGIS. With this method, each tile received its dominant HSG. Likewise, a supervised land use classification was used to extract the major cover types. Afterwards, the curve numbers were calculated from USDA (2009) (Tab. 4-1).

To incorporate the different preconditions of soil wetness before each precipitation event, a further correction step was applied prior to every single simulation iteration. The antecedent soil moisture conditions (ASMC) are categorized into three levels after the style of Sobhani (1975), which can be found in Verma (2017) and can be seen in Tab. 4-1. With the SCS-CN method, the spatially distributed direct runoff for each time step was calculated and implemented in FloodArea.

Table 4-1: List of applied curve numbers according to the specification of hydrological soil groups, cover type, and hydrological condition for each precipitation tile. The CN values are further defined for each ASMC level from I to III (Antecedent Soil Moisture Condition).

Tile Nr.	1	2	3	4	5	6	7	8	9	10	11	12	13	14	15
HSG (Ross et al. 2018)	2 B	3 C	3 C	2 B	3 C	3 C	3 C	3 C	3 C	3 C	3 C	3 C	2 B	3 C	2 B
Cover Type (USDA 2009)	BG*	BG*	BG*	PG*	BG*	BG*	BG*	PG*	PG*	PG*	PG*	PG*	PG*	PG*	PG*
Hydrological condition	Good	Good	Good	Good	Good	Good	Good	Good	Good	Good	Good	Good	Good	Good	Good
Curve Number (CN) according to HSG and cover type (USDA 2009)	48	65	65	61	65	65	65	74	74	74	74	74	61	74	61
ASMC I	28	44	44	40	44	44	44	55	55	55	55	55	40	55	40
ASMC II	48	65	65	61	65	65	65	74	74	74	74	74	61	74	61
ASMC III	70	83	83	80	83	83	83	88	88	88	88	88	80	88	80

*BG: Bush-brush-forbs-grass mixture with brush the major element
*PG: Pasture, grassland, or range continuous forage for grazing

4.2.5. Evapotranspiration from water surfaces

If long periods and large areas are simulated in a study, evapotranspiration (ET) from the flowing water is an important factor that influences the model results. However, evaporation data are difficult to get in large basins with sparse observations. During the SASSCAL I program many meteorological stations were installed in the study area (Helmschrot & Jürgens 2015). However, data for potential evapotranspiration (ETp) is not available. Moreover, all of the stations were installed after the 2009 flood event. Alternatively, literature research provides information about estimated and measured ET and ETp values. A differentiation between these two terms is usually necessary during runoff formation, but when water evaporates from the river surface during the flow process, ET almost equals ETp. In an experiment on three different test sites in the Omusati region (north central Namibia), Kotani et al. (2017) quantified ET during the cultivation period with mean values ranging between 1.4 to 3.8 mm/d and maximum values of ET within a span of 5.4 to 11.2 mm/d. As one of the oldest values in literature, Cunningham et al. (1992) determined ETp from November to March in a range of 190 to 265 mm/month (6.1 to 9 mm/d). When downscaled to the exact time span of the model period, the ETp sum is 895 mm. Mendelsohn & Weber (2011) mention ETp sum of 760 mm from November to March with a daily mean ranging between 4.7 and 7.7 mm. Mendelsohn et al. (2013) sets 1,062 mm for the same time, giving daily mean values from 7.0 up to 10.3 mm. Külls (2000) calculated ET with a Class A pan in Grootfontein southeast of the Etosha Pan. It

resulted in a sum of 827 mm with daily means spanning between 3.8 and 8.4 mm/d (again downscaled to the model time). All research results have one aspect in common: they do not take into account the daily degree of cloud cover, which has a major impact in terms of ET, especially during the rainy season. Therefore, the work of Goormans et al. (2015) was referenced when considering ET. They use a pragmatic and engineering approach by assuming that ET is lower during precipitation events than afterwards. Thus, they make the assumption that no ET is considered on days with more than 2 mm of precipitation and an ET of 8.5 mm must be considered on days with less than 2 mm of precipitation. When this was downscaled and applied to the model time frame and precipitation data, a total sum of 612 mm ET was calculated with daily differentiated ET values reflecting the individual amount of daily precipitation.

There is not an option to consider ET directly in FloodArea during the model run, so ET was subtracted afterwards from the model output water depth layer (Fig. 4-4).

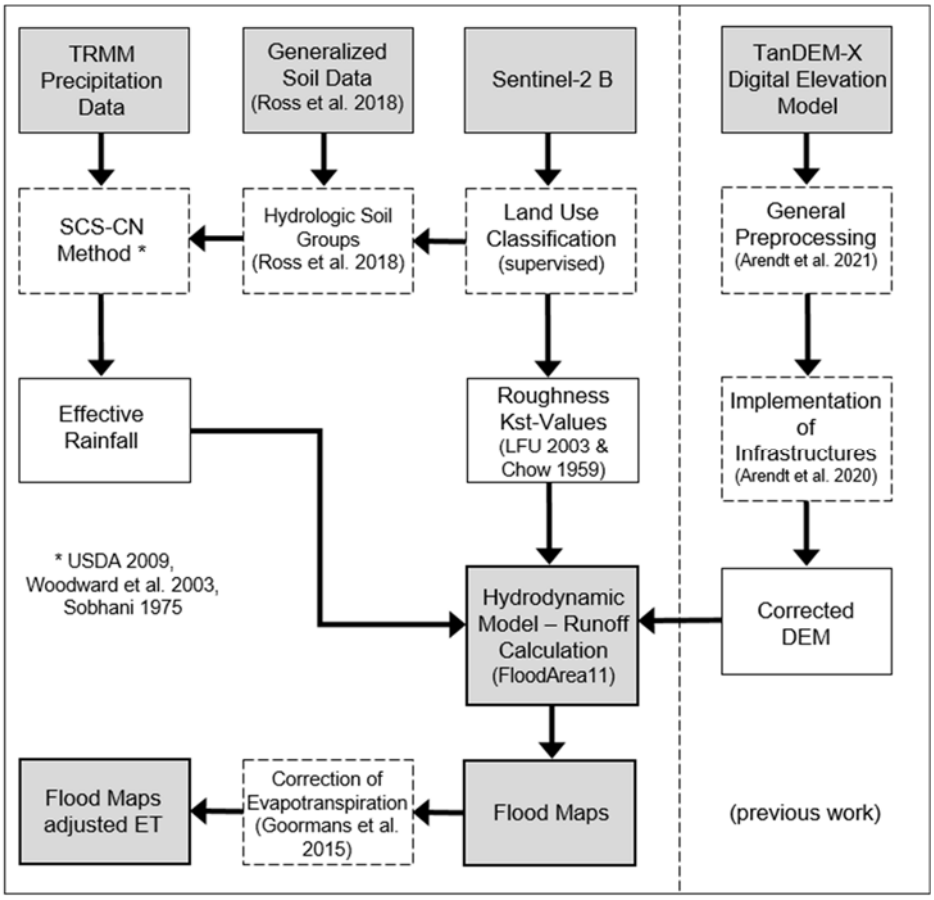

Figure 4-4: Process of data preparation and calculation. Grey boxes: model input/ output data. Dashed boxes: processing steps. White boxes: intermediate products.

4.3. Results

4.3.1. Rainfall characteristics

For the description of the 2008/2009 rainy season flood dynamics, precipitation must first be examined in detail (Fig. 4-4). It is noticeable that the precipitation can be segmented into four phases, which ultimately influence the runoff behavior (Fig. 4-3):

(I) The first phase lasts, with a small interruption, from the end of November to the end of December 2008 and is characterized by persistent precipitation;

(II) This is followed by a phase with dry conditions, which lasts until mid-January;

(III) The second rain phase follows with longer lasting and more intensive rainfall than during the first phase. This phase is characterized by higher peak and daily precipitation values as well as higher average precipitation per day;

(IV) Precipitation decreases at the end of March and runoff lasts until the end of the model period on March 25, 2009.

With the onset of the rainy season in November/December 2008, precipitation occurred mainly in the west. One week later, precipitation also occurred in the northeast and east sections of the study area. At the same time, precipitation also affected areas north and south of Oshakati. The city surface remained dry at first.

4.3.2. 2D-hydrodynamic model results

Two videos are associated with the model results, which can be viewed via an online link provided in section 4.9. Both videos show the modeled surface runoff during the rainy season from Nov 2008 to Mar 2009 (Arendt et al. 2022). One with and one without consideration of evapotranspiration.

According to the rainfall characteristics, a diffuse picture of surface runoff emerges at the beginning of the modeling period, in which significant large scale channel flow is not

recognizable. Only from the 16th model day on (Dezember 11, 2008) larger and coherent surface water areas become apparent in the central and northern area, most with a max. 0.2 m depth. By the end of the first precipitation phase at the 30th model day, interconnectivity and flow processes between the individual Iishana start to become visible (Fig. 4-5 & section 4.9.). The larger Iishana and pans in the north, which were already filled at the beginning of the model period, continue to be filled. A main Oshana channel stands out very clearly, which runs from the northeast along the catchment boundary southward toward Oshakati. While it is wider in the northeast and filled with more water (depths up to 1 m), it becomes narrower in the southern course and is often filled with water only up to half a meter deep. This is joined by another smaller and more branched drainage channel coming from the central area. North of Oshakati, these streams fill the Iishana and pans in and around the city. Water depths range from 0.1 m to 1 m.

In the second, rain-free phase, the surface water drains increasingly towards the south while, at the same time, it accumulates in deeper depressions. The first flow processes come to a standstill. In some Iishana streams, interconnectivity is interrupted. Water levels generally drop to 0.2 m to 0.5 m. The larger individual depressions in the central and northern areas retain surface runoff with a depth of 1 m.

The third phase (second rain phase) begins with heavy rainfall. At first, the smaller but still prominent west-southwest running Iishana stream is reactivated and the precipitation water flows in a channelized manner westward past Oshakati to the south. A few days later, persistent precipitation also leads to increased accumulation of larger volumes of water in the pans in the central area (Angola). A similar pattern is observed in the northwest. The Iishana and pans overflow and reconnect with each other. Distinct flow processes are evident. The Iishana strand fed by the northern and central pans brings large volumes of water toward Oshakati. This is further enhanced by the eastern Iishana strand, which carries the largest volumes of water at this time. On model day 94 (February 27, 2009), the greatest water depths and widest inundations are reached (Fig. 4-5).

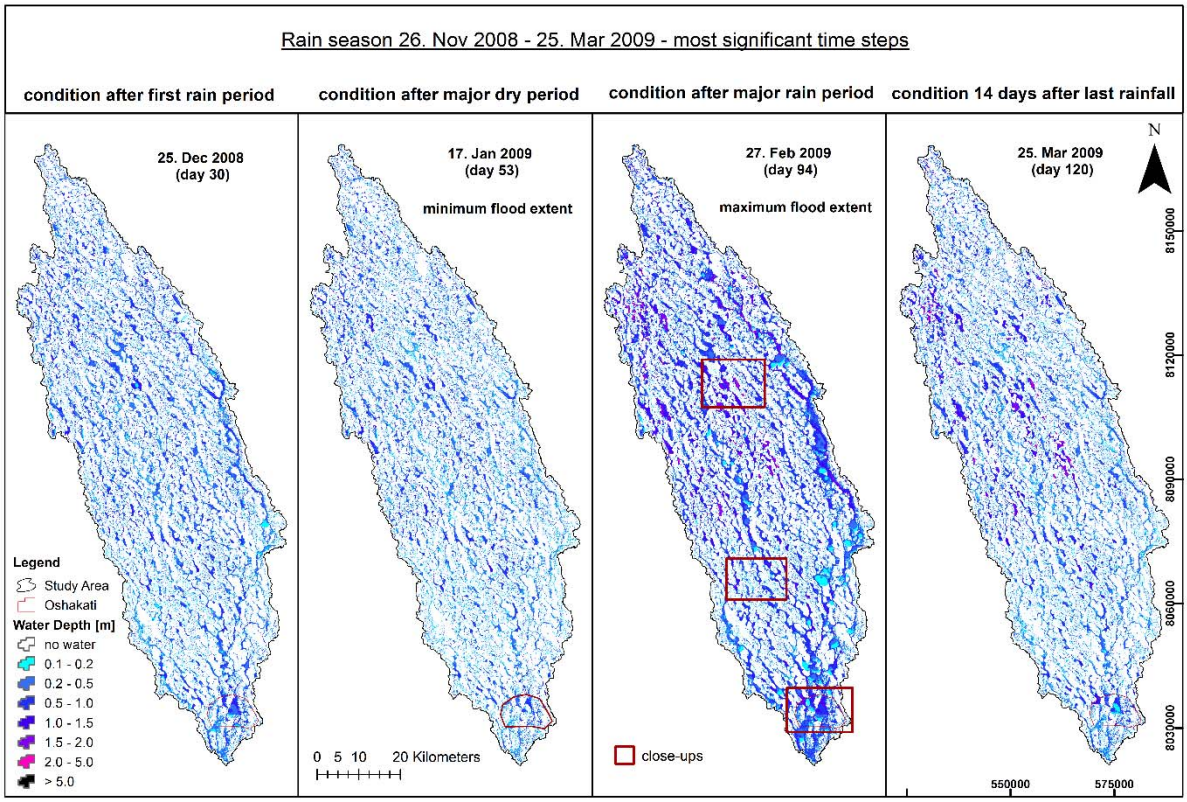

Figure 4-5: The four most significant time steps of inundation during the rainy season from Nov. 2008 to Mar. 2009. An enlarged version can be seen in the appendix (Fig. A-1).

Particularly large, deep, and isolated Iishana (Fig. 4-6 [1]), as well as borrow pits and interconnected Iishana, show very-high water levels since no overflowing has taken place yet. At some locations, water levels ranging from 2 to 5 m are reached. In some borrow pits, the water level also rises to over 5 m. At this point, the average water levels in the ephemeral systems are between 0.5 and 1.5 m.

Crossing the border region between Angola and Namibia, Iishana channels become narrower and take on the pattern of nearly straight lines. Due to the slender morphology of the channels, shallow bank overflows occur in some places with water depths of 0.1 to 0.2 m (Fig. 4-6 [2]).

For Oshakati and the surrounding areas (Fig. 4-6 [3]) channel overflow leads to larger flooding, including back water effects in topographically flat and urban areas. In these flood events, shallow depths of 0.1 to 0.2 m are observed. The estimated flow velocities in the study area are between 0.15 and 0.35 m/s. In particularly narrow channel areas, flow velocities of about 0.5 m/s can be reached. The respective flow velocities are impacted on the one hand by the

respective local gradient and on the other hand by obstructions, such as transverse structures (road dams and embankments).

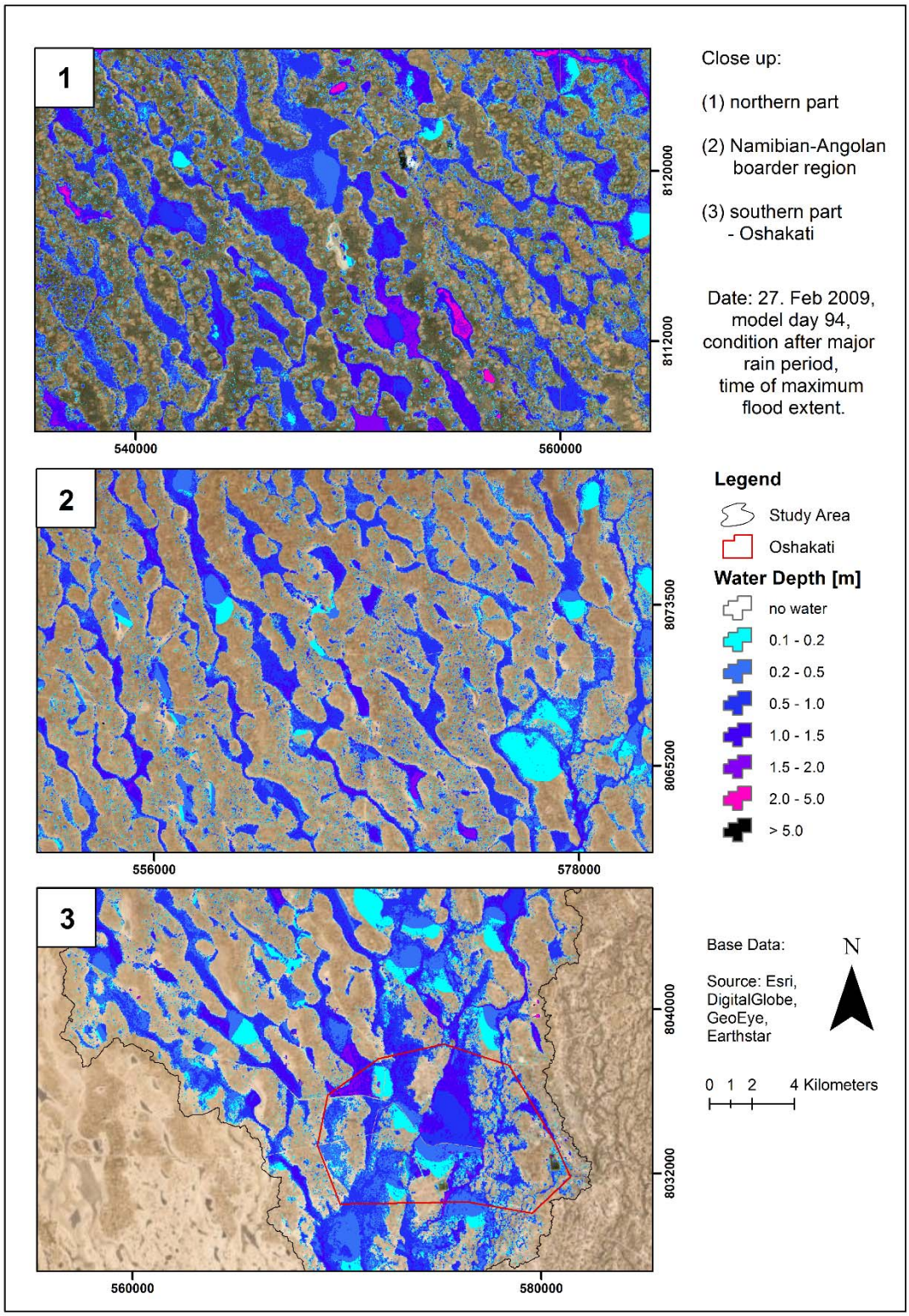

Figure 4-6: Close up of three representative inundation areas from the northern, central and southern part of the study area (also located in Fig. 4-5).

On March 07, 2009, the last precipitation fell during the rainy season (model day 102). March 25, 2009 was chosen as the final day to be evaluated, 14 days after the last rainfall event. In the picture rendered for this day, it can be clearly seen that the surface water flow between the Iishana is mostly disconnected. This is particularly noticeable on the southwestern Iishana strand. The city of Oshakati also experiences minimal flow from the northeast. Most parts of the city are largely dry and water is again concentrated in its original channel beds. Larger sections are now flooded only between 0.1 to 0.2 m in very shallow areas.

In the northern part of the catchment (Angola), wide and deep pans continue to retain larger amounts of water. On the Namibian side, some unconnected Iishana also remain as water reservoirs, while others run dry. South of Oshakati, there is no longer a backwater and the waters have drained further south toward the Lake Oponono area. At this point, the total discernible water volume is about 0.547 km³.

4.4. Evapotranspiration

Figure 4-7 compares two selected time steps, showing the study area with ET from the water surfaces according to Goormans et al. (2015) and comparing it with images of raw model data without ET (see Supporting Information). The first time step compares water levels and maximum inundation at the end of the first (rainfall) phase on January 17, 2009 (model day 53). The first image does not include ET while the second includes an ET of 450.5 mm to date. The next two images on the right (Fig. 4-7) compare the dry weather runoff at the end of the rainy season on March 25, 2009. One image shows no ET, and the other was generated with a total ET of 612 mm.

Without the inclusion of ET, the conditions after the major rain periods show more extensive flooding. In the model, heavy flooding and backwater effects are clearly visible. However, with the consideration of 450.5 mm ET, backwater effects no longer exist, with the exception of some smaller parts in Oshakati. Moreover, interconnectivity and continuous flow processes

are interrupted. The phenomenon of discontinuity on an Oshana mainstream in the southwest of the basin is very evident.

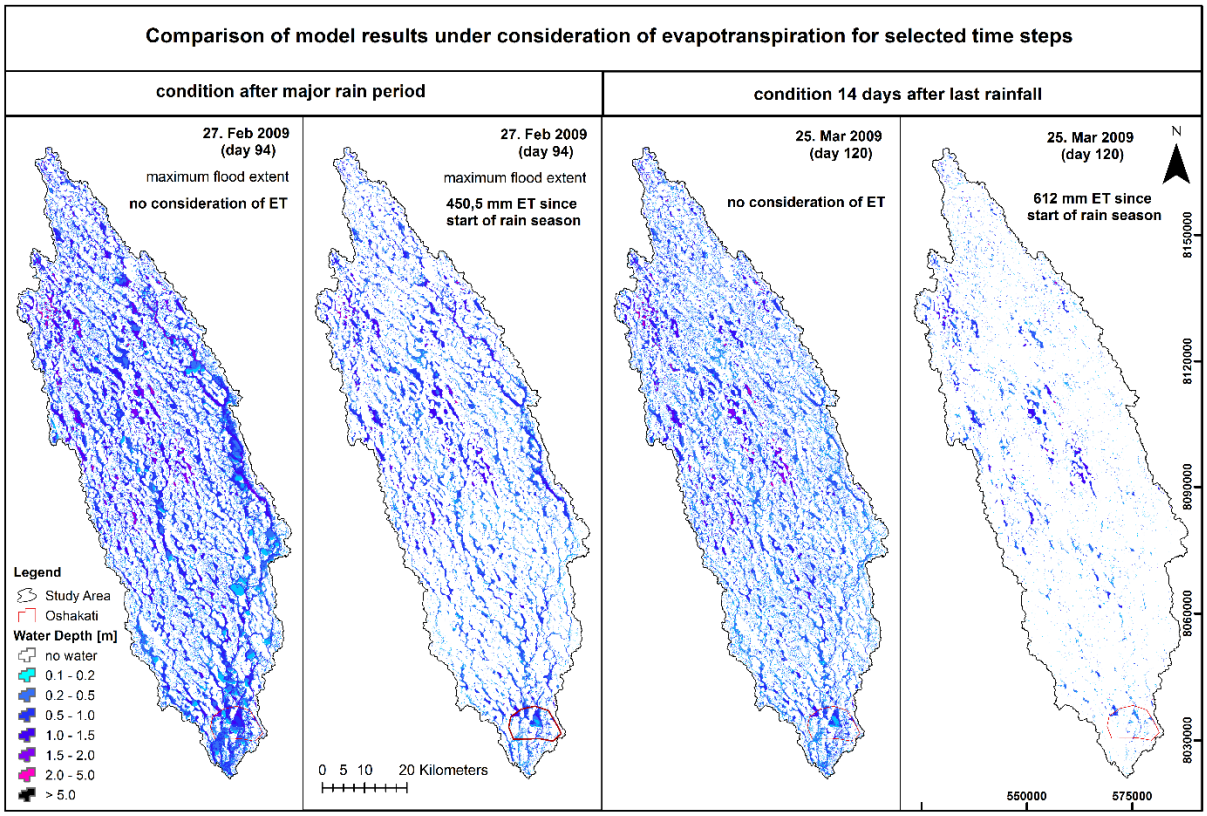

Figure 4-7: Comparison of the model results including and excluding evapotranspiration. An enlarged version can be seen in the appendix (Fig. A-2). Also watch for the Supplementary Information.

The model comparison of the runoff on March 25 including and excluding ET shows large differences in water volume. In the figure depicting the effects of ET, the interconnection and flow processes are completely interrupted. Only larger and deeper pans are retaining water. The flood event appears to be over. The Iishana are no longer overflowing.

The water volumes between the two figures for March 25 differ by a factor of 4.7. If ET is not included, the surface water volume amounts to 0.547 km³, while including ET with 612 mm results in a reduced amount of surface water, lowering it to a volume of 0.116 km³.

4.5. Discussion

Because of a lack of discharge and water level observations, only a tentative evaluation of the model outputs can be done based on the maximum extent of flooded areas extracted from

satellite images. During the rainy season, with its dense and frequent cloud cover, optical satellite data do not provide sufficient information and the extraction of flooded areas for specific dates is not possible. Therefore, to provide at least an estimate of the real flooding conditions, a combination of optical and radar satellite data provided by L. Beck (see Arendt et al. 2021 for details) was used. The data of the multi-temporal analysis represent a cumulative image in which every pixel was marked that was identified as being covered with water for at least one day between October 2008 and September 2009.

The comparison of model outputs with the reference data set is shown in Fig. 4-8.

The overlapping results are also symbolized in green. Accordingly, the spatial distribution of the flooded area corresponds to a match of 100% between the model result and the multi-temporal satellite image analysis (Fig. 4-8).

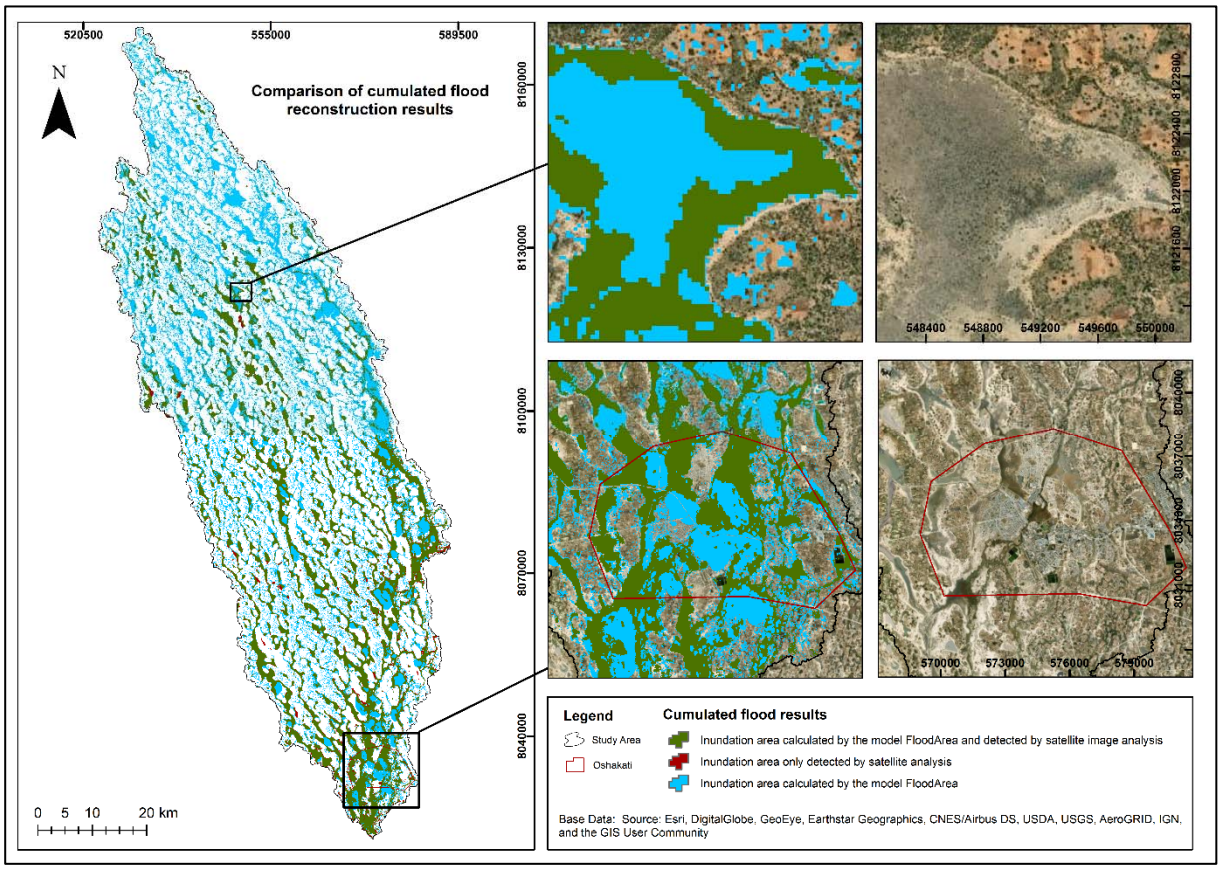

Figure 4-8: Comparison of simulation results with the reference water mask. Green: Areas flooded in model and reference data; Blue: Flooding in the model only; Red: Flooded areas only in the reference mask. An enlarged version can be seen in the appendix (Fig. A-3).

The cumulative inundation area > 0.1 m² amounts to about 1,860 km² according to the calculation with FloodArea. In contrast, the size of the inundation area derived from the satellite images is almost 3 times smaller, measuring only 673 km² in size. An agreement between model and reference data can be achieved for 620 km² only, which is surprisingly low. However, this effect must be attributed to the limitations of the reference data rather than a general lack of model performance.

It is noticeable that the overlap of the results varies spatially according to the application of the two different methods. Thus, there are far more overlapping areas in the southern part of the study area than there are in the northern part. One reason for the difference in detection is due to the different methods and how they deal with land use. In Fig. 4-8, a closer look at the northern example area (both upper right images) shows that the hydrodynamic model is able to capture the water flow in its natural path according to the channel hydraulics and other parameters. The analysis of the satellite images, on the other hand, has problems at this point in distinguishing shallow water areas, dark soils and vegetation. As a result, inundation is greatly underestimated. In particular, the northern (Angolan) part of the study area is much more vegetated and characterized by larger shrubs and contiguous clusters of trees. Another obstacle in multi-sensor analysis is the different spatial resolutions behind it. For example, at coarser resolutions, smaller water areas cannot be recorded and are incorrectly classified as dry. The same can be true for urban areas, in whose narrower streets the water is not detected and the reflectance of the roofs dominates. The resulting mixed pixel effect, which is also associated with the too coarse resolution, makes it difficult to classify the area as flooded (see Fig. 4-8, both image sections, bottom right). If we assume that the hydrodynamics were simulated correctly, the strong overestimation of the flooded areas would be a further result of the limited representation of water surface evaporation. Evaporation plays a central role in the semi-arid study area and significantly influences the model results.

However, as described in the chapter on evaporation, there is little to no area-wide evaporation data available. To completely disregard evaporation leads to a significantly overestimated result. The approach of Goormans et al. (2015) corrects the result, but it also leads to an

overestimation of ET. Compared to a MODIS scene from March 23, 2009 (Fig. A-4), modified by the Darthmouth Flood Observatory (2009), it becomes apparent that the real inundated area is something between the two calculated results in Fig. 4-7 comparing no ET and 612 mm of ET.

Everything indicates that an overestimation of evaporation losses occurred. A new model run with adjusted ET values could remedy this situation. One possibility would be to calculate with the even lower values provided by Külls (2000). Remarkable in these results are the large water reservoirs in the central part of the study area as well as in the northeast and east sections of the Angolan area. Some smaller amounts also remain visible in the border area. In the Namibian area, smaller reservoirs can only be identified in the south around the city of Oshakati. The picture of excessive ET losses therefore shows a clear difference in the remaining water volumes between the north (Angola) and the south (Namibia). The reasons for these differences are minor morphological variations and an increased total precipitation on the Angolan side.

Nevertheless, these data provide excellent insights into the spatial-temporal distribution of water volumes, their surface runoff behavior, and thus the interconnectivity of the Iishana system. In the simulation, three main streamlines could be identified, through which the water volumes are rapidly discharged towards the south. Two of the three join on the Namibian side and subsequently flow through the city of Oshakati and are thus of particular safety relevance with respect to the regional capital. Furthermore, it can be seen that there are larger water bodies on the Angolan side. Close to the Angolan-Namibian border, network structures with individual isolated depressions and pans in between become visible. Further south, the system becomes more diversified again. Throughout the study area, individual large areas flooded to a depth of only 0.1 m are repeatedly identified. These do not correspond completely with comparative data and are likely due to the correction of the digital terrain model. Accordingly, it is an overestimation of the amount of water because these areas have been leveled too much, leaving water on them.

4.6. Conclusions and outlook

This study conducted a transferable 2D-hydrodynamic modeling approach of the region around the Iishana system for the first time ever. The model is based on a single high spatial resolution (25 x 25 m) digital terrain model and covers a long and continuous model period while using temporally and spatially varying precipitation data. In addition, unlike other modeling approaches, the cross-border aspect for the region was fully included. Therefore, the model can be used for scenario calculations of future floods. Based on the TRMM data and with the help of the FloodArea model and its special properties, it was possible to reconstruct flood routing with a high spatial-temporal resolution and to make flood depths and water quantities visible at different time steps. It was also possible to determine the amount of water remaining after a rainy season. This new process helps to better understand the interconnected system, to answer questions about the distribution of the water and its quantity, and to make hazards detectable.

However, the question about the exact amount of remaining water at the end of the rainy season could not be answered yet due to the limited representation of evaporation in the model. Nonetheless, the results provide important initial indications.

Furthermore, the advantage of the model and its input parameters presented here is its transferability. The relatively high calculation period of 24 days in acute hazard cases for flood forecasts can be controlled and lowered by the spatial resolution.

However, there is no natural reliability for normal rain and dry seasons, and variability is high. Therefore, floods and droughts repeatedly lead to crop failures and human and economic losses. This work is part of a broader project that addresses water quantity and quality. In order to better understanding of the flood dynamics of this area, the sub-basin of about 4,600 km² in the eastern part of the Iishana system was selected.

With the help of the 2D-hydrodynamic model FloodArea and the precipitation data of the Tropical Rainfall Measurement Mission (TRMM), the flood event of 2008/2009 was

reconstructed. Furthermore, with the specific model and the TRMM precipitation data, a spatiotemporal precipitation variability could also be reproduced. As a result, flood routing could be performed in addition to data on inundation surfaces, depths, and volumes at different times. In addition, a volume balance of the remaining and available water at the end of the rainy season could be determined.

The exact amount of remaining water depends on the model result used. Currently, ET is a difficult factor to determine and the question of how to accurately calculate it is not yet solved. Not considering ET leads to an obviously overestimated value of 0.547 km³ water remaining while the application of ET results in an underestimated value of 0.116 km³. The true picture might be found somewhere in between. Nonetheless, it gives a first indication of a potential storage volume.

The same problem also applies to the calculation of floodplains, which, neglecting ET, is around 1,860 km². Here, too, this is clearly an overestimated value. Nevertheless, by means of these calculations, three main streams could be identified, two of which join further south and drain through Oshakati. All three streams discharge the water visibly fast. This provides an important indication of a possible safety hazard, especially for the regional capital. In addition, the calculations show that the net-like connectivity of the Iishana system becomes increasingly tighter towards the center of the study area, revealing numerous isolated depressions. In the southern area, the picture again becomes more diffuse. Water depths range from 0.1 m to 14 m, with all areas deeper than 5 m attributed to borrow pits. On average, the water depth is about 0.2 m.

In addition, the result overcorrected by the ET provides important insights. For example, areas where water is available the longest can be identified. These areas are mainly on the Angolan side, in the northeast, east, and central area and in some parts in the transboundary area. Only a few large amounts of water remain in the southern (Namibian) region.

These scientifically relevant findings have a high socio-political value. Although the details regarding ET are not yet conclusive and will require improvement in further work, the study still successfully reveals how flow the Iishana system proceeds. Based on this study, and thanks

to the transferability of the model to the neighboring catchment areas, further work can follow, which can deal with the implementation of water retention measures in the field. An important goal of further work should be to use the knowledge gained here to implement measures for flood protection and water storage, as well as to use synergy effects in order to preserve and increase water resources, even throughout pronounced drought periods.

4.7. Acknowledgements

We thank the German Aerospace Centre (© DLR 2017) for their delivery and support with the TanDEM-X data (Proposal ID: DEM_HYDR1285). We also express gratitude to Dr. Sandro Martinis, Dr. Tobias Ullmann and Lorenz Beck for their support with evaluation data.

4.8. Founding

We are grateful for the financial support by the Department of Earth Science, Freie Universität Berlin. The German Hydrological Society (DHG) supported this work with a scholarship.

4.9. Supporting information

Additional supporting information may be found in the online version of the article at the publisher's website.

With this study two supplementary videos are permanently published (Arendt et al. 2022) via www.refubium.fu-berlin.de and are directly available under:

https://refubium.fu-berlin.de/handle/fub188/34966

5 Synthesis

In order to answer the research questions for this thesis, different methodological approaches were chosen. The methods are again briefly summarized below in response to the research questions. The methods are again briefly summarized below in the responses to the research questions. In addition, there were several research excursions to Namibia, in which large fieldwork was always conducted. However, critical evaluation shows that the results obtained during these excursions always represent a current snapshot. Also, the selected methods are only a fraction of the possible approaches and form, together with the limited research time, a common field of tension.

The purpose of this dissertation is to fill gaps in scientific knowledge about the interconnectivity and runoff behavior of the Iishana system in order to further develop the existing water resource management system.

Answering questions on potential floodwaterwater retention is a core element of this work, enabling water resource management that will significantly overcome drought periods by using synergy effects.

These effects will be intensified through measures combining surface water retention and the specific expansion of existing artificial or natural pans. These multifunctional measures can be related to ‘Green Infrastructure’ and helping to mitigate the impacts of natural hazards such as floods and droughts (EEA 2015).

In this context, artificial pans are defined e.g. as structures build for floodwater retention such as Stengeldämme (see p. 39) or man-made deepened areas on the open country but also borrow pits.

These effects will be intensified through measures combining surface water retention and the specific expansion of existing artificial or natural pans. These multifunctional measures can be related to ‘Green Infrastructure’ and helping to mitigate the impacts of natural hazards such as floods and droughts (EEA 2015).

In this context, artificial pans are defined e.g. as structures build for floodwater retention such as Stengeldämme (see p. 39) or man-made deepened areas on the open country but also borrow pits.

On the opposite side, natural pans are the morphological units that have formed in the terrain due to natural fluvial and aeolian processes over long time and due to their different sediments accumulated in and around (Cunningham et al. 1992) (see also chapter 3).

5.1. Main conclusion

In the following summaries, the main research questions are answered, and a conclusion is drawn:

1. *What impact does the technical technical infrastructure have on the runoff system in the study area?*

This issue was discussed in chapter 2. It became clear that the raw DEM data set is not suitable for modeling due to water-induced interferences, vegetation elements and artificial structures, such as culverts, bridges and road dams, which distort the natural runoff behavior in the current representation. Consequently, in preparation for later modeling of flood events, corrections to the data were required.

Therefore, a field trip was conducted in which about 532 km of road dams were surveyed and more than 1,000 culverts with numerous bridges were mapped. This precise surveying and mapping work provided a crucial contribution for the improvement of the DEM and model results.

The field research showed that, in particular, the road dams located to the north and running orthogonal to the direction of flow have a great influence on the runoff behavior. Backwater

can occur on the north side of these road road dams, massively increasing pressure on these sensitive technical technical infrastructure elements, which are not designed as flood protection. In summary, the infrastructure elements have a great influence on the runoff behavior and can partially influence the flow direction.

Via the implementation of the road dams and culverts, as well as the use of the filter algorithms, the natural geomorphology could be adapted to the natural appearance. This work therefore represents an important basis in the development of a transboundary flood model in the region around the Iishana system.

2. *What quantitative and qualitative characteristics can be attributed to artificial and natural pans, and what contribution can the pans provide in the context of optimized water resource management?*

As discussed in section 1.2, the local population living in the countryside generally uses a wide variety of water sources, depending on availability. Groundwater is rarely used because of its higher salinity (Faulstich et al. 2018; Kluge et al. 2008). Hand-dug wells with depths up to 20 m are often connected to groundwater lenses and are therefore not found throughout the country (Cunningham et al. 1992; Kluge & Polak 2018; Zimmermann 2013). An inexpensive and technically simple solution for increasing necessary water storage lies in the artificial deepening of natural pans. This method allows surface runoff to be utilized in a simple manner (Cunningham et al. 1992; Zimmermann 2013). So far, for this study the term of infrastructure is defined as technical infrastructure. So far, for this study the term of infrastructure is defined as technical infrastructure. Chapter 3 dealt with the topic of pans and their water retention potential.

Different metrics and characteristics of pans were calculated, based on the enhanced TanDEM-X model and with the help of a modified Blue Spot Analysis.

a) *What information can be obtained about the number, location, distribution patterns, and*

connectivity of pans?

In the entire Iishana system, about 190,000 pans have been identified. About one third of these are located in the ephemeral drainage paths of the Iishana and are thus indirectly connected during major runoff events. This information is particularly important in relation to question 2. (c) and is accordingly addressed again in more detail below. Additionally, this study revealed that there are fewer pans in the Angolan part of the study area than there are in the Namibian part. In ,Angola, there also exists a lower density of pans per square kilometer, but a higher number of particularly large pans.

Therefore, this work scientifically confirms, for the first time, the statement of Mendelsohn et al. (2013) that there are significantly more, small (often only 100 m² in size) isolated pans in the southern part of the Iishana system.

The pans in the northern and central parts of the system are fed by both surface runoff and local precipitation. The isolated pans to the south are generally filled solely by local precipitation. Only in the case of particularly large flood events, like most in 2008, 2009 and 2011, they are also partly fed by surface runoff.

b) What metrics (area, volume, and depth) can be attributed to these pans?

The total area of all pans was calculated at about 4,000 km². Proportionally, the northern part, located in Angola, accounts for about 22% of the total area and the Namibian part accounts for 27%. However, when comparing the pan volumes, the differences between the two areas become more obvious. The total volume of all pans is 1.9 km³, with 67% of the volume attributable to Angola and only 33% to Namibia. Thus, the volume of pans in Angola is, on average, about twice as large as that of the pans in Namibia.

In aggregate, the volume of the 75%-quartile is less than 2,100 m³ per pan. The depth of all pans barely exceeds 30 cm on average. Accordingly, the majority of the pans are very shallow.

c) Based on the information obtained previously, can individual pans be identified for development as temporary storage within an integrated water resource management

framework?

The previous calculations have revealed a large number of pans. However, it has been shown that these pans often have a large surface area with a very shallow depth. Considering the semi-arid climate of the region, these disproportionate characteristics have a very unfavorable effect on water retention due to very high evaporation behavior.
Therefore, pans with a significantly better surface-area-to-volume ratio should be sought. By calculating the so-called SA/V rate for all 190,000 pans, it was finally possible to identify those pans showing the best rate of ≤1 m^{-1} for further enhancement (McJannet et al. 2008).

As a result, about 2,000 pans were found. Further evaluation of the data led to the finding that SA/V rates on the Angolan side are, on average, lower than the rates on the Namibian side. Thus, evapotranspiration has a stronger and more negative influence in the Namibian region. Therefore, the focus of measures to develop pans, both for flood retention and to increase the water supply for the dry season, should be in Namibia. The reason for this is the lower water availability in this region due to climate in general.

In all cases, whether the planned development is in Namibia or Angola, the following principles should be observed prior to any augmentation:

(1) Pan must be close to a location with a high demand for water/flood protection;
(2) Pan must be connected to the channel network and, at best, be located within an inundation zone;
(3) Pan needs a low SA/V-ratio to counter the problem of high evaporation rates.

Considering the points just stated and the new findings on hand, the resilience of the local people's livelihood can be increased by following these measures for the expansion of pans and the enhancement of their storage function. Thus, during rainy seasons, the flood peaks can be reduced while at the same time water can be made available for use during the dry periods.

3. *How can the runoff processes of the Iishana system be described and how much water remains in the system immediately after the end of a rainy season?*

The flood event during the 2008/2009 rainy season was chosen for modeling (described in chapter 4). The reason for this was the robust data basis, which showed the least deficiencies for the selected period. In order to minimize the computation time, the flood analysis in the Iishana system focused on the catchment area around the regional capital Oshakati. The selection of this catchment area was made because the flood caused the greatest socio-economic damage in this region, making it particularly important for further considerations.

The model identified three main drainage channels in the catchment area, two of which have a significant influence on flood events in the city of Oshakati. The third channel runs to the west of Oshakati and mainly influences the rural region.

Furthermore, the model revealed that the drainage lines of the Iishana system become narrower from the central to the southern part of the study area. This has a great influence on the flow velocity and thus on the general runoff process, which accelerates as a result.

At the end of the rainy season, the Angolan side of the Iishana system retains more water for a longer period while the Namibian side receives less water, which it retains for a shorter period. This is consistent with the findings generated via question 2 that the pans in the northern part of the catchment have larger volumes.

The simulation showed that the surface runoff both inside and outside the ephemeral runoff paths first accumulates in the pans. The particularly shallow ones quickly overflow and begin to connect with each other first. Corresponding to the prevailing precipitation gradient running from north to south, during persistent precipitation, the interconnectivity starts first in the northern area and continues towards the south.

The model also made clear that an interruption of precipitation at the end of the first third of the rainy season quickly leads to an interruption of interconnectivity. Only with the second and clearly more pronounced precipitation phase do the runoff paths reconnect.

During this second phase, when overflow of the runoff pathways occurs, the water depths average between 0.5 and 1.5 m, although in some areas the depth averages between 2 and 5 m. Backwater effects at infrastructural facilities are also recognizable. The flow velocities vary between 0.15 m/s to 0.35 m/s. In some areas, flow velocities of up to 0.5 m/s occur.

Despite the persistence of precipitation and ongoing runoff processes, the southern pans remain mostly isolated, albeit rim-filled. With the end of the rainy season and the runoff of the flood water from Lake Oponono to the Ethosha pan, the rainwater remaining in the pans can be balanced with regard to volume.

Depending on the amount of evapotranspiration applied in the model, values between 0.116 km³ and 0.547 km³ were determined. At this point, it should be mentioned again that the total volume of all pans in the entire study area calculated in chapter 3 is 1.9 km³.

The study area has a size of about 18,400 km² and the catchment area used in the model has a size of 4,600 km². At a ratio of four to one, this results in a theoretical pan volume of 0.475 km³ for the model region.

Thus, it becomes clear that, without the consideration of evapotranspiration, the model result for the remaining water is too high, not only logically, but also mathematically. The minimum calculated value of 0.116 km³ tends to be closer to reality, even though the current assumption still says that this figure is somewhat underestimated.

Currently, the exact modeling of evapotranspiration is still a major challenge and has not yet been conclusively solved. However, it is clear that the model cannot be calculated without considering ET, because the influence of ET is visibly large.

Nevertheless, the model results provide the first founded information about runoff processes in the Iishana system and give first indications about the volume of potentially retained precipitation. Additionally, the model not only shows how much water is retained, but also where it is retained and where it lasts for the longest amount of time. Thereby a clear difference and gradient becomes visible. This gradient shows a reduction of water availability and longevity from north to south, to the disadvantage of the Namibian part of the study area.

Additionally, for the first time in a scientific framework, the present study succeeded in performing 2D-hydrodynamic modeling in the Ilshana system, which:

- Is based on a single high-resolution digital elevation model
- Draws on a long and continuous precipitation time series
- Considers the precipitation in its temporal as well as spatial variability
- Includes the transboundary aspect and is transferable

The results obtained must not be considered as absolute, as they are the result of methodically obtained snapshots. Nevertheless, many new insights on the Ilshana system were gained with the selected approaches.

For example, the influence of the infrastructure on the runoff behavior in the Ilshana system was made clear for the first time, and a solid basis for subsequent work was created by correcting the digital terrain model.

Furthermore, it was also possible for the first time to scientifically catalog the Ilshana system and its pans by defining quantitative and qualitative characteristics as well as metric properties. Also new are the findings on the storage potential of the pans, particularly their water volumes, water depths and water availability. General knowledge was also obtained on the runoff behavior and its related velocities and areas of risk.

Even if the information on ET has not yet been conclusively clarified and needs to be improved in further research, the study successfully demonstrates how the Ilshana system performs.

Based on this study, and thanks to the transferability of the model to neighboring catchments, further work can follow. An important goal of this work should be to use the knowledge gained here to study and implement flood protection and retention measures. Synergy effects should also be considered and used to preserve precious water resources, even in pronounced drought periods, and to secure the vital supply of water.

5.2. Future perspectives

The final sections are intended to place the latest new findings in the context of future challenges and tasks on different levels.

5.2.1. Sociopolitical context

Flood events, heavy storms, and droughts are intensifying in frequency and amplitude as climate change progresses. In addition, the population in northern Namibia continues to grow. The pressure on the region's water resources continues to increase and will continue in the future.

In this context, further work must first determine the current and future water demand of the people living in the region. For this purpose, the knowledge gained in this study about the metric properties of the pans as well as the hydrodynamic model should be used to estimate flood hazards and to calculate water availability for future scenarios. Combining the current results with the currently missing information, it can be determined whether the water in the pans will be sufficient to irrigate the fields, water the livestock and bridge the water demand during future drought periods.

As scarcity rises, it is obvious that a single strategy for water resource management is not sufficient to meet the increasing demand for water. This work must be seen as a sub-strategy in the effort to cope with water scarcity under changing climatic conditions. Therefore, this study fits as a component approach to other necessary work that still needs to be done.

5.2.2. Scientific perspective

An important area for further investigation is to see if, after accurately taking evaporation into account, the intended increase in water availability through retention is actually achieved. In this context, the factor of possible sedimentation rates must also be considered, because these could reduce the increased volume over time.

Added to this is the challenge posed by the climate change factor. How will the retention potentials behave with higher evapotranspiration rates and possibly less precipitation? Can

the measures actually contribute to a helpful adaptation strategy?

Despite these open questions, which have yet been answered in the framework of the running project, the study provides, for the first time, scientific findings on central questions such as the metric properties of the pans and the number and distribution of these pans in the Iishana system. For the first time, the runoff behavior of a flood was visualized hydrodynamically and characteristics of inundation areas, water depths and flow velocities were determined. The findings for the storage time of rainwater that has fallen during the rainy season are also new. Major challenges still include the adequate consideration of evapotranspiration in the model and, subsequently, the validation of the calculated retention volumes, which could be solved in the future course of the research project.

5.2.3. Potentials in applications & practice

Based on this study, and due to the transferability of the model to neighboring catchments, further work can follow that addresses the modelling of the surrounding catchments, ultimately determining water availability for the watersheds not yet considered.

An important goal of further work should be to use the knowledge gained here for the practical implementation of flood protection and water retention measures as well as the exploration of synergy effects in order to preserve precious water resources and make them usable even in severe dry periods. In addition, questions about technical requirements must also be clarified before the deepening of the pans can take place. As a result, standards need to be set to both protect the structures and ensure safe abstraction of water. This will require bringing other specialists on board, such as hydraulic engineers. The hydrological and geoscientific sciences can certainly provide further support in this regard.

6 References

Achleitner S, Huber A, Lumassegger S, Kohl B, Spira Y, Weingraber F (2020) Pilot Study Upper Austria. Modeling of pluvial floods in response to heavy precipitation events. Guidance for practitioners, https://www.interreg-central.eu/Content.Node/Home/Projects/RAINMAN/Main-Project-outputs-/RAINMAN-LeitfadenEN-V1.0-20200623-(1).pdf (accessed June 25, 2021).

Anders K, Assmann A, Fritsch K (2016) Prospects and requirements for an operational modelling unit in flood crisis situation. Flood Risk 2016, 3rd European Conference on Flood Risk Management, E3S Web of Conferences (7), DOI: 10.1051/e3sconf/20160719002.

Arendt R, Faulstich L, Jüpner R, Assmann A, Lengricht J, Kavishe F, Schulte (2020) A GNSS mobile road dam surveying for TanDEM-X correction to improve the database for floodwater modeling in northern Namibia. Environ. Earth Sci. 2020, 79, 333, https://doi.org/10.1007/s12665-020-09057-5

Arendt R, Reinhardt-Imjela C, Schulte A, Faulstich L, Ullmann T, Beck L, Martinis S, Johannes P, Lengricht J (2021) Natural Pans as an Important Surface Water Resource in the Cuvelai Basin - Metrics for Storage Volume Calculations and Identification of Potential Augmentation Sites. *Water* 13 (2), 177, https://doi.org/10.3390/w13020177

Arendt R, Reinhardt-Imjela C, Schulte A (2022) Hydrodynamic modeling of ephemeral flow in the Iishana channel systems of the Cuvelai Basin - Northern Namibia. Supplementary video material, online accessible: https://refubium.fu-berlin.de/handle/fub188/34966 DOI: 10.17169/refubium-34684.

Arroyo-Suarez E N, Riley J L, Glang G F, Mabey D (2005) Evaluating a Global Differential GPS System for Hydrographic Surveying. Proceedings of OCEANS 2005 MTS/IEEE, Washington DC USA 18-23 Sept, IEEE 1–7, DOI: 10.1109/OCEANS.20051640155.

Assmann A, Jäger S, Fritsch, Brauner C (2013) Risk maps for pluvial flooding and infiltration of a flood risk management process, In: Klinj F, Scheckendiek (ed) Comprehensive Flood Risk Management. Research for policy and practice: 189. Proceedings of the 2nd European Conference on Flood Risk Management. Flood Risk 2012, Rotterdam.

Ata R (2017) Telemac 2D User Manual. Version7.2, April 2017, Paris.

Awadallah A G, Tabet D (2015) Estimating flooding extent at high return period for ungauged braided systems using remote sensing: a case study of Cuvelai Basin, Angola. Nat. Hazards 2015, 77: 255–272, DOI: 10.1007/s11069-015-1600-6.

Balstrøm T (2015) Assessment of Flood Risks for Residential Areas Caused by Cloudbursts. Proceedings of the ESRI User Conference, San Diego, CA, USA, 20–24 July 2015.

Barboux J P (2000) Navigation & Positioning Practices in the Offshore Industry. In: Schürmann B. Noordwijk (ed) Proceedings of the International Symposium GEOMARK 2000 Paris, France, 10-12 April 2000, The Netherlands: European Space Agency (ESA) 2000, ESA SP 458, 49 p.

Bethune S, van der Waal B, Roberts K S (2012) Proposed Flood Mitigation Measures For The Oshakati/Ongwediva Area. Environmental Impact Assessment (EIA), Draft-Scoping Report, May 2012.

Beyer M, Hipondoka M, Hamutoko J, Wanke H (2018) Water resources in the Cuvelai-Etosha Basin. Biodivers. Ecol. 2018, 6: 84–85, DOI: 10.7809/b-e.00308.

Bischofberger J, Schuldt-Baumgart N, Lenzen E (2016) Omeya Ogo Omwenyo - Water is Life. CuveWaters Report; ISOE: Frankfurt/Main, Germany, 2016, DOI: 10.13140/RG.2.1.2287.7047.

Bisnath S, Gao Y (2009) Current State of Precise Point Positioning and Future Prospects and Limitations. In: Sideris M G (ed): Observing our changing earth. Proceedings of the 2007 IAG general assembly Perugia Italy. July 2-13, 2007, Bd 133, Berlin Heidelberg: Springer 2009 (International Association of Geodesy Symposia vol, 133), 615–623, DOI: 10.1007/978-3-540-85426-5_71.

Bisnath S, Wells D, Dodd D (2003) Evaluation of commercial carrier phase-based WADGPS services for marine applications. ION GPS/GNSS 2003 Portland Oregon, 17-27.

Bradbrook K (2006) JFLOW: a multiscale two-dimensional dynamic flood model. Water and Environment Journal (20): 79–86, DOI: 10.1111/j.1747-6593.2005.00011.x.

Cai C, Gao Y (2007) Precise Point Positioning Using Combined GPS and GLONASS Observations. Journal of GPS 6 (1): 13–22, DOI: 10.5081/jgps.6.1.13.

Chow V T (1959) Open-channel hydraulics. New York: McGraw-Hill. Civil Engineering Series 1959.

Cunningham T, Auino E, Marsh A, Seely M (1992) Oshanas: Sustaining People, Environment, and Development in Central Owambo, Namibia. DRFN: Windhoek, Namibia, 1992, ISBN: 978-99916-709-0-4.

Darthmouth Flood Observatory (2009) Floods in southern Africa. Channels of water flowed through normally dry northern Namibia on March 23, 2009. Product date 23.03.2009 https://earthobservatory.nasa.gov/images/37619/floods-in-southern-africa. (accessed November 29, 2021).

De Groeve T (2010) Flood monitoring and mapping using passive microwave remote sensing in Namibia. Geomatics, Natural Hazards and Risk, 2010, Vol. 1, (1): 19-35, DOI: 10.1080/19475701003648085.

Desalegn H & Mulu A (2021) Mapping flood inundation areas using GIS and HEC-RAS model at Fetam River, Upper Abbay Basin Ethopia. Scientific African. Vol. 12. July 2021, e00834, DOI: 10.1016/j.sciaf.2021.e00834.

Digital Atlas of Namibia (2016) Available online: https://www.uni koeln.de/sfb389/e/e1/download/atlas_namibia/haupt_namibia_atlas.html (accessed October 26, 2016).

Dixon K (2006) StarFire: A Global SBAS for Sub-Decimeter Precise Point Positioning. Proceedings of the 19th International Technical Meeting of the Satellite Division of the Institute of Navigation (ION GNSS 2006), Fort Worth TX, September 2006. pp. 2286-2296.

Dutt V B S S I, Rao G S B, Rani S S, Babu S R, Goswami R G, Kumari Ch U (2009) Investigation of GDOP for Precise user Position Computation with all Satellites in view and Optimum four Satellite Configurations. Journal Ind. Geophys. Union Vol.13, No (3) 139-148.

European Environment Agency (2015) Exploring nature-based solutions. The role of green infrastructure in mitigating the impacts of weather- and climate change-related natural hazards. EEA Technical Report, No. 12/2015, DOI: 10.2800/946387

European Environment Agency (2015) Exploring nature-based solutions. The role of green infrastructure in mitigating the impacts of weather- and climate change-related natural hazards. EEA Technical Report, No. 12/2015, DOI: 10.2800/946387

Faulstich L, Schulte A, Arendt R, Kavishe F, Lengricht J (2018) Die Qualität der intensiv genutzten Oberflächengewässer im Cuvelai-Becken (Nord-Namibia) zum Ende der Trockenzeit 2017. In: Chifflard P, Karthe D, Möller S (eds) Geographica Augustana, Beiträge zum 49. Jahrestreffen des Arbeitskreises Hydrologie, Göttingen, Germany, 23–25 November 2017; Universität Augsburg: Augsburg, Germany, 2018, Band 26, pp. 9–21.

Filali-Meknassi Y, Ouarda T B M J, Wilcox C (2014) Data Access, Availability and Quality Assessment for the Development of a Flood Forecasting Model for Namibia. Technical Report UNESCO 78, Windhoek, Namibia, 2014. Document code: WIN/2014/IHP/01.

Fritsch K, Assmann A, Tyrna B (2016) Long-term experiences with pluvial flood risk management, E3S Web of Conferences 7, 04017 (2016), Flood Risk 2016. 3rd European Conference on Flood Risk Management, DOI: 10.1051/e3sconf/20160704017.

Gao Y, Wojciechowski A, Chen K (2005) Airborne kinematic positioning using precise point positioning methodology. Geomatica Vol. 59 No (1): 29-36.

Gaughan A E, Staub C G, Hoell A, Weaver A, Waylen P R (2016) Inter- and Intra-annual precipitation variability and associated relationships to ENSO and the IOD in southern Africa. Int. Journal of Climatology 2016, (36): 1643–1656, DOI: 10.1002/joc.4448.

Ge M, Gendt G, Rothacher M, Shi C, Liu J (2008) Resolution of GPS carrier-phase ambiguities in Precise Point Positioning (PPP) with daily observations. Journal Geod. 82 (7): 389–399, DOI: 10.1007/s00190-007-0187-4.

Gebbers R, Adamchuk V I (2010) Precision agriculture and food security, In: Science (New York N,Y,) 327 (5967) 828–831, DOI: 10.1126/science.1183899.

Geomer GmbH. FloodAreaHPC-Desktop user manual. v. 10.3, 2017.

Goormans T, van Looveren R, Mufeti, P, Wynants, J (2015) Building a Hydrological and Hydrodynamic Model while facing Challenges in Data availability in the Oshana Region of Central Northern Namibia. Proceedings of the E-Proceedings of the 36th IAHR World Congress, The Hague, The Netherlands, 28 June–3 July 2015. In: Mynett A (ed) IAHR: Madrid, Spain, 2015, pp. 5222–5233, ISBN: 978-1-5108-2434-8.

Goudie A, Viles H (2015) Landscape and Landforms of Namibia, Springer Heidelberg, ISBN: 978-94-017-8020-9.

Goudie A, Viles H A (2015) Landscapes and Landforms of Namibia. World Geomorphological Landscapes. Springer, Dordrecht, The Netherlands, 2015, ISBN: 978-94-017-8020-9.

Grim S (2012) Abflusslose Senken - Instrumente in der Landschaftsanalyse und Indikatoren Rezenter Krustenbewegungen. Ph.D. Thesis, Johannes-Gutenberg-Universität, Mainz, Germany, 2012.

Hamatoku J T, Wanke H, Koeniger P, Beyer M, Gaj M (2017): Hydrogeochemical and isotope study of perched aquifers in the Cuvelai-Etosha Basin, Namibia. Isotopes in Env. a. Health Stud., pp. 1-18, DOI: 10.1080/10256016.2016.1273913.

Hatch R, Sharpe T S, Galyean P (2003) StarFire: A Global High Accuracy Differential GPS System. Proceeding of the 2003 National Technical Meeting of The Institute of Navigation Anheim, CA 2003, pp. 562-573.

He K (2015) GNSS kinematic position and velocity determination for airborne gravimetry, PhD Thesis (Scientific Technical Report 15/04) Potsdam: Deutsches GeoForschungsZentrum (GFZ), 158 p.

Helmschrot J, Jürgens N (2015) Integrated SASSCAL research to assess and secure current and future water resources in Southern Africa. Hydrological Science and Water Security: Past, Present and Future. Proceedings of the 11th Kovacs Colloquium, Paris, Rance, June 2014. IAHS Publ. 366. 2015, DOI: 10.5194/piahs-366-168-2015.

Himmelsbach Th, Beyer M, Wallner M, Grünberg I, Houben G (2018) Deep, semi-fossil aquifers in southern Africa: A synthesis of hydrogeological investigation in northern Namibia. In: Revermann R, Krewenka K M, Schmiedel U, Olwoch J M, Helmschrot J, Jürgens N (eds): Climate change and adaptive land management in southern Africa – assessments, changes, challenges, and solutions. Biodiv a. and Ecol. (6): 66-74, DOI:10.7809/b-e.00306.

Hipondoka M H T (2005) The Development and Evolution of Etosha Pan. Ph.D. Thesis, Julius-Maximilians-Universität, Würzburg, Germany, 2005, 152 p.

Hurn J (1989) GPS: a guide to the next utility, Sunnyvale Trimble Navigation 1989. 76 p., ISBN: 10-9992537019.

Hüser K, Besler H, Blümel W D, Heine K, Leser H, Rust U (2001) Namibia: Eine Landschaftskunde in Bildern; Klaus Hess Verlag: Göttingen, Germany, 2001, ISBN: 978-3-933117-14-4.

Jenson S K, Domingue J O (1988) Extracting topographic structure from digital elevation data for geographic information-system analysis. Photogramm. Eng. Remote Sens. 1988, (54): 1593–1600.

Jokinen A S (2014) Enhanced ambiguity resolution and integrity monitoring methods for Precise Point Positioning. PhD thesis at Imperial College London, Centre for Transport Studies, Department of Civil and Environmental Engineering, 231 p.

Kaplan E, Hegarty C (2005) Understanding GPS Principles and Applications, Principles and Applications. 2nd ed. Norwood: Artech House 2006, 726 p., ISBN: 1580538940.

Kapuka A, Hlásny T (2020) Social Vulnerability to Natural Hazards in Namibia: A District-Based Analysis. Sustainability 2020, (12): 4910, DOI: 10.3390/su12124910.

Kazmierski K (2018) Performance of Absolute Real-Time Multi-GNSS Kinematic Positioning, In: Artificial Satellites Vol. 53 No. (2): 75-88, DOI: 10.2478/arsa-2018-0007.

Kazmierski K, Hadas T, Sosnica, K (2018) Weighting of Multi-GNSS Observations in Real-Time Precise Point Positioning, Remote Sensing 10 (1) 84, DOI: 10.3390/rs10010084.

Kerdiles H, Rembold F, Pérez-Hoyos A (2015) Seasonal Monitoring in Namibia. Ad Hoc Report. Severe drought affecting cereal production and pastoral areas in northern and central Namibia. Joint Research Centre of the European Union, 2015, Technical Report, 20 pp. http://the-eis.com/elibrary/sites/default/files/downloads/literature/Seasonal%20Monitoring%20in%20Namibia_2015.pdf (accessed June 25, 2021).

Klintenberg P, Mazambani C, Nantanga K (2007) Integrated Water Resources Management in the Namibian Part of the Cuvelai Basin, Central Northern Namibia, CuveWaters Papers No. 2; ISEO: Frankfurt/Main, Germany, 2007.

Kluge T, Liehr S, Lux A, Moser P, Niemann S, Umlauf N, Urban W (2008) IWRM concept for the Cuvelai Basin in northern Namibia. Phys. Chem. Earth Parts ABC 2008, (33): 48–55, DOI: 10.1016/j.pce.2007.04.005.

Kluge T, Polak M (2018) Water supply infrastructure and sanitation in central-northern Namibia. In: Kramm J, Jokisch A, Müller K, (eds): Integrated Water Resources Management in Water-Scarce Regions. IWA Publishing: London, UK, 2018, pp. 19–22, ISBN: 978-1-78040-790-6.

Knoop V L, de Bakker P F, Tiberius C C J M, van Arem B (2017) Lane Determination With GPS Precise Point Positioning, IEEE Trans. Intell. Transport. Syst. 18 (9): 2503–2513, DOI: 10.1109/TITS.2016.2632751.

Kotani A, Hiyama T, Ohta T, Hanamura M, Kambatuku J R, Awala S K, Iijima M (2017) Impact of rice cultivation on evapotranspiration in small seasonal wetlands of north central Namibia. Hydrological Research Letters 11(2): 134–140. 2017, DOI: 10.3178/hrl.11.134.

Kuliwoye E K (2010) Flood Hazard Assessment by means of Remote Sensing and Spatial analyses in the Cuvelai Basin, Case Study Ohangwena Region – Northern Namibia. 2010 Master thesis Seminar Series Nr. 218.

Külls C (2000) Groundwater of the North-Western Kalahari, Namibia. Estimation of recharge and quantification of the flow system. Doctoral thesis. Würzburg, University of Würzburg, 2000, 230 p.

Kundzewicz Z W, Kanae S, Seneviratne S I, Handmer J, Nicholls N, Peduzzi P, Mechler R, Bouwer L M, Arnell N, Mach K, Muir-Wood R, Brakenridge G R, Kron W, Benito G, Honda Y, Takahashi K, Sherstyukov B (2014) Flood risk and climate change: global and regional perspectives. Hydrological Sciences Journal 59, No. (1): 1-28, DOI: 10.1080/02626667.2013.857411.

Langley R B (1999) Dilution of Precision, GPS World (May 1999), pp. 52–68.

Leandro J, Chen A S, Schumann A (2014) A 2D parallel diffusive wave model for floodplain inundation with variable time step (P-DWave). Journal of Hydrology. Vol. 517. pp. 250-259, DOI: 10.1016/j.jhydrol.2014.05.020.

Leica Geosystems AG (2018) Sensor specifications. Available online: https://leica-geosystems.com/-/media/Files/LeicaGeosystems/Products/Datasheets/Leica_Viva_ GS16_DS.ashx?la=en&hash=EB1C7278B6E75F4ADDF9E80849879557 (accessed September 14, 2018).

Li X, Ge M, Dai X, Ren X, Fritsche M, Wickert J, Schuh H (2015) Accuracy and reliability of multi-GNSS real-time precise positioning: GPS GLONASS BeiDou and Galileo, J. Geod 89 (6): 607–635, DOI: 10.1007/s00190-015-0802-8.

Liu T, Yuan Y, Zhang B, Wang N, Tan B, Chen Y (2017) Multi-GNSS precise point positioning (MGPPP) using raw observations. J. Geod 91 (3): 253–268, DOI: 10.1007/s00190-016-0960-3.

Liu T, Zhang B, Yuan Y, Li M (2018) Real-Time Precise Point Positioning (RTPPP) with raw observations and its application in real-time regional ionospheric VTEC modeling, J. Geod 92 (11): 1267–1283, DOI: 10.1007/s00190-018-1118-2.

Luetkemeier R, Liehr S (2019) Integrated responses to drought risk in Namibia and Angola. Watersolutions, 2019, (3): 56–60, P-ISSN: 2509-2731.

Luetkemeier R, Stein L, Drees L, Liehr S (2017) Blended Drought Index: Integrated Drought Hazard Assessment in the Cuvelai-Basin. Climate 2017, 5, (3) 51, DOI:10.3390/cli5030051.

Mandl D, Frye S, Sohlberg R, Cappelaere P, Handy M, Grossman R (2012) The Namibia Early Flood Warning System a CEOS pilot project. IEEE International Geoscience and Remote Sensing Symposium (IGARSS) 2012, 22-27 July 2012 Munich Germany Annual IEEE Computer Conference, Piscataway NJ: IEEE, pp. 3521–3524, DOI: 10.1109/IGARSS.2012.6350660.

Manning R (1891) On the flow of water in open channels and pipes. Transactions of the Institution of Civil Engineers of Ireland. 20, pp. 161–207.

Martinis S, Kersten J, Twele A (2015a) A fully automated TerraSAR-X based flood service. ISPRS J. Photogramm. Remote Sens. 2015, 104, pp. 203–212, DOI: 10.1016/j.isprsjprs.2014.07.014.

Martinis S, Kuenzer C, Wendleder A, Huth J, Twele A, Roth A, Dech S (2015b) Comparing four operational SAR-based water and flood detection approaches. Int. J. Remote Sens. 2015, 36, pp. 3519–3543, DOI: 10.1080/01431161.2015.1060647.

McBenedict, B, Hauwanga W N, Wanke H, Chimwamurombe P M, Hang'ombe B M (2019) Seasonal Health Risks Due to Zoonotic Pathogens from Hand-dug Well Water in Ohangwena and Omusati Regions of Namibia. J. Pure Appl. Microbiol. 2019, 13, pp. 1583–1593, DOI: 10.22207/JPAM.13.3.31.

McJannet D, Cook F, Burn S (2008) Evaporation Reduction by Manipulation of Surface Area to Volume Ratios: Overview, Analysis and Effectiveness. Urban Water Security Research Alliance Technical Report No. 8, CSIRO: Canberra, Australia, 2008.

Mendelsohn J, Weber B (2011) Cuvelai: The Cuvelai Basin, its Water and People in Angola and Namibia = Povos e águas da bacia do Cuvelai em Angola e Namibia, Occasional paper, Development Workshop Angola: Luanda, Angola, 2011, ISBN: 978-99916-780-6-1.

Mendelsohn J M, Jarvis A, Robertson T (2013) A Profile and Atlas of the Cuvelai-Etosha Basin. RAISON and Gondwana Collection: Windhoek, Namibia, 2013, ISBN: 978-99916-780-7-8.

Miller R M, Pickford M; Senut B (2010) The geoglogy, paleontology and evolution of the Etosha Pan, Namibia: Implications for terminal Kalahari deposition. South Afr. J. Geol. 2010, 113, pp. 307–334; DOI: 10.2113/gssajg.113.3.307.

Mitchell A (1999) The ESRI Guide to GIS Analysis. ESRI: Redlands, CA, USA, 1999, ISBN: 978-1-879102-06-4.

Mufeti P, Rientjes T, Mabande P, Maathuis B (2013) Application of a satellite based rainfall-runoff model: A case study of the Trans Boundary Cuvelai Basin in Southern Africa. Proceedings of the European Space Agency Living Planet Symposium, Edinburgh, UK, 9–13 September 2013, Ouwehand L (ed): ESA Communications: Noordwijk, The Netherlands, 2013; SP-722, ISBN: 978-92-9221-286-5.

Mukul M, Srivastava V, Jade S, Mukul M (2017) Uncertainties in the Shuttle Radar Topography Mission (SRTM) Heights: Insights from the Indian Himalaya and Peninsula, Scientific reports 7, 41672, DOI: 10.1038/srep41672.

Müller I, Hipondoka M, Winkler K, Geßner U, Martinis S, Taubenböck H (2018) Monitoring flood and drought events - Earth observation for multiscale assessment of water-related hazards and exposed elements. Biodivers. Ecol. 2018, (6): 136–143, DOI: 10.7809/b-e.00315.

Namibia Statistics Agency (2014) Namibia 2011 Census Population Projections 2011 to 2041. Namibia Statistics Agency: Windhoek, Namibia, 2014.

Namibia Statistics Agency (2013) Namibia 2011 Population and Housing Census Atlas; Windhoek, Namibia, 2013.

Ngula Niipele, J, Chen J (2019) The usefulness of alos-palsar dem data for drainage extraction in semi-arid environments in The Iishana sub-basin. J. Hydrol. Reg. Stud. 2019, (21): 57–67, DOI: 10.1016/j.ejrh.2018.11.003.

Nguno A, Angombe M (2011) Mapping of clay and salt pans in northern Namibia using remote sensing and field spectral techniques. 35th Canadian Symposium on Remote Sensing pp. 2–4.

Nielsen N H, Larsen M R A, Rasmussen S F (2011) Development of a screening method to assess flood risk on Danish national roads and highway systems. Water Sci. Technol. 2011, (63): 2957–2966, DOI: 10.2166/wst.2011.157.

NovAtel Inc. (2015) An Introduction to GNSS, GPS GLONASS BeiDou Galileo and other Global Navigation Satellite Systems. Second Edition, Canada (2015), ISBN: 978-0-9813754-0-3.

Nujić M (2016) HYDRO_AS-2D–2D-Strömungsmodell für die wasserwirtschaftliche Praxis. Benutzerhandbuch, Version4.2.1, In: Hydrotec Ingenieurgesellschaft für Wasser und Umwelt mbH (ed), September 2016, Rosenheim.

Pekel J-F, Cottam A, Gorelick N, Belward A S (2016) High-resolution mapping of global surface water and its long-term changes. Nature 2016, 540, pp. 418–422, DOI: 10.1038/nature20584.

Perez-Ruiz M, Upadhyaya S K (2012) GNSS in Precision Agricultural Operations. In: Elbahhar F B, Rivenq A (eds): New Approach of Indoor and Outdoor Localization SystemsIntechOpen Ltd.: London, UK, 2012, ISBN: 978-9535107750.

Persendt F C, Gomez C (2016) Assessment of drainage network extractions in a low-relief area of the Cuvelai Basin (Namibia) from multiple sources: LiDAR, topographic maps, and digital aerial orthophotographs. Geomorphology 2016, 260, pp. 32–50, DOI: 10.1016/j.geomorph.2015.06.047.

Persendt F C, Gomez C, Zawar-Reza P (2015) Identifying hydro-meteorological events from precipitation extremes indices and other sources over northern Namibia, Cuvelai Basin. Jàmbá: Journal of Disater Risk Studies, 2015, Vol. 7, No (1), DOI: 10.4102/jamba.v7i1.177.

Pipaud I, Loibl D, Lehmkuhl F (2015) Evaluation of TanDEM-X elevation data for geomorphological mapping and interpretation in high mountain environments — A case study from SE Tibet China. Geomorphology 246, pp. 232–254, DOI: 10.1016/j.geomorph.2015.06.025.

Rättich, M, Martinis S, Wieland M (2020) Automatic Flood Duration Estimation Based on Multi-Sensor Satellite Data. Remote Sens. 2020, 12 (4), 643, DOI: 10.3390/rs12040643.

Reason C J C, Smart S (2015) Tropical southeast Atlantic warm events and associated rainfall anomalies over southern Africa. Front. Environ. Sci. 2015, 3, 24, DOI: 10.3389/fenvs.2015.00024.

Rizzoli P, Martone M, Gonzalez C; Wecklich C, Borla Tridon D, Bräutigam B, Bachmann M, Schulze D, Fritz T, Huber M (2017) Generation and performance assessment of the global TanDEM-X digital elevation model. ISPRS J. Photogramm. Remote Sens. 2017, 132, pp. 119–139, DOI: 10.1016/j.isprsjprs.2017.08.008.

Ross W C, Prihodko L, Anchang L, Kumar S, Ji W, Hanan N P (2018) Data Descriptor: HYSOGs250m, global gridded hydrologic soil groups for curve-number-based runoff modeling, 2018, Sci. Data 5:150091, DOI: 10.1038/sdata.2018.91.

Rutzinger M, Höfle B, Geist T, Stötter J (2006) Object-based building detection based on airborne laser scanning data within GRASS GIS environment. In: Bodum L (ed): Proceedings of the UDMS 2006: Urban Data Management Symposium, Aalborg, Denmark, 15–17 May 2006, UDMS: Delft, The Netherlands, 2006, pp. 7.37–7.48.

Seely M, Henderson J, Heyns P, Jacobson P, Nakale T, Nantanga K, Schachtschneider K (2003) Ephemeral and endoreic river systems: Relevance and management challenges. In Transboundary Rivers, Sovereignty and Development: Hydropolitical Drivers in the Okavango River Basin, In: Turton A, Ashton P, Cloete E (eds): AWIRU: Pretoria, South Africa, 2003, pp. 187–212.

Shifidi V T (2014) Socio-Economic Assessment of the consequences of flooding in Northern Namibia, Thesis (MA) Stellenbosch University (2014-12), 248 p.

Shifidi V T (2016) Impact of flooding on rural livelihoods of the Cuvelai Basin in Northern Namibia. J. Geogr. Reg. Plan. 2016, 9, pp. 104–121, DOI: 10.5897/JGRP2015.0536.

Shrivathsa B, Panjwani J (2017) Lane Detection using GPS-PPP and VISUAL Method. Asian Journal of Applied Science and Technology (AJAST) Vol. 1, Issue 5, pp.137–141.

Skakun S, Kussul N, Shelestov A, Kussul O (2014) Flood Hazard and Flood Risk Assessment Using a Time Series of Satellite Images: A Case Study in Namibia. Flood Hazard and Flood Risk Assessment, Risk Anal. 2014, 34, pp. 1521–1537, DOI: 10.1111/risa.12156.

Skog I, Handel P (2009) In-Car Positioning and Navigation Technologies - A Survey, IEEE Trans. Intell. Transport. Syst. 10 (1): 4–21, DOI: 10.1109/TITS.2008.2011712.

Smith B (2003) Accuracy and resolution of shuttle radar topography mission data. Geophys. Res. Lett. 30 (9), 47 p., DOI: 10.1029/2002GL016643.

Sobhani G A (1975) Review of selected small watershed design methods for possible adoption to Iranian conditions. 1975. MS Thesis, Utah State University, Logan, UT. In: Verma S, Verma R K, Misha S K, Singh A, Jayaraj G K (2017) A revisit of NRC-CN inspired models coupled with RS and GIS for runoff estimation. Hydrological Sciences Journal, 2017, Vol. 62, No. 12, pp. 1891-1930, DOI: 10.1080/02626667.2017.1334166.

Stengel H W, Wipplinger O, Lempp F (1963) Wasserwirtschaft in S. W. A. / Waterwese in S. W. A. Water affairs in S. W. A., Afrika-Verlag Der Kreis: Windhoek, Namibia, 1963.

Strickler A (1923) Beiträge zur Frage der Geschwindigkeitsformel und der Rauhigkeitszahlen für Ströme, Kanäle und geschlossene Leitungen (Contributions concerning the question of the flow velocity formular and roughness values for streams, channels and conduits). Bern: Mitteilungen des Amtes für Wasserwirtschaft. 1923. 16. 77.

Sturm M, Zimmermann M, Schütz K, Urban W, Hartung H (2009) Rainwater harvesting as an alternative water resource in rural sites in central northern Namibia. Phys. Chem. Earth Parts ABC 2009, 34, pp. 776–785, DOI: 10.1016/j.pce.2009.07.004.

Tarboton D G (1997) A new method for the determination of flow directions and upslope areas in grid digital elevation models. Water Res. 1997, 33, (2): 309-319, DOI: 10.1029/96WR03137.

Teunissen P J G, Khodabandeh A (2014) Review and principles of PPP-RTK methods. J. Geod. 89 (3): 217–240, DOI: 10.1007/s00190-014-0771-3.

Twele A, Cao W, Plank S, Martinis S (2016) Sentinel-1-based flood mapping: A fully automated processing chain. Int. J. Remote Sens. 2016, 37, pp. 2990–3004, DOI: 10.1080/01431161.2016.1192304.

Tyrna B, Assmann A, Fritsch K, Johann G (2018) Large-scale high-resolution pluvial flood hazard mapping using the raster-based hydrodynamic two-dimensional model FloodAreaHPC. Journal of Flood Risk Management, 11, pp. 1024-1037, DOI: 10.1111/jfr3.12287.

United Nations Office for Coordination of Humanitarian Affairs Regional Office for South Africa [UN-OCHAROSA] (2018) Water ways, roads, points of interest, administrative boundaries. https://data.humdata.org/search?ext_subnational=1&ext_geodata=1&groups=nam&q=&ext_page_size=25 desc (accessed February 16, 2018).

United States Department of Agriculture [USDA] (2009) Hydrologic Soil Groups. Part 630 Hydrology, Engineering Handbook, 2009, Chapter 7, 210-VI-NEH, 7 p., https://directives.sc.egov.usda.gov/OpenNonWebContent.aspx?content=22526.wba (accessed June 25, 2021).

Van Der Waal B (1991) Fish life of the oshana delta in Owambo, Namibia, and the translocation of Cunene species. Madoqua 17: 201-209.

Verma S, Verma R K, Misha S K, Singh A, Jayaraj G K (2017) A revisit of NRC-CN inspired models coupled with RS and GIS for runoff estimation. Hydrological Sciences Journal, 2017, Vol. 62, No. 12, pp. 1891-1930, DOI: 10.1080/02626667.2017.1334166.

Wang L, Li Z, Ge M, Neitzel F, Wang Z, Yuan H (2018) Validation and Assessment of Multi-GNSS Real-Time Precise Point Positioning in Simulated Kinematic Mode Using IGS Real-Time Service. Remote Sensing 10 (2), 337, DOI: 10.3390/rs10020337.

Wanke H, Beyer M, Hipondoka M, Hamutoko J, Gaj M, Koeniger P, Himmelsbach T (2018) The long road to sustainability: Integrated water quality and quantity assessments in the Cuvelai-Etosha Basin, Namibia. Biodivers. Ecol. 2018, 6, pp. 75–83, DOI:10.7809/b-e.00307.

Wanke H, Nakwafila A, Hamutoko J T, Lohe C, Neumbo F, Petrus I, David A, Beukes H, Masule N, Quinger M (2014) Hand dug wells in Namibia: An underestimated water source or a threat to human health? Phys. Chem. Earth Parts ABC 2014, Vol. 76, p. 104–113, DOI: 10.1016/j.pce.2015.01.004.

Wendleder A, Wessel B, Roth A, Breunig M, Martin K, Wagenbrenner S (2013) TanDEM-X Water Indication Mask: Generation and First Evaluation Results. IEEE J. Sel. Top. Appl. Earth Observations Remote Sensing 6 (1): 171–179, DOI: 10.1109/JSTARS.2012.2210999.

Wessel B (2016) TanDEM-X Ground Segment - DEM Products Specification Documen. Public Document TD-GS-PS-0021, Issue 3.1, EOC, DLR: Oberpfaffenhofen, Germany, 2016.

Wieland M, Martinis S (2019) A Modular Processing Chain for Automated Flood Monitoring from Multi-Spectral Satellite Data. Remote Sens. 2019, 11(19), 2330, DOI: 10.3390/rs11192330.

Woltersdorf L, Liehr S, Döll P (2015) Rainwater Harvesting for Small-Holder Horticulture in Namibia: Design of Garden Variants and Assessment of Climate Change Impacts and Adaptation. Water, 2015, 7, pp. 1402–1421, DOI: 10.3390/w7041402.

Woodward D E, Hawkins R H, Jiang R, Hjelmfelt junior A T, Van Mullem J A, Quan D Q (2003) Runoff curve number method: examination of the initial abstraction ratio. 2003 World Water and Environmental Resources Congress, Philadelphia, 2003, pp. 1-10, DOI: 10.1061/40685(2003)308.

Xu H (2012) Application of GPS-RTK Technology in the Land Change Survey. Procedia Engineering 29, pp. 3454–3459, DOI: 10.1016/j.proeng.2012.01.511.

Zimmermann M (2013) Sustainable Transformations of Water Supply Regimes. The Cuvelai-Etosha Basin in Central Northern Namibia. Schriftenreihe IWAR; Inst. IWAR: Darmstadt, Germany, 2013, ISBN: 978-3-940897-22-0.

Zimmermann M (2010) The coexistence of traditional and large-scale water supply systems in central northern Namibia. J. Namib. Stud. 2010, 7, pp. 55–84, ISSN: 1863-5954.

Zumberge J F, Heflin M B, Jefferson D C, Watkins M M, Webb F H (1997) Precise point positioning for the efficient and robust analysis of GPS data from large networks. J. Geophys. Res. 102 (B3), pp. 5005–5017, DOI: 10.1029/96JB03860.

Appendix

Table A-1: Satellite data used for validation and its properties.

Sensor	Product Name	Final Pixel Spacing (m)	Coverage (km: Range × Azimuth)	Polarizations/Bands
Radar	ALOS PALSAR–FBS GEC *	6.25	70 × 90	SinglePol HH
	ALOS PALSAR–FBD GEC *	13	70 × 90	DualPol HH + HV
	ALOS PALSAR–PLR GEC *	12.5	30 × 90	QuadPol HH + HV + VH + VV
	ALOS2 PALSAR–SM³ FBD 1.1 *	10	70 × 70	DualPol HH + HV
	Envisat ASAR–IMP	12.5	70–90 × 110–130	SinglePol (VV|HH)
	Envisat ASAR–WSM	75	400–450 × variable	SinglePol (VV|HH)
	Sentinel-1B GRD	10	250 × 175	DualPol VV + VH
	TSX-ScanSAR	7.5	100 × 150	SinglePol HH
	TSX-Stripmap	2.5	15–30 × 50–75	SinglePol HH
	TSX-Spotlight	2	10 × 10	SinglePol HH
Optical	Landsat 5 L1	30 (bands 1–5, 7)	170 × 183	7
	Landsat 8 L1	30 (bands 1–7, 9–11)	170 × 185	11

* Product Level: ESA **GEC** = JAXA **1.5**, ESA **SLC** = JAXA **1.1.**

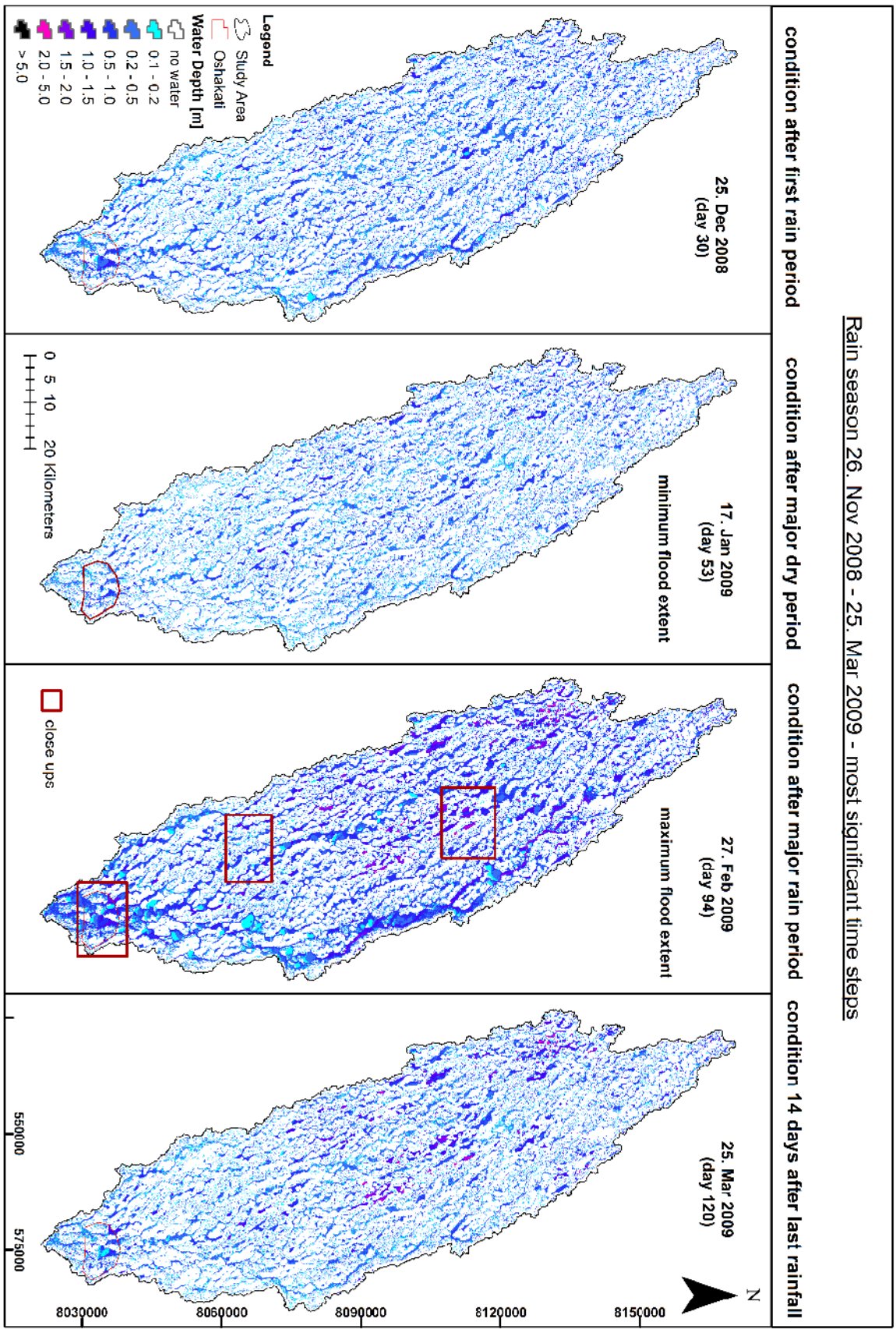

Figure A-1: The four most significant time steps of inundation during the rainy season from Nov 2008 to Mar 2009.

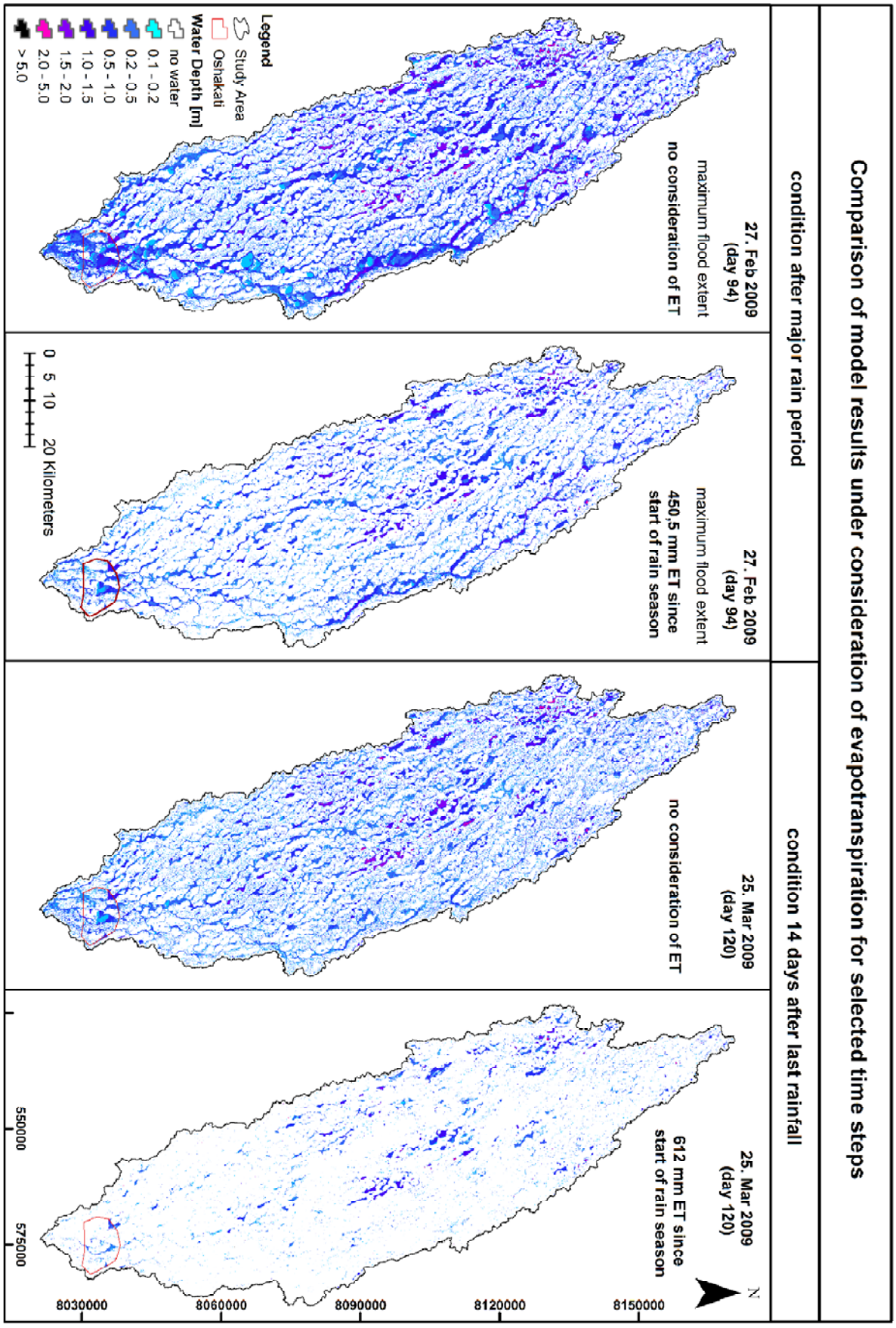

Figure A-2: Comparison of the model results including and excluding evapotranspiration.

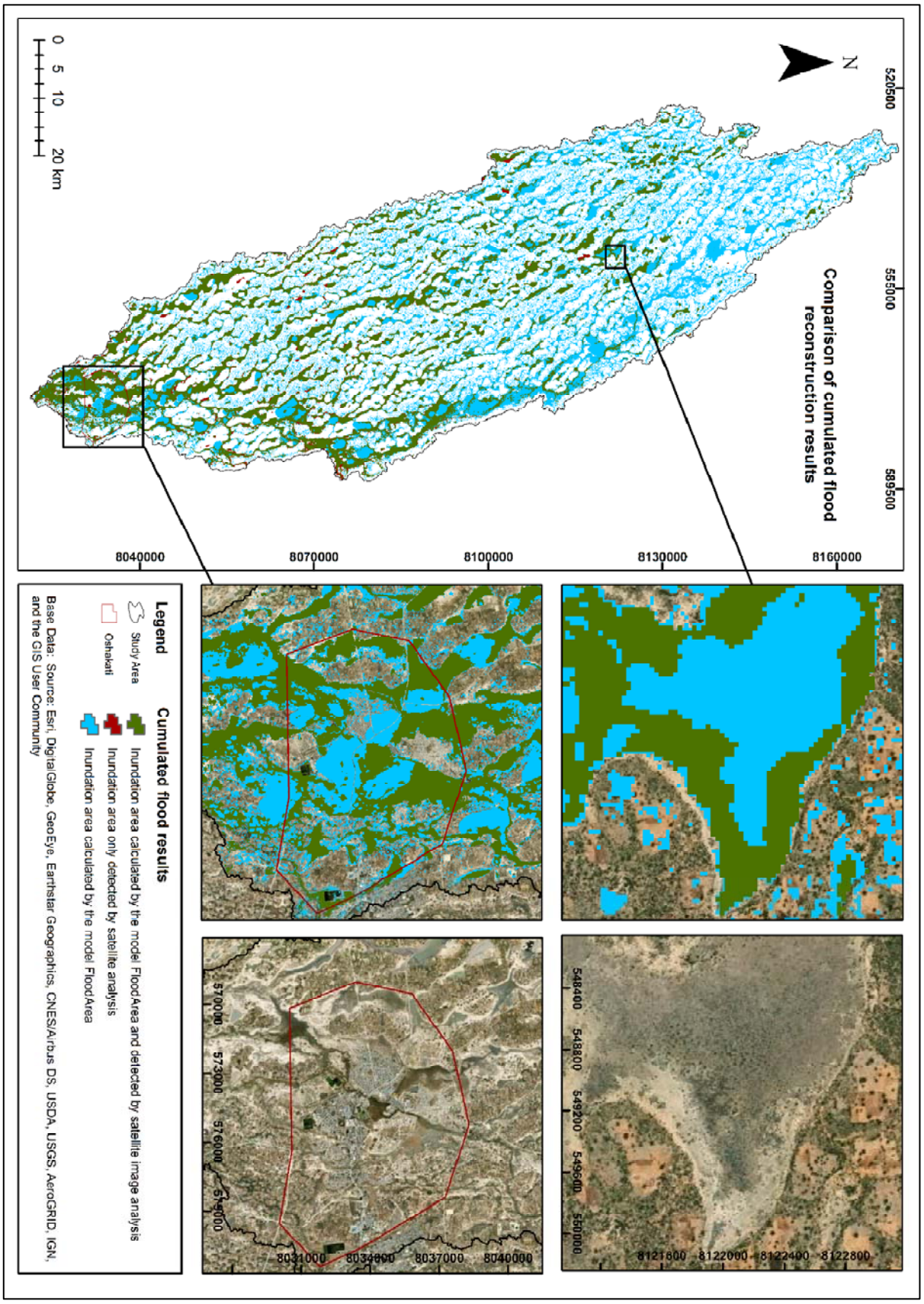

Figure A-3: Comparison of simulation results with the reference water mask. Green: Areas flooded in model and reference data; Blue: Flooding in the model only; Red: Flooded areas only in the reference mask.

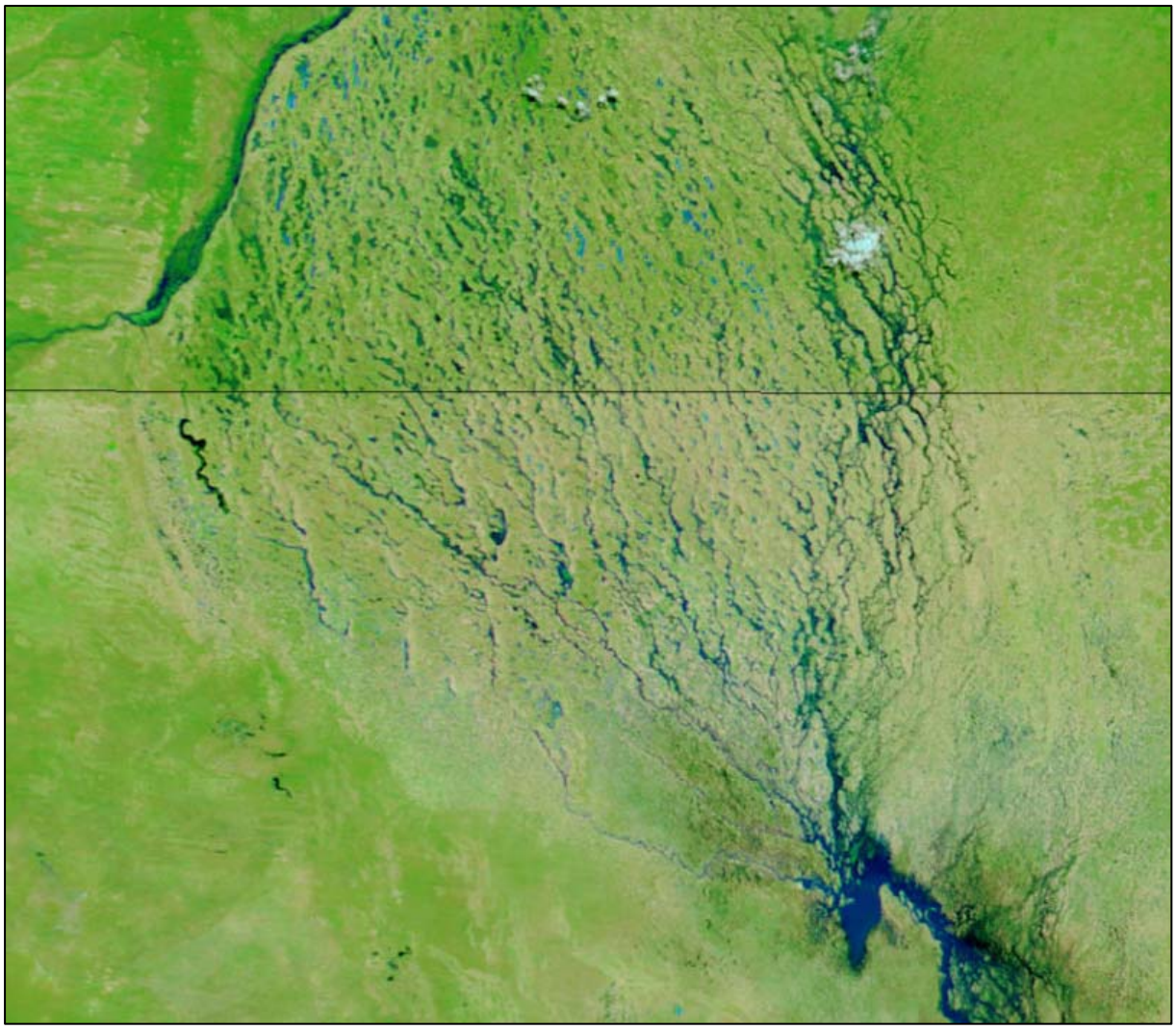

Figure A-4: MODIS scene from March 23, 2009, modified by the Darthmouth Flood Observatory (2009). Black line represents the border between Angola (above black line) and Namibia (below black line). Green colors are related to vegetation; blue colors are defined as (flood-) water.